Université de Montréal

Role of the host protein DDX3X in HSV-1 nuclear egress

Par
Muhammad Rehan

Département de microbiologie, infectiologie et immunologie

Faculté de médecine

Mémoire présenté à la Faculté de médecine
en vue de l'obtention du grade de Magister scientiae
en Microbiologie/ immunologie

November, 2023

Université de Montréal

Département de Microbiologie, Infectiologie, et Immunologie, Faculté de Médecine

Ce mémoire (ou cette thèse) intitulé(e)

Role of the host protein DDX3X in HSV-1 nuclear egress

Présenté par

Muhammad Rehan

A été évalué(e) par un jury composé des personnes suivantes

Dr. Guy Lemay
Président-rapporteur

Dr. Roger Lippé
Directeur de recherche

Dr. Andrés Finzi
Membre du jury

Résumé

HSV-1 et HSV-2, tous deux des virus à ADN double brin de la sous-famille des *Alphaherpesvirinae*, ont une prévalence subclinique chez près de 67 % de la population mondiale. Au cours de leur réplication virale intra-nucléaire, quatre types de capsides (procapsides, capsides A, B et C) sont produites tandis que seules les capsides C contiennent de l'ADN mature. Compte tenu de leur plus grande taille (125 nm) que les pores nucléaires (30 à 50 nm), ils quittent le noyau par une voie inhabituelle appelée sortie nucléaire. Notre laboratoire a précédemment découvert que le HSV-1 incorpore 49 protéines hôtes distinctes, dont DDX3X, une hélicase à ARN de type DEAD (Asp-Glu-Ala-Asp) dépendante de l'ATP qui module l'expression génique des virus à ADN et à ARN. DDX3X est redirigé vers la membrane nucléaire interne à la fin de l'infection et interagit avec pUL31, un composant du complexe de sortie nucléaire viral, pour favoriser la sortie nucléaire des capsides virales vers le cytoplasme. Cependant, la nature exacte de ces interactions reste incertaine. D'autre part, notre laboratoire a également signalé que PCBP1 est spécifiquement présent sur les capsides C et que sa déplétion entraîne une réduction du titre viral. PCBP1 est connu pour se lier à l'ARN poly (c) via les domaines d'homologie K (KH) et joue un rôle dans la stabilisation de l'ARNm, le contrôle transcriptionnel, la traduction de l'ARN, l'immunité antivirale et la modulation de la propagation virale. À l'aide de microscopie confocale et d'études de co-immunoprécipitation, le présent travail révèle que DDX3X interagit avec les deux composants du complexe de sortie nucléaire, à savoir pUL31 et pUL34, et que cette interaction est indépendante de leur phosphorylation par la kinase pUS3 qui module normalement leur localisation. De plus, nous montrons également que DDX3X interagit avec PCBP1, ce qui pourrait expliquer la sélection préférentielle des capsides C lors de la sortie nucléaire. Cette étude constitue un pas en avant dans la cartographie des interactions complexes entre protéines hôtes multiples et partenaires viraux et pour élucider leur rôle possible dans l'évasion sélective énigmatique des capsides C du HSV-1.

Mots-clés: HSV-1, sortie nucléaire, DDX3X, PCBP1.

Abstract

HSV-1 and HSV-2, both double-stranded DNA viruses of the *Alphaherpesvirinae* subfamily, reportedly have sub-clinical prevalence in nearly 67% of the world population. During their intra-nuclear virus replication, four types of capsids (procapsids, A, B, and C capsids) are produced while only C-capsids contain mature DNA. Given their larger size (125 nm) than the nuclear pores (30-50 nm), they exit the nucleus by an unusual route called nuclear egress. On the other hand, our lab previously found that HSV-1 incorporates 49 distinct host proteins, including DDX3X, a DEAD (Asp-Glu-Ala-Asp) box ATP-dependent RNA helicase that modulates gene expression of both DNA and RNA viruses. We also showed that DDX3X is redirected to the inner nuclear membrane late during the infection and interacts with pUL31, a component of the viral nuclear egress complex, to promote the nuclear exit of the viral capsids to the cytoplasm. However, the exact nature of such interactions remains elusive. On the other hand, our lab also reported that PCBP1 is specifically present on the C-capsids, and its depletion causes a reduction in viral titer. PCBP1 is known to bind with poly(c) RNA through K-homology (KH) domains and plays a role in mRNA stabilization, transcriptional control, RNA translation, antiviral immunity, and the modulation of viral propagation. Using confocal microscopy and co-immunoprecipitation studies, the present work reveals that DDX3X interacts with both components of the nuclear egress complex, i.e., pUL31 and pUL34, and that this interaction is independent of their phosphorylation by the pUS3 kinase that normally modulates their localization. Moreover, we also show that DDX3X interacts with PCBP1, which could explain the preferential selection of the C-capsids during the nuclear egress. This study is a step forward to map the complex multiple host protein interactions with viral partners and elucidate their possible role in the enigmatic selective escape of HSV-1 C-capsids.

Keywords: HSV-1, Nuclear egress, DDX3X, PCBP1.

Table of Contents

List of Tables

List of Figures

List of Abbreviations

3-O-S-HS	3-O-Sulfated Heparan sulfate
ADP	Adenosine diphosphate
AGO2	Argonaute 2
ATP	Adenosine triphosphate
AZFa	Azoospermia factor
BCA	Bicinchoninic acid
BGS	Bovine growth serum
BRCA1	Breast Cancer gene 1
BSA	Bovine Serum Albumin
CamKIIα	Ca2+/calmodulin (CaM)-dependent protein kinase II
CCL5	Chemokine (C-C motif) ligand 5
CD1d	Cluster of Differentiation 1
CDK	Cyclin-dependent kinase
cGAS/STING	Cyclic GMP–AMP synthase/Stimulator of interferon gene
CKIs	Cdk inhibitors
CNS	Central nervous system
Co-IP	Co-immunoprecipitation
CRM1	Chromosomal Maintenance 1
CSFV	Classical Swine Fever Virus
CVSC	Capsid vertex-specific component
DCs	Dendritic cells
DENV	Dengue virus
DICE	Dual-integrase cassette exchange
DNA	Deoxyribonucleic acid
dNTP	Deoxynucleotide triphosphate
dsRNA	double-stranded RNA
E	Early
EBV	Epstein-Barr Virus
eIF	Eukaryotic initiation factor
EJC	Exon junction complex
eNOS	Endothelial nitric oxide synthase
ER	Endoplasmic reticulum
ERK	Extracellular signal-regulated kinase
FBS	Fetal bovine serum
FRET	Fluorescence Resonance Energy Transfer
FRMP	Fragile X mental retardation protein
G3BP1	Ras GTPase-activating protein (GAP)-binding protein 1
gRNA	Genomic RNA

GTP	Guanosine triphosphate
H/P	Helicase-Primase complex
HCF-1	Host cell factor 1
HCMV	Herpes cytomegalovirus
HCV	Hepatitis-C virus
HEV	Hepatitis-E virus
HFMD	Hand, Foot, and Mouth disease
HIV-1	Human immunodeficiency virus 1
hnRNP	Heterogeneous nuclear ribonucleoproteins
hpi	Hours post-infection
HPV-16	Human papilloma virus-16
HSPGs	Heparan sulfate proteoglycans
HSV-1	Herpes simplex virus 1
HSV-2	Herpes simplex virus 2
HVEM	Herpesvirus entry mediator
IAV	Influenza A virus
ICCS	Image cross-correlation spectroscopy
ICP	Infectious cell polypeptide
IE	Immediate early
IFN-β	Interferon-beta
ILEI	Interleukin-like epithelial-mesenchymal transition inducer
INM	Inner nuclear membrane
IR	Inverted Repeats
IRES	Internal ribosome entry sites
IRF3	Interferon regulatory factor 3
JAK-1	Janus Kinase 1
JEV	Japanese encephalitis virus
KD	Knockdown
KHSV	Kaposi's sarcoma-associated herpesvirus
KLF4	Krüppel-like factor 4
LC3B	Light chain 3B
LCD	Low-complexity domains
LMNA	Lamin A/C gene
MAPK/JNK	Mitogen-activated protein kinase/ Jun N-terminal kinase
MAVS	Mitochondrial antiviral-signaling protein
MCC	Mander’s correlation coefficient
MCMV	Murine Cytomegalovirus
MDA5	Anti-Melanoma Differentiation-Associated gene 5
MHC-I	Major histocompatibility complex type 1
miRNA	Micro RNA
MOI	Multiplicity of infection
mRNA	Messenger ribonucleic acid

ND10	Nuclear domains 10
NEC	Nuclear egress complex
NES	Nucleus export signal
NF-κB	Nuclear factor kappa light chain enhancer of activated B-cells
NLS	Nuclear localization signal
nm	Nanometer
NMR	Nuclear magnetic resonance
NPC	Nuclear pore complex
nRNAs	non-coding RNA
NS5	Non-structural protein 5
NXF1	Nuclear RNA export factor 1
OCT-1.	Octamer motif-binding protein
ONM	Outer nuclear membrane
ORF	Open reading frame
Ori	Origin of Replication
p300/CBP	CREB binding protein
PBST	Phosphate-buffered saline with Tween 20
PCC	Pearson's correlation coefficient
PDB	Protein Data bank
PFA	Paraformaldehyde
PFU	Plaque forming units
PKC	Protein kinase C
PM	Plasma membrane
PNS	Peripheral nervous system
PPIs	Protein-protein interactions
PRRs	Pattern Recognition Receptors
PRV	Pseudorabies virus
PTM	Post-translation modification
PVDF	Polyvinylidene fluoride or polyvinylidene difluoride
RBD	RNA binding domain
RBP	RNA binding protein
RdRp	RNA-dependent RNA polymerase
RIG-I	Retinoic acid-inducible gene I
RIPA	Radio immune assay
RLR	RIG-I-like Receptors
RNA	Ribonucleic acid
RNAi	RNA interference
RNAPII	RNA polymerase II
RNPs	Ribonucleoproteins
RPMI	Roswell Park Memorial Institute
rRNA	Ribosomal ribonucleic acid

SDS-PAGE	Sodium dodecyl sulfate-polyacrylamide gel electrophoresis
SNR	Signal-to-noise ratio
SP1	Superfamily 1
ssDNA	Single-stranded DNA
STAT-2	Signal transducer and activator of transcription
STD	Sexually transmitted disease
TAP	Tandem affinity purification
TBK1	Tank binding kinase 1
TFIIA	Transcription factor II A
TGN	Trans-Golgi network
TLRs	Toll-like receptors
TNF-α	Tumor necrosis factor-alpha
TREX	Transcription and Export
TRIM-25	Tripartite motif-containing protein 25
TTS2	Tripartite terminase subunit 2
UL	Unique long
US	Unique short
UTR	Untranslated region
Vhs	virion host shutoff protein
vRNP	Viral ribonucleoprotein
VSV	Vesicular Stomatitis
VZV	Varicella zoster virus
WB	Western blot
WNT/β-catenin	Wingless/Integrated
WT	Wild type

کب تک چلے گا انگلی روایت کی تھام کر

اب وقت ہے سو رسم درایت کو عام کر

رہ رہ کر چھیڑ ساز حیات دوام کا

اے آدمی تو موت کا جینا حرام کر

“How long will the finger of tradition last?

Now is the time, so publicize the ritual

Stay and stay alive

O man, forbid the life of death”

Acknowledgments

Thousands of miles away from my sweet home in a graduate school of my dream University, a community effort helps me to thrive here. For this, I offer my special and sincerest gratitude to my mentor, Dr. Roger Lippé, for his excellent supervision and invaluable support. I appreciate his patience during a period of my persistent obstinacy and lack of tolerance. I express my profound gratitude for the multitude of opportunities bestowed upon me, as well as his invaluable counsel, constructive comments, and unwavering support throughout my experimental and thesis work provided by him. I have had a great learning experience in his laboratory, and I am eagerly anticipating the forthcoming stages of this scientific endeavor.

I extend my sincere gratitude to my immediate family members for instilling a sense of excitement and pleasure in my engagement with the field of science. Although we lost him more than a decade ago, I still remember my father's encouragement in accepting the challenges of science which will remain a lifelong inspiration for me. Mother, my closest confidant, and ally, you are the epitome of courage in my life, and I am indebted to you for all that I currently possess and for all future accomplishments. I am exceedingly fortunate and honored to have you as my maternal figure. I am sincerely thankful to my both siblings, especially my sister Javeria Umber, for her invaluable support and consistent ability to amuse me.

I would like to express my appreciation to all my lab fellows for the positive experiences we shared in the laboratory, the instances where we worked together to achieve the same goals, and the occasions where we had pieces of enjoyment. I appreciate your support in understanding and thriving in a multicultural environment, your consistent dedication to ensuring my satisfaction, and your adept handling of my idiosyncrasies. Josiane, a kind-hearted fellow, I appreciate your support in hands-on experience in lab experiments. Bita, Negar, Yulia, and Jonas, your influence has significantly altered my overarching outlook on science and life. I am especially thankful to Catherine and Sandrine Marqueteau, our lab managers, for their support and mentorship.

Last but not least, I extend my gratitude to the Higher Education Commission Pakistan (HEC) for their financial assistance and to all members of the Université de Montréal for their technical support. I am thankful to have met Waqas Nawaz Khan for his guidance in troubleshooting my problems.

Chapter 1: Introduction

1.1 History and Taxonomic Classification

The first description of Herpes simplex virus dates to ancient Greek records when a Greek physician Hippocrates II, coined the term "έρπης" meaning "to crawl" or "to creep" to describe the spreading ulcerative skin lesions. Although the herpetic lesions were characterized in classical literature, back in 1839 Vidal was the first person to discover the possibility of person-person transmission of herpes simplex virus (1).

Based on virion morphology, cell tropism, and physio-clinical characteristics, the family *Orthoherpesviridae* together with the families *Malacoherpesviridae* and *Alloherpesviridae* is categorized into the order *Herpesvirales* inside the kingdom *Heunggongvirae* (2). Till today, 9 members from three subfamilies (α-, β-, and γ-) have been recognized in mild to severe human infections, including *alphaherpesviruses* (HSV-1, HSV-2, and VZV), *betaherpesviruses* (HCMV, HHV-6A, HHV-6B, and HHV-7), and *gammaherpesviruses* (EBV and KSHV) (3). Based on phylogenetic analysis, *Orthoherpesviridae* subfamilies are estimated to have diverged from a common ancestor approximately 400 million years ago and later evolution gave rise to 135 species afflicting both human and non-human hosts (4).

1.2 General Characteristics of Herpes Simplex Virus

1.2.1 Clinico-Pathological Features

Herpes simplex virus -1 (HSV-1), a prototypical alphaherpesvirus, binds with its respective receptors and typically causes mild to severe orolabial ulcerative skin lesions (cold sores/oral herpes/gingivostomatitis) in children and adults and establishes latency in the peripheral nervous system (PNS) (5). Sometimes complications cause keratitis, conjunctivitis, and even blindness. HSV-2 causes genital herpes, an important sexually transmitted disease (STD) (6). HSV-1 has also been reported as a mild cause of genital herpes (7). HSV-1 has a high prevalence during childhood, though some studies reported delayed acquisition from childhood to adulthood in developed countries (8). Depending upon the viral strain and site of infection, skin lesions develop within 2-20 days post-infection. These oral/skin lesions are 1–2 mm blisters that coalesce to form small, irregular, painful, and shallow ulcers, demarcated from healthy skin by a yellowish-grey erythematous pseudo-membrane. These ulcers usually heal in 7-14 days, leaving no scars (9, 10).

In rare cases, these oro-mucosal lesions can be followed by anorexia, lethargy, pyrexia, hypersalivation, dysphagia, headache, and bilateral cervical lymphadenopathy (11).

Neonates can get herpes infections either during intrauterine life from asymptomatic mothers, particularly during the third trimester (5-8% cases) or during post-partum contact with hospital individuals (8-10% cases) (12, 13). With no complete virus clearance, 50% of surviving neonates live with lifelong complications, including vision impairment, psychomotor retardation, and learning disabilities (14).

1.2.2 Epidemiology

HSV-1 has an estimated presence of 4.8 billion people, which is nearly 67% of the total world's population (15, 16). Risk factors associated with variation in the global prevalence of HSV-1 include socioeconomic status, age, race, and geographic region. HSV-1 is slightly more prevalent in females (~66%) as compared to males (~61%). The highest disease prevalence is reported in African countries while the lowest numbers are reported in the South and North American regions (17, 18). HSV-2 has been diagnosed in more than 400 million people, totaling around 13% of the worldwide population (19). As it is not possible to differentiate between HSV-1 and HSV-2 in genital herpes with current serological tests, the total estimate for HSV-1 is still low, accounting for about 5% of cases of genital herpes (20). In addition, the likelihood of recurrent genital herpes is greater with HSV-1 (15%) than that of HSV-2 infection (0.01%) (21).

Recently, the characterization of a widely spread "HSV-2 lineage" originating from the African population shows fewer recombination events with HSV-1, suggesting the possibility of virus diversification first in ancient African populations and then its possible spread to other parts of the world (22). Based on such geographic analyses, HSV-1 strains are categorized into three "phylogroups" i.e., I (America and Europe), II (Asia, America, and Europe), and III (Africa) (23). In addition to newly recognized lineage, phylogroup III's distribution, which is basal to Eurasian phylogroups, indicates that the appearance and subsequent spread of genetic variation in HSV-1 coincided with the human "out-of-Africa" migration model, where the dispersal of human beings from Africa to Europe and then to Asia happened about 55,000 years ago and brought this novel HSV lineage with them (22, 24, 25). This "out-of-Africa" human dispersal theory was also proposed for the varicella-zoster virus (VZV) and human betaherpesvirus-6 (26).

1.2.3 HSV-1 interaction with the immune system

Both innate and adaptive immune responses sense herpesviruses. The innate immune response requires membrane-bound toll-like receptors (TLRs) and cytosolic pattern recognition receptors (PRRs) (27), while $CD8^+$ T cells are crucial components of the adaptive immune response (28). Different PRRs recognize the cytosolic genomic DNA of HSV-1. TLR2-mediated pro-inflammatory cytokines production after onset of HSV-1 infection in mice causes the accumulation of polymorph inflammatory cells in the brain while TLR3 produces type-I and type-III interferons (IFNs) in fibroblasts (29, 30). In conventional dendritic cells (DCs) and murine macrophages, TLR9 recognizes cytosolic viral DNA with the stimulation of C-C motif chemokine ligand-5 (CCL5) and tumor necrosis factor-alpha (TNF-α) production (31). RLR/MAVS/MDA5 dependent HSV-1 recognition and IFN-production are important components of antiviral immune response (32).

The IFN-induction in HSV-1 infection is independent of *de-novo* viral genes synthesis and requires only viral entry into the cell (33). Different viral proteins interact with cellular factors to escape antiviral immunity. The pUS3 phosphorylation of retinoic acid-inducible gene-I (RIG-I) at the serine in position 8 prevents the tripartite motif-containing proteins-25 (TRIM25) mediated RIG-I-MAVS binding and subsequent type-1 IFN production (34). The pUL37 deamination of asparagine residues in RIG-I hampers its ability to sense viral RNA and consequently suppresses the immune response (35). The HSV-2 virion host shutoff (vhs) protein blocks the double-stranded RNA (dsRNA) antiviral pathway by inhibiting the expression of both MDA5 and RIG-I (36). The N-terminus of HSV-1 gL inhibits the nuclear translocation of p65 and significantly downregulates the NF-κB-mediated IFN-β production. The HSV-1 vhs, pUS3, pUL24, pUS11, ICP34.5 ICP0, ICP27, and pUL42 binding with NF-κB-subunits (p50 and p65) inhibits the nuclear translation of NF-κB and other effectors of innate immune response (37, 38). Some studies also reported the decreased levels of JAK1 and STAT-2 in HSV-1 infected cells partially attributed to either vhs or ICP27 interactions with the immune system (39, 40). ICP47 interferes with ER-transport of antigenic peptides and inhibits major histocompatibility complex (MHC) class I-mediated activation of cytotoxic T-lymphocytes (41). The HSV-1 gE and gI complex, which exhibit antibody bridging activity, inhibits IgG-mediated complement neutralization, phagocytosis, and cellular cytotoxicity (42). gC binding with the complement factors (C3b and C5) inhibits complement-mediated virus neutralization and cell lysis of HSV-1 infected cells (43).

1.3 Mature HSV-1 virions

Like other members of *Orthoherpesviridae*, HSV-1 contains five structural components: i) an electron-dense double-stranded DNA (dsDNA) core, encapsidated in ii) an icosahedral capsid, covered by iii) proteinaceous tegument layer, surrounded by iv) a polymorphic lipid envelope, and flanked by v) viral glycoproteins (Figure 1.1) (44, 45).

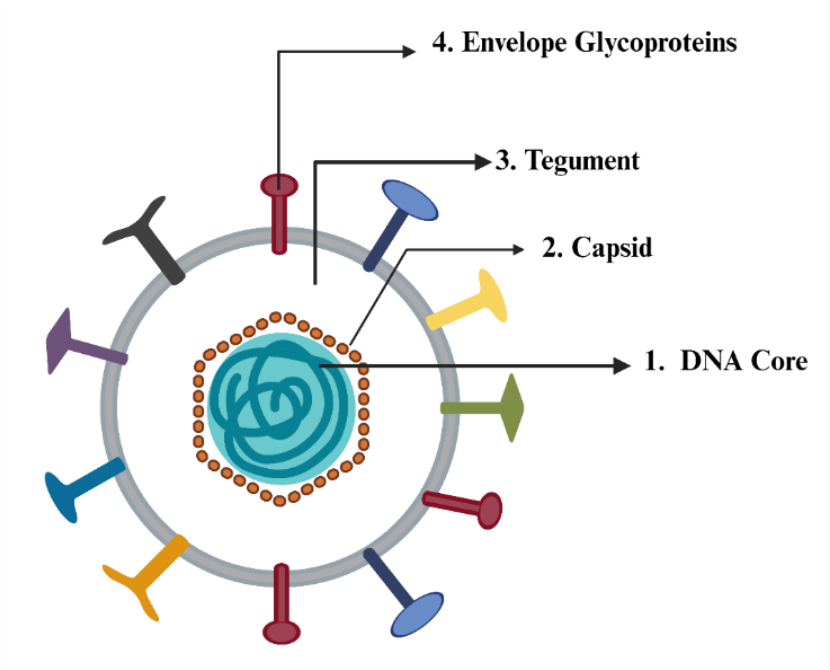

Figure 1.1: Structural components of mature HSV-1 virion.
Adapted with permission from *Heming et al.,* 2017 (45) and modified with BioRender.com.

1.3.1 Genome

HSV-1 contains a large 152 kb long dsDNA with 68% GC content. The genome is made up of two covalently linked segments named unique long (U_L) and unique short (U_S) flanked by inverted long (R_L) and short (R_S) repeats (Figure 1.2) (46). The terminal repeats better known as direct repeats (DR1), a 400 bp sequence present at the end of each terminus, help in genome circularization after HSV-1 entry into the host cells. DNA exists in four isomeric forms due to the capacity of both U_L and U_S segments to invert at a relatively high frequency (47). Dispersed between these segments, 94 open reading frames (ORFs) encode 84 distinct genes, out of which, 40 genes are called "core genes", as they are evolutionarily conserved and shared by all members of the *Orthoherpesviridae* family (48, 49). Upon entry, the viral DNA is delivered to the host cell's nucleus through the nuclear pore complex (NPC).

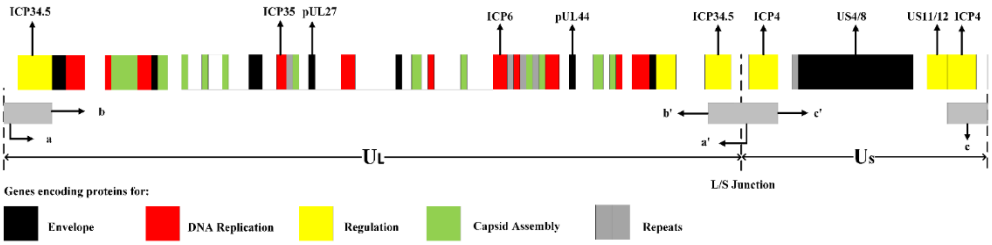

Figure 1.2: Genome map of HSV-1.

This figure illustrates the HSV-1 genome organization with genes encoding proteins required for virus replication, regulation, and envelopment. Adapted with permission from *Argnani et al.,* 2005 (46) and modified with Microsoft Visio.

1.3.2 Capsid

The delicate HSV-1 DNA is tightly packed in an icosahedral capsid, 125 nm in diameter with a ~15 nm thickness, which results in high (18-20 atmospheres) internal DNA pressure (50). The mature capsid comprises 162 capsomeres with defined faces and vertices. The 150 hexon faces and 12 geometrically defined penton vertices that make up these capsomeres combine to form an icosahedron with a triangulation number of T=16. The inner shell of each capsid contains 1100 copies of a scaffold protein (VP22a or ICP35) encoded by the UL26.5 gene. The outer shell contains 955 VP5 copies on both pentons (five copies each) and hexons (six copies each), encoded by HSV-1 UL19. Both hexons and pentons are connected by a triplex, comprised of one VP19c and two VP23 copies and 320 triplexes interlink the capsomeres to each other (51). Twelve vertices contain pUL17 and pUL25 and form a so-called capsid-vertex specific component (CVSC). DNA enters and exits the capsid through a unique portal which is surrounded by 12 copies of pUL6 and contains pUL25 in a unique conformation distinct from other vertices (52, 53).

1.3.3 Tegument

The tegument is a dense amorphous protein layer between the capsid and viral lipid envelope. HSV-1 tegument contains 23 viral proteins and incorporates 49 host proteins, many of which are important for virus replication and egress (54, 55). A complex network of protein-protein interactions (PPIs) holds tegument proteins together even upon biochemical removal of the viral envelope (56). This asymmetric, amorphous protein network is concentrated near the distal pole, an envelope pole located farthest from the capsid. The process of viral tegumentation is complex and sequential during virus egress as it is influenced by different stages of the viral life

cycle including capsids trafficking and docking to nuclear pores (57), genome replication (58), regulation of host-proteins expression (59), and immune evasion (60). The proteins are added first in the nucleus (ICP0, ICP4, pUL36, pUL37, VP22, vhs, pUS3, pUL7, and pUL51), and others are likely added as the capsids travel in the cytoplasm and finally at the site of secondary envelopment i.e., trans-Golgi network (TGN) or endosomal vesicles (61-63).

1.3.4 Envelope

The viral envelope contains asymmetrically arranged 15 viral proteins, out of which 3 are non-glycosylated (pUL20, pUL45, and pUS9) and 12 are glycosylated (gB, gC, gD, gE, gG, gH, gI, gJ, gK, gL, gM, and gN). Four of these glycosylated proteins i.e., gB, gD, and gH/gL are essential for HSV-1 attachment and entry into the host cells (64, 65), while the other 11 proteins facilitate virus entry, syncytia formation, and cell-cell spread during infection (66). The virus acquires its lipid envelope either from endosomal vesicles (67) or from TGN during the secondary envelopment (68).

1.4 Life cycle

The HSV-1 life cycle can be lytic or lead to viral latency when the genome largely remains quiet in neuronal cells of trigeminal ganglia. The replication cycle begins with virus attachment to host-cell receptors, followed by entry, gene expression, genome replication, assembly, and egress of mature virions, which takes approximately 18-24 hours in permissive cells (69).

1.4.1 Attachment and entry into the host cells

Five viral glycoproteins i.e., gB, gC, gD, and gH/gL interact with host cell receptors for pH-dependent or pH-independent endocytosis of the viral genome depending on the cell type (70). The HSV-1 receptors are cell type-specific and include heparan sulfate proteoglycans (HSPGs) and nectin-1 for fibroblasts, neuronal cells, and epithelial cells (71), while 3-O-sulfated heparan sulfate (3-O-S-HS) and herpesvirus entry mediator (HVEM) are primary receptors for ocular epithelium and the rare infection occurring in T-cells (72). These interactions are multistep with the initial gB or gC binding with HSPGs followed by gD interaction with nectin-1. This induces conformational changes in the viral gB fusion protein, leading to fusion with the plasma membrane (PM), which also requires the gH/gL viral complex. After fusion, most tegument proteins are released into the cytoplasm and the viral capsids are delivered to the nucleus through microtubules (73). At the NPC, the viral proteins (pUS3, pUL36, and pUL37) interact with Nup214, Nup358,

and Importin-β to inject the viral genome into the nucleus (74). The expulsion of the viral genome from the capsid is mediated by the highly pressurized DNA within the capsids (75).

1.4.2 Gene expression

The HSV-1 viral genes are transcribed by the host's RNA polymerase-II (RNAPII) in an orderly cascade regulated by host-viral protein interactions. During the lytic infection, three different kinetic groups of genes named the immediate early (IE or α) genes, early (E or β) genes, and late (L or γ) genes (76), are orderly expressed. IE genes can be transcribed without any *de novo* viral protein synthesis. The incoming tegument protein VP16 interacts with host cell factor-1 (HCF-1) and Octamer motif-binding protein (OCT-1) upstream of IE gene promoters and recruits transcription factors (TFIIA) to transcribe IE genes. IE genes encode pUS1, pUS1.5, pUS12, ICP0, ICP4, and ICP27 and induce the expression of later genes. Twelve early genes are involved in viral replication and nucleic acid metabolism (Table 5.1 in Annex) (77). Late genes are divided into two types: γ1 (leaky late) and γ2 (true late) genes. γ1 proteins are detectable in small concentrations before virus replication, however, both groups require DNA replication for their optimal expression and are essential for assembly and packaging of virions. ICP4 tightly regulates transcription and efficient early to late switch without any other interacting partner and increases the transcription of different viral genes (78). In addition to the TATA box, several transcription initiator elements (INRs) flanking initiation sites are also important for late gene regulations (79). After viral DNA replication, the viral proteins involved in transcription leave nuclear domain-10 (ND10) foci where they first accumulate to newly assembled replication compartments, which provide transcription factors important for early to late switch (80).

After transcription, newly transcribed viral mRNA must be transported to the cytoplasm for subsequent translation and post-translational modifications (PTMs). An HSV-1 ICP27 interaction with nuclear export receptor TAF/NXF1 suppresses host nucleocytoplasmic mRNA translocation and promotes the export of intronless viral mRNAs to the cytoplasm. Transcription is tightly coupled with DNA replication and the underlying mechanism is still enigmatic (81). A viral RNase (VHS) eventually degrades both host and early viral mRNAs, thereby promoting late viral transcripts (82).

1.4.3 Replication

HSV-1 encodes three *cis*-acting origins of replication: two within the terminal repeats of the short segment (OriS) and one (OriL) between the pUL29 and pUL30 genes of the U_L region (83). Seven early viral proteins compose the core replication machinery. These include the DNA polymerase (pUL30), helicase-primase complex (H/P complex) (pUL5, pUL8, pUL52), single-stranded DNA (ssDNA) binding protein (ICP8), processivity factor (pUL42), and origin binding protein (pUL9) (84). pUL9 has intrinsic helicase and ATPase activity required to unwind dsDNA and binds with both OriS and OriL to initiate replication (85). ICP8 has template annealing capacity, binds to ssDNA and pUL9, and forms filaments. ICP8 stimulates both the H/P complex and pUL30 and interacts with other cellular and viral proteins to facilitate viral genome replication. The H/P complex is a heterodimer that contains ATPase, 5′–3′ helicase, primase, and DNA binding properties and is recruited to the replication fork after the pUL9 interaction with ICP8. pUL8 is required for H/P nuclear localization, pUL5 assists in dsDNA unwinding while pUL52 adds RNA primers, which serve as a template for DNA synthesis (86, 87).

pUL30 is a viral polymerase that can add 30 nucleotides per second during elongation and correct mismatched nucleotides in the 3’ to 5’ direction (88). pUL30 also prevents base dissociation once stabilized by pUL42 on the DNA strand. Moreover, pUL42 decreases the premature dissociation of pUL30 by 10 folds without affecting its association rate (89). HSV-1 replicates in two stages resulting in concatemeric DNA, that is longer than the HSV-1 genome and cleaved later, which sometimes is recombination dependent. Recombination rescues replication at the stalled fork and produces concatemers (Figure 1.3) (90, 91).

1.4.4 Capsid assembly and genome packaging

During intranuclear replication of HSV-1, four morphologically distinct types of capsids are formed; i) Procapsids and thermo-stable A-capsids, B-capsids, and C-capsids (92). Procapsids are fragile precursor capsids, first formed during the replication cycle, and contain a large spherical amorphous outer double shell (93). A- capsids are the least abundant of the three stable capsid types, contain no DNA, and arise from unsuccessful DNA packaging. B-capsids are 20%-30% of all capsid forms that contain scaffold protein and do not interact with DNA packaging machinery. C-capsids are mature products of replication and contain mature infectious DNA (94). The

minimum number of viral proteins required to form procapsids includes VP5, VP19C, pre-VP22a, VP23, and UL26 gene products (95).

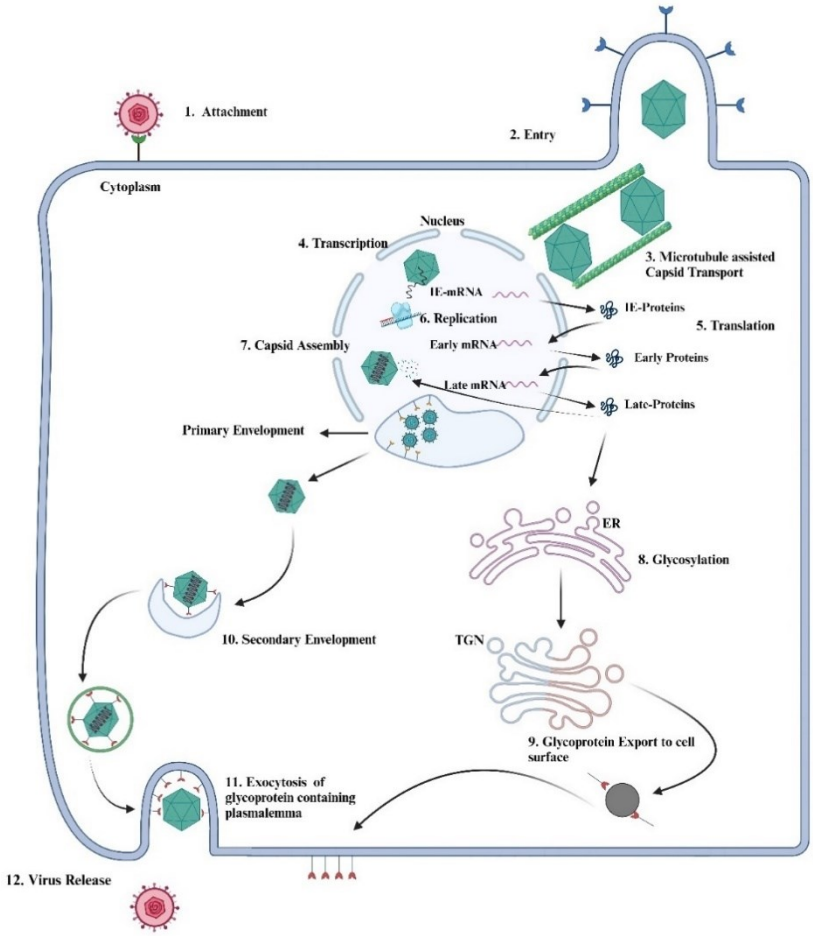

Figure 1.3: Lytic life cycle of HSV-1.

This figure illustrates the complete steps of virus replication from entry to gene expression and to egress of mature capsids. Adapted with permission from *Ibáñez et al., 2018* (91) and modified with BioRender.com.

The first step in capsid assembly is forming a portal ring followed by VP5 interaction with the scaffold pre-VP22a and UL26 gene products inside the nucleus of HSV-1 infected cells. Next, the proteolytic cleavage of the scaffold yields an angularized icosahedral capsid with T=16 symmetry (96). The exact order of this cleavage step is not completely known. However, during capsid maturation, the processing of UL26-encoded protease yields VP24, and the presence of this protease domain on defective icosahedral B-capsids suggests it could happen before the

encapsidation event (97). CVSC proteins (pUL17 and pUL25) are assembled on these capsids along with the packaging triplex (pUL15, pUL28, and pUL33) before encapsidation and their concentration depends on capsid type (98). Successful DNA encapsidation requires seven viral gene products (pUL6, pUL15, pUL17, pUL25, pUL28, pUL32, and pUL33). If any one of these proteins is depleted, it results in the accumulation of B-capsids and concatemeric DNA (99). Moreover, pUL21 interacts with CVSC and is required for genome retention inside capsids, which suggests its indirect role in genome packaging (100).

1.5 Nuclear egress

Nuclear pores allow the transfer of molecules between 25 to 39 nm (101). Due to its much larger size, HSV-1 capsids cannot exit the nucleus through nuclear pores and adopt an unusual mechanism called nuclear egress. Three models are proposed to describe the capsid's exit from the nucleus. The first “single envelopment” model suggested that capsids acquire the primary envelope by budding through the INM into the PNS. Since the PNS is contiguous with the ER, the capsids would subsequently be transported to the cell’s surface through the biosynthetic pathway (102). However, no electron micrographs of virions inside the Golgi have ever been identified, which is requisite for the glycosylation of 12 viral glycoproteins (103). The second “nuclear pore” model suggests that the enlarged nuclear pores allow the capsids to pass through them (104). In support of this model, only one study identified the translocation of HIV-1 capsids (~120 nm × 60 nm) through the NPC, which is the maximum cargo in NPC recognized to date. However, Mettenleiter’s lab suggested that HSV-1 could only pass through the NPCs in extreme conditions (105). The third model was proposed by Stackpole in 1969, which suggested a three-step envelopment-deenvelopment-reenvelopment, egress of the capsids (106). In this model, the capsids bud through the INM into the PNS for primary envelopment, and then these enveloped virions fuse with the ONM to release unenveloped capsids into the cytoplasm. Finally, the cytoplasmic capsids acquire their final envelope by budding into the TGN or endocytic vesicles. Most recent studies support this model (107, 108).

The nucleus undergoes a complete architectural reshaping because of wild-type (WT) infection, with dense chromatin being moved to the periphery to make enough room for the growing replication compartment and capsid docking. Nucleocapsid movement inside the nucleus is passive, but induction of the virus-induced channels allows capsid passage through dense

chromatin (57, 109). The following section explains this envelopment-deenvelopment-reenvelopment model in detail along with contributing proteins.

1.5.1 Nuclear egress complex (NEC)

The efficient escape of newly assembled DNA-filled capsids requires a structurally intact and rightly positioned nuclear egress complex (NEC) (100). The HSV-1 NEC is composed of two viral proteins named pUL31 (NEC1) and pUL34 (NEC2) (110). Both proteins are essential for the proper positioning of NEC and are conserved among all members of the *Herperviridae* family (111). The absence of any of the two proteins along with pUS3 causes impaired viral replication, retention of capsids inside the nucleus, and vesiculation of the nuclear membrane in the PNS (112, 113). In HSV-1, at least four other viral proteins regulate NEC. pUL13, a viral kinase that phosphorylates pUS3, co-localizes with pUL31 and regulates NEC localization (114). pUS3, another viral kinase, phosphorylates both NEC proteins and is required for the even distribution of NEC throughout the nuclear rim (115). ICP22, encoded by the UL49 gene, and ICP4 have a pUL31-dependent association with the NEC and are involved in the proper trafficking of the heterodimer to the INM (116). Furthermore, VP13/14, encoded by UL47, and pUL21 are also associated with proper NEC positioning (117, 118). The currently accepted model suggests the trafficking of pUL31 from the cytoplasm to the inner nuclear membrane (INM), where it interacts with pUL34 to form NEC, and this interaction also retains NEC at the INM (119). This model suggests that some unknown viral or host protein interacts with pUL31 N-terminus (44 amino acids) to prevent its pre-mature interaction with pUL34 in the cytoplasm before reaching the nuclear periphery (120, 121). The NEC binds with lamin A/C (LMNA), disrupts their interaction with emerin, and recruits different isoforms of protein kinase C (PKC) that aid in the dissolution of nuclear lamina and drive budding of nucleocapsids (122). Overexpression of the NEC alone can form vesiculation of the nuclear envelope and recruit nuclear capsids to the INM. Recent studies also suggested that NEC can act as an adapter protein to initiate the membrane budding and recruit other proteins (123).

Recent studies have proposed 5 different crystal structures of NEC in *alpha-* and *betaherpesviruses* including HSV-1 (PDB ID: 4ZXS) (124), human cytomegalovirus (HCMV) (PDBs: 5D5N and 5DOB) (125), and pseudorabies virus (PRV) (PDBs: 5E8C and 4Z3U) (126). NEC is an elongated cylindrical heterodimer with pUL34 at the base and pUL31 at the top of the

complex. Both proteins have unique folds. The globular core or conserved region-I of pUL31 forms an extended N-terminal hook that wraps downward around pUL34 while conserved region-III of pUL34 binds with the remaining structures of pUL31, resulting in an extremely stable heterodimer (127).

1.5.2 pUL31

pUL31 is 306 amino acids long, soluble, hydrophobic, and nucleotidylated phosphoprotein (128). Its large C-terminus contains four conserved regions while the N-terminus is highly variable (129). The C-terminus contains a binding site for its interaction with pUL34 (130) and also interacts with nuclear capsids. The smaller N-terminus is critical for virus propagation (121), contains bipartite NLS (131), and is a substrate of pUS3 phosphorylation (as reviewed in 1.5.4). This PTM is significantly important for HSV-1 viral replication and nuclear egress. Moreover, pUL31 mutants lacking an N-terminus are retained in the cytoplasm even if co-transfected with pUL34 (132). Furthermore, the N-terminus of pUL31 is critical for the recruitment and intranuclear translocation of capsids to the vicinity of INM (121). Through the central pore channel, pUL31 is actively recruited to the INM in the presence of pUL34 (133), where it interacts with and recruits other viral partners to the nucleocapsid budding sites, including gD and gM (134), and is considered important for DNA packaging and virion assembly (135). One study found HSV-1 pUL31 closely associated with newly replicated DNA (136). Studies using pUL31 orthologs from Epstein-Barr virus (EBV) and murine cytomegalovirus (MCMV) also revealed its unique role in DNA packaging (137, 138). pUL31 also promotes gene expression early after HSV-1 infection and is associated with the cell's failure to activate MAPK/JNK kinase and NF-kB (135). Deletion of pUL31 has a minor effect on total viral DNA concentration but causes a three to four-fold decrease in viral yield and monomeric to concatemeric DNA ratio compared to WT infection (139). However, the reduction in viral titer is not seen in all cell lines (140). pUL31 directly interacts with C-capsids and the pUL31-bound capsids are recruited at the INM (141). This role is also supported by our previous lab findings where pUL31 interacts with the C-terminal of DDX3X, re-localize it to the INM late during HSV-1 infection, which could be associated with capsids recruitment at the INM and selective egress of C-capsids (142).

1.5.3 pUL34

pUL34 is a type-II integral membrane phosphoprotein that can be anchored to both ER and nuclear membranes (143). pUL34 is anchored to the INM through its transmembrane helix located on the hydrophobic C-terminal domain with some residues extended to peri-nuclear space (PNS) (144). It also contains a nucleoplasmic domain (247-long amino acid motif) that binds to pUL31 which is important for their retention at INM (115). Several N-terminal residues (between amino acids 137 to 181) also interact with pUL31 and are required for vesicle formation at the PNS (145). pUL34 deletion causes a two-to-five-fold decrease in virus yield. Nuclear capsids can assemble in the absence of pUL34 but are unable to bud through the INM (146). pUL34 recruits pUS3 and PKC and has an indirect role in chromatin restructuring during egress in coordination with pUS3 (reviewed in 1.5.4) (147). pUL34 could facilitate the nuclear egress through four potential means: i) pUL34 could mediate a direct interaction between the INM and nucleocapsids; ii) pUL34 could interact with other viral proteins to redirect them to the INM for egress, and iii) its interaction with nuclear lamins re-structures this physical barrier, since in the absence of pUL34, nuclear lamina remains intact with the accumulation of incoming nuclear capsids in the nuclei due to failure of egress. Finally, iV) pUL34 also induces membrane curvature around the capsids (148-151).

1.5.4 pUS3

HSV-1 encodes a 481-amino acids long inner tegument associated protein pUS3, a serine/threonine kinase, which is not conserved in other Herpes subfamilies (152). pUS3 is an important virulence factor required for infecting the peripheral and central nervous system (153). It is auto-phosphorylated at Ser-147 and phosphorylated by pUL13 and pUS3 activity in egress is pUL13 dependent (154). pUS3 is multifunctional with 23 known viral and host substrates (155), acts as an anti-apoptotic factor (156), interacts with microtubule network by phosphorylating dynein (157, 158), prevents histone deacetylation to promote gene expression (159), and regulate the intracellular trafficking of host and viral proteins (160). The most critical function of pUS3 is to assist preferential egress of HSV-1 nuclear capsids through de-envelopment (161). Another study supported this role where primary enveloped nuclear capsids were trapped in the PNS in cells infected with the US3-null virus (162). In addition to capsids, pUS3 absence also causes accumulation in the PNS of other viral proteins required for viral infectivity and secondary envelopment including gK (163).

pUS3 phosphorylates pUL31 at six serine residues, including Ser-11, 24, 26, 27, 40, and 43. pUS3 dead kinase mutations or alanine substitutions at these six serine residues misplace the NEC in punctate structures around INM and produced invaginations of nuclear membrane similar to those produced by depleting the whole protein (110, 132). pUS3 also phosphorylates pUL34 at Ser-198 and Thr-195. However, alanine substitutions at those sites have little impact on NEC localization (164). pUS3 additionally phosphorylates lamin A/C and emerin to modify the nuclear architecture, localization, and conformation which assist in the egress of nucleocapsids (147, 165). pUS3 also promotes pUL47 nuclear localization by phosphorylating it at Thr-685, Ser-77, and Ser-88, which in turn interacts with the NEC to regulate nuclear egress (166).

1.6 HSV-1 incorporates host proteins

Viruses hijack the host cell's metabolic and protein synthesis machinery and incorporate various host cellular proteins (167). These host proteins assist viruses in their successful entry, invasion, replication, egress, and spread in infected cells (168). Through mass spectrometry analysis, our lab found that HSV-1 mature extracellular virions incorporate 49 distinct host proteins (55). Furthermore, small interfering RNA (siRNA) screening revealed that 15 of these host proteins were important for *in-vitro* HSV-1 propagation. The ATP-dependent DDX3X was at the top of the list, interfering the most with the HSV-1 life cycle (54).

1.7 DDX3X

RNA helicases are categorized into six superfamilies (169). One of the largest ATP-dependent RNA helicase family in eukaryotes, the DEAD (Asp-Glu-Ala-Asp) box helicases, are included in the superfamily 2 (SF2) and are known to have roles in every stage of RNA metabolism (170). The human genome encodes two functional genes paralogs: DDX3X and DDX3Y, which share 92% amino acid homology (171). First identified in 1997, DDX3X is an important ATP-dependent RNA helicase of this DEAD-box family with a relaxed ability to bind different possible substrate stereoisomers (172-175). DDX3X is located on the X-chromosomes at position p11.3-11.23 (176), while DDX3Y is localized on the AZFa region of the Y chromosome (177). DDX3Y is only expressed in sperm germ cells and is important for male fertility (177, 178). DDX3X escapes human female X-chromosomal inactivation (179) and is ubiquitously expressed in various body tissues (180). There are 37 known human DEAD-box proteins and DDX3X is highly conserved (181). The other known orthologs of the human DDX3X include *Saccharomyces*

cerevisiae Ded1p (182), Drosophila Belle (183), Mice PL10 (184), Xenopus An3 (185), and Rat mDEAD3 (186). Despite their sequence homology, these proteins do not necessarily complement each other in *in vitro* assays (187).

DDX3X is a 73 kDa polypeptide with 662 amino acids and contains a helicase core along with two RecA-like domains (188). It also contains twelve helicase motifs for RNA binding (motifs Ia, Ib, Ic, IV, IVa, V, and VI) (189) and ATP hydrolysis (Q, I, II/DEAD, VI) (Figure 1.4) (174, 190), flanked by disordered terminals. At both C- and N-terminus domains, structurally adaptable low complexity domains (LCD) flank the helicase core (191, 192). These LCDs have extra-catalytic regulatory functions and structurally distinguish DDX3X from other members of the DEAD-box helicase family (193). Recent studies revealed DDX3X's capability of oligomerization and remodeling of the secondary structures of bound RNAs by hydrolyzing ATP to ADP (194). This makes it a highly multifunctional host protein with known roles in important cellular processes including RNA metabolism (195), nucleo-cytoplasmic RNA transport (196), regulation of cell cycle (197), apoptosis (198), IFN production (199), gene instability (200), regulation of gene expression (201), metabolic stress (202), embryo development (203), intellectual disabilities (204), DNA damage and tumorigenesis (205).

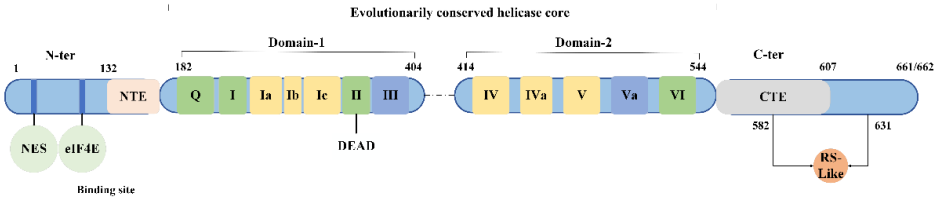

Figure 1.4: Structural organization of DDX3X.

This figure illustrates the structural domains of DDX3X. The helicase motifs represent ATP binding and hydrolysis (green), RNA binding (yellow), and linkage between ATP and RNA binding sites (blue). Adapted from *Mo et al., 2021* (190) and modified with Microsoft Visio.

1.7.1 Sub-cellular localization of DDX3X

The N-terminus of DDX3X contains a leucine-rich nuclear export signal (NES), which is associated with exportine-1/CRM1 mediated nuclear export (206), while an RS (arginine/serine) like region in the C-terminus interacts with the nuclear export receptor TAP (207). DDX3X has a nucleo-cytoplasmic distribution, but some studies reported it predominantly localized to the

cytoplasm (207, 208). The subcellular localization of DDX3X is important as it is correlated with disease progression and tumorigenesis (209, 210). Studies have reported DDX3X localization to other cell organelles in different pathophysiological conditions, including the mitochondria (208), centrosome (211), and nucleolus (209). DDX3X has also been reported inside stress granules (212). Our lab also reported that DDX3X is redirected to the INM where it co-localizes with large nuclear capsid blebs (~4 μm) in approximately 15-20% infected cells late during HSV-1 infection. As VP5 did not concentrate at the INM in the absence of DDX3X and its presence depends on DDX3X and C-capsids, this points to these large blebs being the aggregates of C-capsids coming for egress (142).

1.7.2 DDX3X interaction with RNAs

DDX3X reportedly binds to almost every transcribed mRNA (213) preferably with their G-rich sequences and 5'-UTRs (214). DDX3X lacks inherent RNA sequence-specificity and can recognize complex higher order (secondary) RNA structure (TAR hairpin) in close proximity to the 5′ m7GTP cap moiety (213). DDX3X can also bind with higher-order structures in both ssRNA and dsRNA (215). However, for dsRNA, DDX3X can only interact with either 3' or 5'overhangs (194). *In vitro* studies show that DDX3X can unwind DNA-RNA and RNA-RNA duplexes, which require the presence of ATP. However, it is still unclear to which extent it can unwind DNA-DNA duplexes (182).

1.7.3 DDX3X regulates gene expression

1.7.3.1 Transcription

DDX3X is involved in the transcriptional regulation of gene promoters. For example, DDX3X interaction with YY1 positively regulates the transcription of genes associated with WNT/β-catenin signaling (216), which is important in cancer progression. In addition, DDX3X negatively regulates the E-cadherin promoter (217) and upregulates the promoters of $p21^{waf1/cip}$ (218) and IFN-β genes by binding with transcription factor SP1 (219). DDX3X promotes the recruitment of p300/CBP and IRF3 to the IFN-β promoter (220) and interacts with TBK1 to upregulate the IFN-β promoter (219).

1.7.3.2 mRNA splicing and RNA export

DDX3X contains 7 serine-arginine dipeptides in its C-terminus RS-domain (between amino acids 582-632), structurally resembling other splicing factors (221). Recent studies have identified DDX3X in human spliceosomes, spliceosomal B complexes, and messenger ribonucleoproteins (mRNPs), along with the presence of spliced mRNAs and exon junction complex (EJC) core proteins (196, 222). However, DDX3X involvement in pre-mRNA splicing is still elusive. The presence of NES suggests that DDX3X could already be associated with mRNA before exiting the nucleus (223). Moreover, the recruitment of EJC and TREX complex during splicing promotes its nuclear export (224). In contrast, DDX3X knockdown shows minimal effect on splicing, pointing to another scenario where DDX3X interacts with RNPs only to promote the RNA export after splicing and itself has little or no active role in splicing events (225). To support this hypothesis, studies reported DDX3X interactions with Exportin-1 and NFX-1, proteins involved in mRNA export (218). However, the depletion of DDX3X has no statistically significant impact on the nuclear export of the β-globin reporter gene (226) or poly(A)+ mRNA (227). These findings suggest that DDX3X could be associated with the export of certain specific mRNAs and not with the export of all mRNA types. In addition to FRMP, hnRNPU, DDX1, and Staufen1, DDX3X has also been recognized as a component of kinesin-associated transport granules essential for neuronal transport of β-actin and CaMKIIα mRNA (228, 229). However, the knockdown of DDX3X affects neither the granule assembly nor the RNA export and its actual role needs to be explored further.

1.7.3.3 Translation

mRNA is translated into functional protein by two mechanisms in eukaryotes named i) cap-independent and ii) cap-dependent translation (230). DDX3X regulates protein synthesis by interfering with both mechanisms of translation. On the one hand, DDX3X suppresses cap-dependent translation by interacting with the eIF4E complex, thus inhibiting the eIF4E-eIF4G interaction and overall protein synthesis in liver cancer (231). In contrast, DDX3X binds with the eIF4F complex and positively regulates cap-dependent translation of mRNA transcripts with structured 5'-UTR (232). Another study reported that DDX3X interacts with eIF3 and cap-binding protein complex (CBC) to upregulate the translation of uORF-containing mRNAs, which plays a significant role in the metastatic invasion of tumors (233). DDX3X may also interact with eIF3 and 40S ribosomes in HeLa cells to facilitate the 80S-ribosomal assembly and protein synthesis,

but the exact mechanism is still ambiguous (193, 234). On the other hand, a study reported that a DDX3X interaction with eIF3 (subunits j and e) and PRL-13 facilitates the IRES-mediated cap-independent translation (235). DDX3X interaction with (GGGGCC) nRNAs effectively prevents repeat-associated non-AUG (RAN) translation (236) and its knockdown (KD) was associated with aberrant perturbations in elongation and ribosomal recycling (185).

1.7.4 Cell cycle and Tumorigenesis

DDX3X is implicated in the regulation of cell cycle, apoptosis, and tumorigenesis. Contradictory studies reported DDX3X as both a tumor suppressor and an oncogene (237). Cyclin-dependent kinases (CDKs), cyclin-dependent kinase inhibitors (CKIs), and cyclins are major regulators of the cell cycle (238). DDX3X positively regulates the cell cycle by regulating the mRNA translation of both cyclin D1 and E1 (239). In contrast, some studies reported that DDX3X suppresses cell growth by interacting with the p53-DDX3X-p21 axis. P21, a typical CKI, interacts with cyclin/CDK complexes to stop cell growth. DDX3X stimulates the binding of SP1 to the p21 promoter and increases its interaction with p53 in lung cancer (240). The depletion of DDX3X causes rapid G1-S phase transition or complete G1-phase arrest in lung, prostate, colorectal, and breast cancers (241, 242), which could result from the reduced cyclin E1 due to its upregulation by DDX3X (239). Moreover, DDX3X also inhibits the Kruppel-like factor-4 (KLF4) expression, which is then followed by upregulation of CDK2 and CCNA2 expression (243). Furthermore, DDX3X also regulates the cell cycle and survival in the early stages of mouse embryogenesis. In addition, DDX3X is also involved in cell adhesion, motility, and metastatic invasion of cancerous cells via its interaction with Rac1- signaling pathway (244).

1.7.5 DDX3X in viral infections

As obligate intracellular pathogens lack essential genes for their own replication, several viruses hijack DDX3X for their successful infection. The role of DDX3X in viral infections can be divided into three categories: i) replication; ii) regulation of viral gene expression; and iii) antiviral innate immunity. Until today, DDX3X has been implicated in the regulation of 18 virus species belonging to 12 different genera (Table 1.1). DDX3X interacts with 7 subcellular compartments associated with viral entry, gene expression, nuclear egress, energy needs, and assembly of the lipid envelope (Figure 1.5) (245, 246).

Table 1.1. List of viruses interacting with DDX3X

Species	Genus	Genome	Reference
Herpes simplex virus-1 (HSV-1)	Simplexvirus	dsDNA	(201)
Human cytomegalovirus (HCMV)	Cytomegalovirus	dsDNA	(247)
Hepatitis-B virus (HBV)	Orthohepadnavirus	dsDNA	(248)
Vaccinia virus (VACV)	Orthopoxvirus	dsDNA	(249)
SARS-CoV-2	Betacoronavirus	ssRNA	(250)
Respiratory syncytial virus (RSV)	Orthopneumovirus	ssRNA	(251)
Hepatitis-C virus (HCV)	Hepacivirus	ssRNA	(252)
Human immunodeficiency virus (HIV)	Lentivirus	ssRNA	(253)
Human para-influenza virus-3 (HPIV-3)	Respirovirus	ssRNA	(251)
Lymphocytic choriomeningitis virus (LCMV)	Mammarenavirus	ssRNA	(254)
Lassa mammarenavirus (LASV)	Mammarenavirus	ssRNA	(254)
Junín virus (JUNV)	Mammarenavirus	ssRNA	(254)
Norwalk-like viruses (NLV)	Norovirus	ssRNA	(255)
Coxsackie B	Enterovirus	ssRNA	(256)
EV-71	Enterovirus	ssRNA	(257)
Japanese Encephalitis virus (JEV)	Ortholavivirus	ssRNA	(258)
West Nile virus (WNV)	Orthoflavivirus	ssRNA	(259)
Zika virus (ZIKV)	Orthoflavivirus	ssRNA	(260)
Dengue virus (DENV)	Orthoflavivirus	ssRNA	(261)
Influenza-A virus (IAV)	α-influenza virus	ssRNA	(262)
Red-spotted grouper nervous necrosis virus (RGNNV)	Betanodavirus	ssRNA	(263)
Snakehead vesiculovirus (SHVV)	Perhabdovirus	ssRNA	(264)

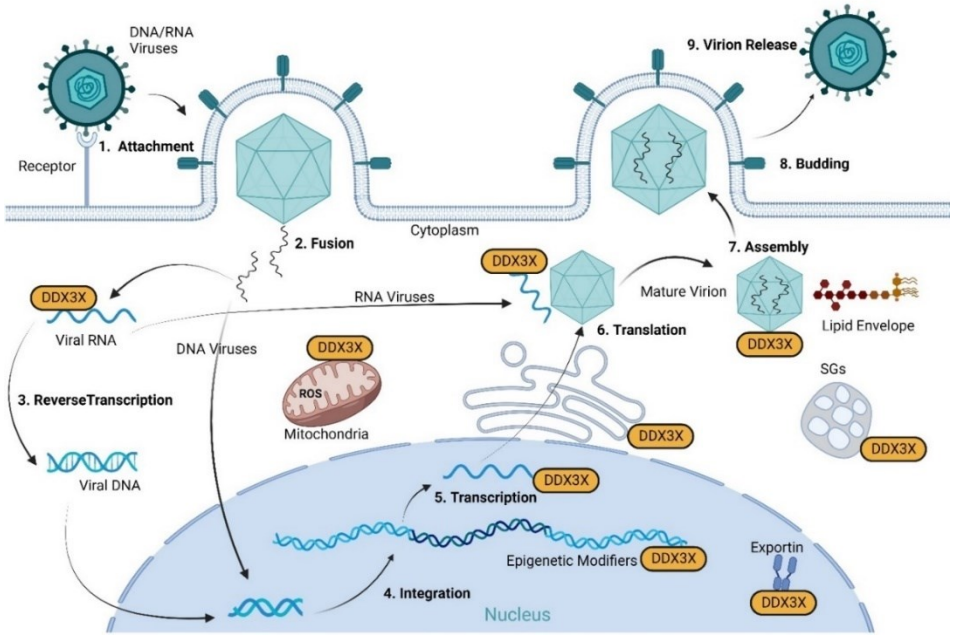

Figure 1.5: Schematic Illustration of putative multiple subcellular compartments where DDX3X can interact with viruses.

Adapted with permission from *Winnard Jr et al., 2021* (245) and modified with BioRender.com.

Experimental and computational studies predicted DDX3X interaction with fragment1 in 5'-UTR of **SARS-CoV-2** (265) is considered proviral in its replication (266). Similarly, one proteomic study identified DDX3X as a SARS-CoV-2 interacting partner along with 104 other host proteins in Huh7 and Calu3 cells. SGs surface protein G3BP1 interacts with the SARS-CoV-2 nucleocapsid (Np) protein, co-localizes with RNA foci, and its inhibition by DDX3X significantly lowered the viral titers (250, 267).

Exportin-1 mediated nuclear export of un-spliced vRNPs (Rev-bound RRE-RNA) transcripts is the final step in the replication cycle of **human immunodeficiency virus-1** (**HIV-1),** which requires NES and RanGTP independent DDX3X interaction with CRM1 (268). DDX3X depletion in HeLa cells restricts the translation of HIV-1 gRNA without significantly impacting the global translation. Ectopic expression of siRNA DDX3 or mutation (S382L) in the motif-III linked with ATP hydrolysis of DDX3X fully restores HIV-1 translation, which suggests its indispensable role in HIV-1 life cycle in addition to the nuclear export but in an ATP independent fashion (232).

DDX3X interacts with the N-terminus (amino acids 16-36) of the **hepatitis C virus (HCV)** core protein in both the cytoplasm and nucleus and its depletion inhibits viral replication. After HCV infection, DDX3X is redirected from the nucleus to the cytoplasm, accumulating in discrete foci near ER and co-localizing with the viral core protein. Upon binding the HCV 3'-UTR, DDX3X is redirected to cytoplasmic SGs, which are involved in liquid-liquid phase condensation required for the virus replication (252, 269, 270).

Japanese encephalitis virus (JEV) NS5 (methyltransferase/RNA polymerase) and NS2B-NS3 (serine protease) are essential for genome replication of the virus (258). DDX3X co-localizes with the viral RNA, interacts with NS3, NS5-RdRp, and NS5-MTase on both 3'- and 5'-UTRs, and its depletion causes a significant reduction in viral replication and protein expression (271). **Dengue virus (DENV)** infection of A549 cells upregulated DDX3X transcription and similarly, viral replication was upregulated in siRNA-DDX3X treated HEK293T cells (261).

Proteomic analysis revealed that mature **human cytomegalovirus (HCMV)** virions incorporate DDX3X in a pp65/pUL83-dependent manner and that HCMV infection upregulates DDX3X (247). Proteomics studies from our lab reported mature **HSV-1** virions incorporate DDX3X, which promotes HSV-1 viral infectivity, propagation, replication, and regulation of gene expression (201). Our recent lab findings indicated a novel role of DDX3X in HSV-1 nuclear egress. Hence, the DDX3X C-terminus physically interacts with pUL31 and stimulates mature virions to incorporate pUS3 and reshape nuclear architecture during capsid egress (142).

Though host-pathogen interactions remain enigmatic, the above data overall indicated the importance of DDX3X in the life cycles of both DNA and RNA viruses, positioning it as a potential pan-antiviral host protein for the development of broad-spectrum antivirals.

1.8 PCBP1

Some heteromeric protein complexes bind to newly synthesized and transcriptionally active RNAs (272). These heteromeric RNA binding proteins (RBPs) are largely composed of heterogeneous nuclear ribonucleoproteins (hnRNPs) (273). RBPs are classified by the structural and functional homology of their RNA-binding domains (RBDs) (274) and have diverse biological functions such as cell signals transduction (275), telomere synthesis (276), transcription (277), splicing (278), mRNA stability (279), translation (280), and post-translational modifications (281).

The K-homology (KH) domain of the RNA binding family consists of Poly(C)-binding proteins i.e., PCBP1-4 or alternatively called hnRNP E1– 4/ hnRNP-K/J or αCP1– 4. They contain evolutionarily conserved ~70 amino acid-long triplicate copies of the KH-RNA binding domain (Figure 1.5) (282, 283). Based on sequence similarity, KH-domains were first discovered in hnRNP K as 45- amino acids long triple repeats and later recognized in PCBP 1-4 and other proteins, including FMR1, a multifunctional RBP important for neuronal development (284-286). NMR spectroscopy reveals that the KH-domain structure consists of βααββα fold and strands of β-pleated sheet strongly packed against 3 α-helices hydrophobic residues (287). In addition to this βααββα fold, KH-domains can also be categorized into 2 groups: Type-I contains C-terminal βα extension while Type-II contains αβ extension on the N-terminus (288, 289). Poly(rC)-binding protein-1 (PCBP1) or hnRNP E1, is a 356 amino acid long intron-less protein (290), that shares an ~88% homology with PCBP2 (291). PCBP1 is involved in RNA metabolism, a classic hnRNP characteristic, but also exhibits some novel functions, such as interaction with the immune system, metastasis, iron transport, and modulation of viral infections (292), which are discussed in detail in the following sections.

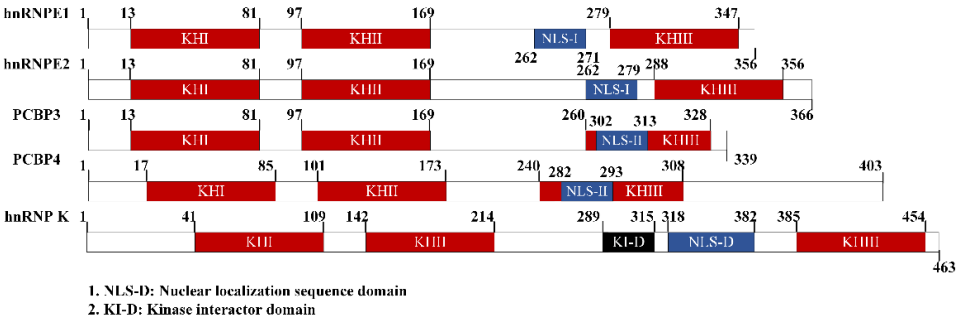

Figure 1.6: PCBPs multidomain structure with colored KH domains.
Adapted with permission from *Makeyev and Lieberhaber, 2002* (293) and modified with Microsoft Visio.

1.8.1 Cellular localization of PCBP1

Structural analysis of PCBP1 revealed the presence of two functionally independent nuclear localization signals named NLS-I and NLS-II with diverse biological functions both in the nucleus (transcriptional gene regulation and RNA splicing) and cytoplasm (translation) (290). NLS-I, an evolutionarily conserved 9-amino acids motif, is located in the variable region linking

the KH2 and KH3 domains, while a variable 12-amino acid long NLS-II is present in the KH3 domain (294, 295). Deletion of NLS-I is sufficient to block the nuclear localization of PCBP1 while for PCBP2, both NLS-1 and NLS-II need to be mutated (296). PCBP1, PCBP2, and hnRNP K are primarily localized to the nucleus, with PCBP1 being specifically enriched in the nuclear speckles and PCBP-3 and PCBP-4 are predominately cytoplasmic (297, 298). Nuclear speckles are interchromatin organelles with higher concentrations of snRNPs and other protein splicing factors, suggesting their close association in modulating gene expression (299). Phosphorylation of PCBP1 by mitogen-induced p21-activated kinase 1 (Pak1) on Thr 60 and 127 increases its nuclear retention (296, 300). Although PCBP1 is ubiquitously expressed, its localization pattern is different depending on cell type. PCBP1 was abundantly nucleocytoplasmic in Chief cells (stomach epithelial cells) while it was limited to the nucleus in Parietal cells (301). Transient change in the subcellular location of any protein could significantly alter its interactions with other proteins (302).

1.8.2 PCBP1 in the regulation of gene expression

PCBP1 can control gene expression at multiple cellular levels as a transcriptional activator, translational repressor, and RNA splicing regulator (303). In addition to RNA binding, studies reported that PCBP1 can bind to pyrimidine/polypurine (PPR) rich regions in 3'-UTR of ssDNA and dsDNA (296). This property is very important in the transcriptional gene regulation of several proteins. For instance, PCBP1 binds to AU-rich sequences in the promoter region of eukaryotic initiation factor 4E (eIF4E) (304), μ-opioid receptor (MOR) (305), BRCA1, interleukin-like EMT inducer (ILEI) (306), β-globin (307), tyrosine hydroxylase (308), collagen type I and III (309), renin (310), erythropoietin (311), neurofilament-M and actively regulates their transcription (312). PCBP1 was the only protein among many interacting partners of PPR, whose concentration was decreased in the presence of a non-functional BRCA gene in breast cancer cells (312). μ-opioid receptor (*Mor*) has a critical role in the use of analgesics to alleviate pain in terminal cancer and develop dependence and tolerance (313), and is mostly expressed in the CNS. PCBP1 binds to a 26-nucleotide ssDNA CR-element in the promoter region of *Mor* and tightly regulates its expression by acting as both a negative and positive modulator of transcription (314, 315). Different PTMs including phosphorylation confer structural and functional changes in PCBP1, important for transcriptional regulation of gene expression and change in its localization. Mitogenic stimulated PAK1 phosphorylation of PCBP1 on Thr 60 and 127 restricts its binding and

increases translational inhibition of the DICE minigene (316). It also positively mediates PCBP1 interaction with U2 snRNP and CAPER-α to promote alternative splicing (316, 317)

Regulating the stability and degradation of mRNA is critical to regulate gene expression (318). It involves complex interactions between hnRNPs and *cis*-acting sequences mostly present in AU-rich elements (AREs) of 3'-UTRs and are responsible for mRNA instability (319). hnRNPs were recognized to influence structural and functional interactions of the human α-globin mRNA stability complex, interacting with CR-elements in 3'-UTR of this complex (320). The following proteins are involved in this complex: PCBP1, PABP, PCBP2, and hnRNP D, out of which PCBP1 is an essential part of this complex (321). Interaction with this complex increases the half-life of mRNAs by protecting them from de-adenylation (322). Since then, other studies suggested that PCBP1 interacts with various mRNAs for their stability. For instance, PCBP1 also binds with endothelial nitric oxide synthase (eNOS), $p21^{WAF1}$, and p63 through 3'-UTR CR-element (323-325). The binding of PCBP1 with eNOS mRNA protects it from miRNA-mediated repression (323). PCBP1 also interacts with 5'-UTR and maintains mRNA stability of EV71 (326), *c-myc*, and PRL-3 (327). PCBP1 can negatively affect the stability of p62/SQSTM1 and LC3B (328). The expression of p53-activated $p21^{WAF1}$ is associated with cell cycle G1 arrest and depletion of both PCBP1 and PCBP2 enhanced mRNA stability of $p21^{WAF1}$ (329).

1.8.3 PCBP1 in viral infections

HSV-1 C-capsids preferentially escape the nucleus and finding PCBP1 specifically on these viral capsids suggests a putative role of PCBP1 in the HSV-1 selective nuclear egress (330). Preliminary work from our lab suggests that PCBP1 is needed for optimal HSV-1 replication. Interestingly, PCBP1 also interacts with HSV-1 pUL24, which has been implicated in HSV-1 nuclear egress (331), consistent with PCBP1's involvement in that process (Thornbury, in preparation). Furthermore, one study recently suggested that PCBP1 could be involved in the assembly, secretion, and egress of HCV virions (332). Studies reported proviral effects of PCBP1 for enterovirus 71 (EV71) (333), Kaposi's sarcoma-associated herpesvirus (KSHV) (334), poliovirus (292), and classical swine fever virus (335). In contrast, PCBP1 also shows antiviral effects against HPV-16 (336), Hepatitis-E virus (HEV) (337), HCV (338), HIV-1 (339), influenza virus (340), and vesicular stomatitis virus (VSV) (341).

1.8.3.1 PCBP1: A proviral host protein

PCBP1 acts as a proviral host factor by interacting with viral and other host proteins to manipulate the host immune system, and positively regulate IRES activation. Poliovirus and EV71 are ssRNA viruses of *Picornaviridae*, and cause poliomyelitis and hand-foot-and-mouth disease (HFMD) respectively (342). Both viruses contain nucleotide motifs in their 5'-UTR, essential for their viral RNA replication and IRES-mediated translation. The EV71 5'-UTR contains six stem loops/SLs (domains). This cloverleaf-like stem-loop I (SL-I), found within 1 to 87 nucleotides in 5'-UTR, is critical for virus replication and virulence (343). PCBP1 KH1 domain binds to SL-I and SL-IV of EV71 and poliovirus (292, 326). PCBP2 binds even more strongly to SL-IV and IRES than PCBP1 and complements its depletion in poliovirus-infected cells (344). PCBP1 binds to KSHV ORF57, an HSV-1 ICP-27 homolog, a protein detrimental to mRNA biogenesis (345). This interaction causes IRES-mediated translation of host protein XIAP (X-linked inhibitor of apoptosis) but does not impact IRES-mediated translation of KSHV vFLIP. Here PCBP1 possibly acts as an anti-apoptotic factor on KSHV infection's reactivation. However, the exact mechanism of favoring IRES-mediated KSHV translation is still under investigation (346).

1.8.3.2 PCBP1: An antiviral host protein

PCBP1 interacts with the VSV phosphoprotein (P), and its overexpression inhibits viral mRNA synthesis at the primary transcription levels without significant impact on overall genome replication (347). ORF2, a sub-genomic RNA, encodes the major HEV capsid and is involved in virus attachment with host receptors, uptake, trafficking, replication, and pathogenesis (348). PCBP1 interacts with the ORF2 genomic promoter, and its depletion causes a significant increase in HEV viral replication (349). Similarly, PCBP1 inhibits the translation of human papillomavirus-16 (HPV-16) late genes (350). HPV-16 capsid proteins L1 and L2 mRNA expression is blocked in normal cells as they are only expressed in terminally differentiated cells. HnRNP K, PCBP1, and PCBP2 bind to 3'-UTR of L2 mRNA resulting in a 4-fold reduction in HPV CAT gene expression. PCBP1 also inhibits the translation of L2 mRNA which gives insight into the antiviral role of PCBP1 (351, 352). Similarly, PCBP1 inhibits the activation of IFN-β, ISRE, and NF-κB-Luc in SeV-infected HEK293 cells (353).

Chapter 2: Study Objectives

This study aimed to evaluate the possible role of DDX3X in the preferential egress of HSV-1 C-capsids. We studied 1) the impact of phosphorylation on the DDX3X nuclear localization and the formation of large capsid (VP5) blebs; 2) the impact of pUs3 phosphorylation on pUL31 interaction with DDX3X; 3) whether DDX3X interact directly with pUL31 and/or pUL34; 4) probe the PCBP1 interaction with DDX3X; 5) examine if PCBP1 interacts with pUL31 and pUL34 separately.

Chapter 3: Methods

3.1 Cells and Viruses

HeLa cells were grown (in 10 cm Petri and 6-well plates) in DMEM supplemented with 5% BGS, 2 mM L- glutamine, and 1% P/S at 37°C in a 5% CO_2 incubator for 24 hours. Vero cells expressing the HSV-1 pUL31 (CV31 cells) were provided by Dr. Richard Roller. Vero and CV31 cells were grown in DMEM containing 10% heat-inactivated FBS, 2mM L-glutamine (and for the CV31 cells, 200 µg/mL Hygromycin B; Gibco™). HEK293T cells were grown (on coverslips in 6-well plates) in DMEM containing 10% FBS, 2 mM L-glutamine, and 1% P/S (penicillin/streptomycin). 143B cells were grown in DMEM containing 10% FBS, 1% 5-bromo-2'-deoxyuridine (BuDR), and 1% P/S. A solution of poly-L-lysine was mixed (1:10) in ultra-pure water (Sigma-Aldrich), 5 mL was added to 10 cm Petri's for 5 minutes at room temperature, and plates were washed three times with sterile 1x PBS. HEK293 Flp-In GS-DDX3X (142) cells were seeded in these plates provided with DMEM containing 10% FBS, 2 mM L-glutamine, and 200 µg/mL Hygromycin B. Throughout this study, we used two viral strains, i.e., 1) HSV-1 WT (F), provided by Dr. Beate Sodeik (Institute der MHH, Germany), and 2) strain F HSV-1 US3K220A/vRR1204 viral mutant encoding a kinase-dead pUS3 protein, graciously provided by Dr. Richard Roller (Department of Microbiology and Immunology, Carver College of Medicine, University of Iowa). These viruses were propagated on Vero cell monolayers to generate stocks.

A day before infection, cells were seeded in a volume so that they attained 70%-80% confluency in approximately 24 hours. The next day, cells were trypsinized and counted using a hemocytometer to determine the volume of virus needed to achieve the multiplicity of infection (MOI) of 5. The virus stocks were diluted to the required concentrations in 0.1% Roswell Park Memorial Institute (RPMI) media. Cells were either mock infected or infected with HSV-1 (F) WT, and US3K220A at an MOI of 5. After adsorption, 10 mL DMEM was added to each plate and placed in the incubator for 11 to 48 hours as indicated in the figure legends.

3.2 PCR and Sequencing

To confirm the mutation in the vRR1204/US3K220A virus, PCR and sequencing were performed. The cells were lysed with 1x PBS, centrifuged @ 300 x *g*, and DNA was extracted following the manufacturer's protocol. DNA concentration was determined with a Nanodrop-1000

spectrophotometer (Thermo Scientific). Primers (F: 5'-CAAACCTTCCCACACCACAC-3'; R: 5'-ACGGTGGTGGTATACGGATC-3'), flanking 931 bp region of HSV-1 (F) US3, were designed using Primer3. One microgram of DNA was used as a template in PCR. After gel electrophoresis, the gel was purified following the instructions provided by the manufacturer (Monarch DNA Gel Extraction Kit/ T1020), and the purified PCR product was then sent for sequencing. Sequencing files were then aligned and visualized with SnapGene.

3.3 Transfections

pRR1238 (HSV-1 WT pUL34 plasmid) and pRR1334 (HA-tagged HSV-1 pUL31 plasmid) were kind gifts from Dr. Richard Roller. The plasmids were either individually (1.5 µg) or together (0.75 µg each) diluted into 50 µL of serum-free DMEM containing high glucose (4.5 g/L). LipoD293™ (SignaGen® Laboratories) @ 4.5 µL was gently mixed with 50 µL serum-free DMEM with high glucose. Both reagents were pooled at a 3:1 transfection reagent: DNA ratio, vortexed or gently pipetted up and down for 15 seconds and incubated at room temperature for 15 minutes without any disturbance for the formation of DNA-transfection complex. This complex was added to each well drop by drop, gently mixed by swirling, and incubated at 37°C. For the mock condition, only transfection media (4.5 µL) diluted in 50 µL high glucose DMEM was gradually used. Given their high rate of transfection, either 143B or HEK293 cells were used for transfections. For Western blotting, the cells were harvested 48 hours post-transfection. As a positive control for pUL31 or pUL34, cells were infected with HSV-1 (F) WT at MOI 5 and harvested 12 hpi. Thirty-five micrograms of each cell lysate were loaded on 5-20% gradient gel to confirm pUL34 plasmid expression compared to WT infection. For confocal microscopy, the cells were fixed after 24 hours post-transfection with 4% PFA and immunostained with anti-pUL34, anti-HA, and R648/rabbit anti-DDX3X antibodies and prepared for confocal microscopy. Alternatively, the samples were stained for anti-pUL31 or pUL34 and anti-PCBP1 antibodies**.**

3.4 Western Blotting

Total cell lysate from infected cells was harvested with manual scrappers in 1x PBS. The cell lysates were centrifuged at 800 x *g* in a refrigerated centrifuge for 5 minutes and then re-suspended in RIPA lysis buffer (50 mM Tris-HCL ph7.4, 150 mM NaCl, 1 mM EDTA, and 1% SDS) with the addition of a protease inhibitor cocktail containing chymostatin (5 µg/mL), leupeptin (0.5 µg/mL), aprotinin (2.5 µg/mL), and pepstatin (0.5 µg/mL) in dimethyl-sulfoxide

(DMSO). Samples were gently rotated for 1 hour at 4°C, sheared 3 times through $27^{1/2}$-gauge needles, sonicated 10 "On/Off cycles" with intensity 8 on a Microcup-horn sonicator (Fisher Scientific Sonic Dismembrator Model 100), and centrifuged for 20 minutes at 12,000 x *g* (4°C). The supernatants were put into fresh Eppendorf vials. Protein concentrations were measured with a Pierce™ BCA Protein Assay Kit (Thermo Scientific/Cat no. 23225) according to the manufacturer's protocol. Thirty-five micrograms of the total cell lysates were loaded on 5-20% gradient polyacrylamide gel in a sample buffer (2% SDS 2%, 50 mM Tris-HCl/pH 7.4, 10% glycerol, 2% β-mercaptoethanol, 0.1% and bromophenol). After their migration, the proteins were transferred to PVDF membranes (Bio-Rad), and then incubated in a blocking buffer (5% skim milk) for 1 hour at room temperature. The primary antibodies were diluted in an antibody dilution buffer containing 5% BSA in 1x PBST mixed with 0.1% Tween-20, while the secondary antibody dilution buffer contained 5% skim milk in 1x PBST (0.1% Tween-20 in 1x PBS, pH 7.4). The following day, the membranes were washed with 1x PBST) three times and incubated with the appropriate secondary antibodies at room temperature for 1 hour. After washing three times with 1x PBST, an enhanced chemiluminescence substrate (Bio-Rad) was added to the membranes, and the proteins were visualized using the Bio-Rad ChemiDoc XRS+ system. The intensity of signals was quantified with the ImageJ software.

3.5 Confocal laser scanning microscopy (CLSM)

HeLa cells were grown on coverslips in 6-well plates in DMEM until they reached 70% confluence. The cells were either mock-treated (-ve CTL) or infected for 11 hours with HSV-1 (F) WT and US3K220A at an MOI of 5 and fixed with 4% paraformaldehyde (PFA) for 15-20 minutes at room temperature. The cells were permeabilized and then blocked in blocking buffer (0.3% Triton X-100 and 5% heat-inactivated bovine serum in 1x PBST) at room temperature for 60 minutes. The coverslips were washed with 50 µL sterilized 1x PBS for 5 minutes and immunostained with 30 µL primary antibody dilution (1:1 mix of rabbit anti-DDX3X/R648 and mouse anti-VP5 antibodies; details are given in Table 3.3) overnight at 4°C. On the next day, 50 µL 1x PBS was used three times to wash coverslips for 5 minutes each at room temperature and incubated with 50 µL fluorochrome-conjugated secondary antibodies dilution (1:1 mix of Alexa Flour 488 and 568; details given in Table 3.4) at room temperature for 1 hour. Both primary and secondary antibodies were diluted in dilution buffer containing 1% BSA in 1x PBST. Again 50

µL of 1x PBS was used three times to wash coverslips for 5 minutes each at room temperature, and Hoechst 33342 (5 µg/mL) was added in 1:200 Dako Fluorescent antifade Mounting Medium to stain the nuclei. The glass slides were washed with 70% ethanol and dried with Kim wipes. Coverslips were dipped 3 times in Milli-Q ultra-pure water and gently placed over 10 µl of mounting medium (Dako, Sigma-Aldrich) overnight at room temperature. Coverslips were examined with a Leica TCS SP8-DLS confocal microscope and images were taken with an HC PL APO 63x/1.40 CS2 oil objective and laser intensities of each channel were appropriately adjusted to avoid image saturation.

The impact of pUS3 viral kinase on the intracellular distribution of DDX3X was analyzed with the LAS X (Leica) software. The Gaussian filter was used to define the nuclei and the click-draw option was used to set cell boundaries. Two-hundred infected cells for each condition (wild-type vs mutant virus) were counted using VP5 as a marker of HSV-1 infection. In parallel, the VP5 distribution was categorized into a) nucleocytoplasmic; b) diffuse nuclear; c) small nuclear foci; and d) medium-sized nuclear foci up to 2 µm or large foci up to 4 µm.

3.6 Co-localization analyses

To determine the co-localization of DDX3X and pUL31, two strategies were used. In the first, Vero or CV31 cells were mock treated for 11 hours. The cells were fixed and processed for immunofluorescence as indicated above. Ten random images from each condition (CV31 and Vero Mock) were selected and exported using LAS X software. The images were processed with Fiji/ImageJ software (JACoP plugin) using Pearson's Correlation Coefficient (PCC) (354). The average correlation "r" between DDX3X and HSV-1 pUL31 was shown on a scale from -1- to +1. Alternatively, Mander's Correlation Coefficient (MCC) was used (355). In that tool, the degree of co-localization ranges from 0 (no lo-localization) to 1 (perfect co-localization). In the second strategy involving pUL31 or pUL34 transfected cells, 30 cells from the mock or transfected conditions were selected with ImageJ software and subjected to co-localization analysis using the JACoP plugin. Co-localization was quantified using PCC and MCC tools (as described above). Also, for PCPB1, 30 cells were quantified per condition.

3.7 Immunoprecipitations

HEK293 Flp-In GS-DDX3X cells (stably expressing GS-DDX3X) were either mock-treated or infected with HSV-1 (F) WT and US3K220A at an MOI of 5. After 12 hpi, the cells were lysed with RIPA lysis buffer. The cell lysates were centrifuged at 800 x *g*, in a refrigerated centrifuge for 5 minutes, and pellets were re-suspended in RIPA lysis buffer containing 1x CLAP (10^7 cells/mL). The cell lysates were incubated on ice for 1 hour and centrifuged for 20 minutes at 14,000 RPM in a microfuge. The supernatants were discontinuously sonicated for 10 seconds. Lysates were first incubated with 6 µL goat pre-immune serum for 1 hour at 4°C with gentle rotation to block non-specific binding. Pierce™ Protein G Agarose beads @ 50 µL (50% slurry), were washed three times with lysis buffer @ 2,000 RPM for 1 minute each, and the supernatants were removed to add 1 mL lysis buffer. The cell lysate was added to the beads and incubated overnight at 4°C with gentle rotation. The following day, beads were centrifuged at 800 x *g* for 2 minutes and the flow-through was kept for future analysis. The beads were harvested by centrifuging @ 2,000 RPM for 1 minute, washed once with lysis buffer having a higher NaCl concentration (500 mM) and twice with lysis buffer containing a lower concentration of NaCl (150 mM). Thereafter, 50 µL (2X sample buffer and β-mercaptoethanol) were added to re-suspend the bead pellets. Proteins were denatured by heating for 5 minutes at 95°C on a hot plate, centrifuged for 2 minutes at 2, 000 RPM, and supernatants were loaded on 5-20% gradient polyacrylamide gel to do the normal western blot (as described above).

3.8 Statistical analyses

The data were subjected to One-way analysis of variance (ANOVA) with Welch Post-hoc test, bilateral Student's two-tailed *t*-test, and Nested *t*-test using GraphPad Prism v9 (USA) and Python 3.8.5. Data was considered statistically significant when $p \leq 0.05$.

Table 3.1. Primary Antibodies Used in WB, IP, and Co-IP

Antibody	Origin	Lab No.	Dilution	Species
R648/DDX3X	Dr. Arvind Patel	AB153D	1:2000	Rabbit
DDX3X	BioLegend (658602)	AB200	1:1000	Mouse

DDX3X	GeneTex (GTX54030)	AB201	1:200 (IP)	Rabbit
US3	Dr. Bruce Banfield	AB213	1:500	Rat
UL34	Dr. Susane Bailer	AB132	1:2000	Rabbit
11E2 (ICP8)	Abcam (ab20194)	AB128	1:2000	Mouse
ICP5	East Coast Bio HA-018	AB42	1:2000	Mouse
GAPDH	Millipore Sigma (MAB374)	AB205	1:5000	Mouse

Table 3.2. HRPO-conjugated secondary antibodies used in WB

Antibody	**Origin**	**Dilution**	**Species**
GARab-HRPO	Bethyl Laborateries	1:5000	Goat
GAM-HRPO	Jackson ImmunoResearch	1:10000	Goat
GARat-HRPO F (ab') 2	Jackson ImmunoResearch	1:1000	Rabbit

Table 3.3. Primary antibodies used in IF microscopy

Antibody	**Origin**	**Lab No.**	**Dilution**	**Species**
R648/DDX3X	Dr. Arvind Patel	AB153D	1:200	Rabbit
DDX3X	GeneTex (GTX54030)	AB201	1:200	Rabbit
UL34	Dr. Richard Roller	AB84	1:1000	Chicken
UL31	Dr. Bruce Banfield	AB211	1:200	Rat
ICP5	East Coast Bio HA-018	AB42	1:100	Mouse
VP22	Dr. Joel Baines	AB169	1:200	Chicken
hnRNP E1 (PCBP1	Santa Cruz (sc-137249)	AB209	1:200	Mouse
PCBP1	Invitrogen (PA5-65369)	AB225	1:200	Rabbit
FLAG-M2	Sigma-Aldrich	AB235	1:500	Mouse
ICP4	Abcam (6514)	AB115	1:100	Mouse

Table 3.4. Fluorophore-conjugated secondary antibodies used in IF microscopy

Antibody	Origin	Dilution	Species
CAR Alexa 488	Molecular Probes	1:1000	Chicken
CAM Alexa 488	Molecular Probes	1:1000	Chicken
DAC Alexa 488	Invitrogen	1:1000	Donkey
GARab Alexa 568	Molecular Probes	1:1000	Goat
GAM Alexa 568	Molecular Probes	1:1000	Goat
GAC Alexa 568	Molecular Probes	1:1000	Goat
GAR Alexa 647	Molecular Probes	1:1000	Goat
DAM Alexa 647	Molecular Probes	1:1000	Donkey

Chapter 4: Results

4.1 Confirmation and Gene expression of the US3 kinase mutant

To confirm the effect of HSV-1 pUS3 phosphorylation on DDX3X re-localization to the INM and its interaction with DDX3X (one of our primary objectives), we resorted to an HSV-1 pUS3 strain F mutant having a lysine to alanine substitution at an amino acid position 220, which abolishes the kinase activity of pUS3 (146). To validate this dead kinase mutation, we designed PCR primers flanking a 931 bp region of HSV-1 US3 using Primer3. Then, we infected HeLa cells with this mutant virus strain, and for positive control, we used the WT (F) strain. After 24 hours, we prepared cell lysates and extracted the DNA. After PCR and purification by gel electrophoresis (Figure 4.1A), we sent the amplicon to "Génome Québec" for sequencing. We then aligned the sequences with that of the complete HSV-1 (F) US3 sequence from NCBI (GU734771). This confirmed the mutation (Figure 4.1B).

We also confirmed the gene expression of this mutant strain by Western blotting. We used HeLa cells since this is the cell line in which we originally discovered that DDX3X is incorporated into mature virions (54) and where most of our characterization took place (142). We infected the cells with both WT and mutant (US3K220A) strains for 24 hours, prepared cell lysates, quantified the protein contents by a BCA assay, and loaded equal amounts of proteins on 5-20% gradient SDS polyacrylamide gel. WB analyses of pUS3 and the control VP5 major viral capsid protein confirmed the expression of the mutant gene (Figure 4.2). This was also true in the classical Vero cell line most labs use to study this virus. We then quantified this gene expression using ImageJ and found that the US3K220A strain showed statistically significant reduced gene expression as compared to the WT strain (Figure 4.3).

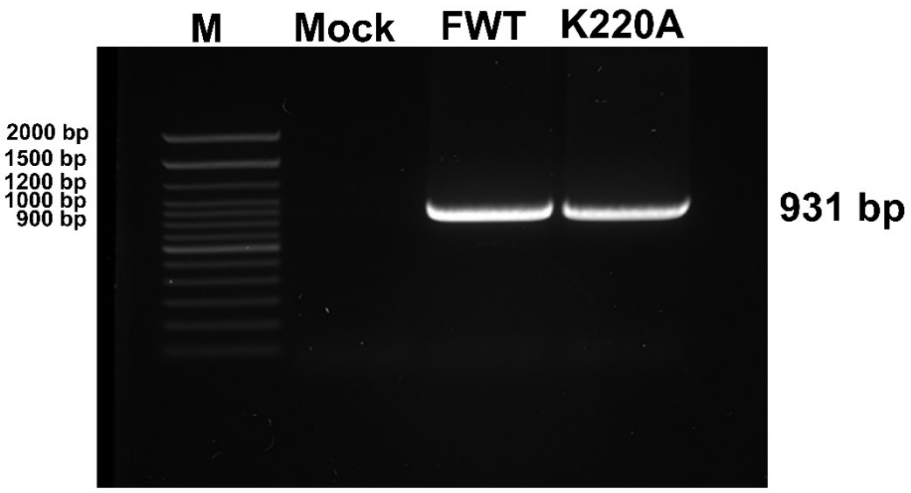

Figure 4.1: Confirmation of dead kinase mutation through PCR

HeLa cells were infected with HSV-1 (F) WT and US3K220A at an MOI of 5. Cells were harvested, and the total DNA was extracted and used as a template for PCR using US3-specific primers. The amplified PCR product was run on 1.5% agarose gel for 40 minutes. The gel-purified PCR product was sent for sequencing, which confirmed the lysine substitution by alanine at AA position 220.

A 12 hpi

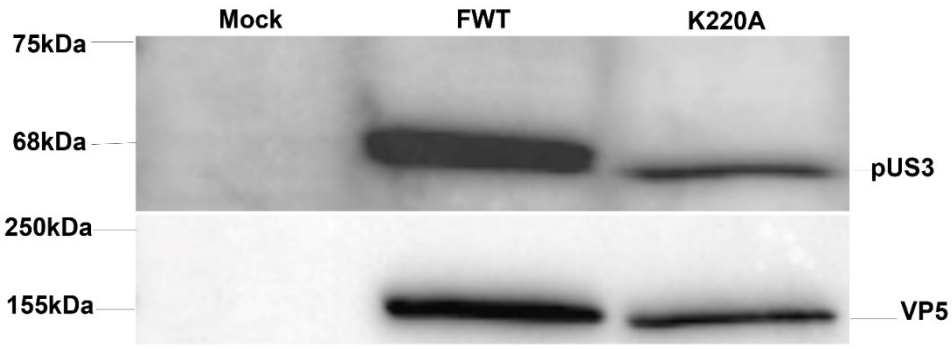

B 24 hpi

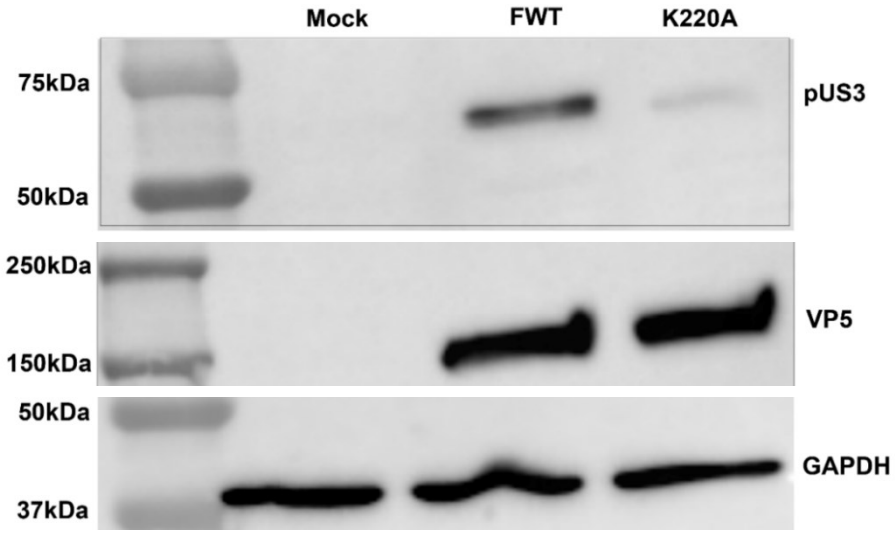

Figure 4.2: US3K220A Gene expression in HeLa cells

HeLa cells infected with HSV-1 (F) WT and US3K220A at a MOI of 5 were harvested A) 12 hpi or B) 24 hpi, in RIPA lysis buffer. Fifty micrograms of proteins were loaded on a 5-20% SDS gradient gel and immunoblotted (i) overnight with monoclonal Rat anti-pUS3 antibody (1:500; expected mw of 68 kDa), (ii) as loading control with mouse anti-VP5 (1:2000; expected mw of 155 kDa), or (iii) mouse anti-GAPDH (1:10000; expected mw of 37 kDa). All blots were visualized with ChemiDoc. The blots are representative of 3 independent experiments.

A 12 hpi

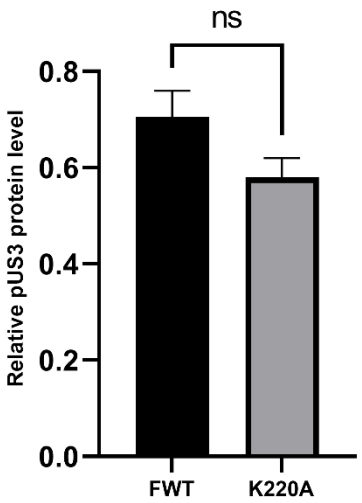

B 24 hpi

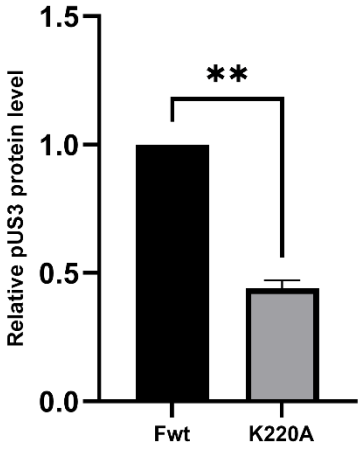

Figure 4.3: Quantification of US3K220A gene expression

To quantify and compare the gene expression of US3K220A with HSV-1 F (WT) A) 24 hours, B) 12 hours post-infection, immunoblots were quantified using ImageJ. The graph bars are representative of the statistical mean and SEM. The independent Student's *t-test* was performed, **p < 0.01; ns: non-significant*. The graphs represent 3 independent experiments. The data are normalized to the VP5 signal.

4.2 Phosphorylation impacts DDX3X localization

pUS3 is a viral kinase whose enzymatic activity plays an important role in nuclear egress through its interaction with NEC and other host proteins. DDX3X has a nucleo-cytoplasmic distribution in uninfected cells. Previously, our lab found that HSV-1 redirects DDX3X to the INM

late during an infection when newly assembled capsids are egressing (142). DDX3X also co-localizes with large nuclear capsid aggregates, thought to be C-capsids, as DDX3X co-localizes with VP5, the major capsid protein (142). Our objective was to determine if the viral kinase activity has any impact on DDX3X nuclear localization. For this, HeLa cells were infected for 11 hours with both the WT and US3K220A viruses and prepared for confocal microscopy. We randomly selected 200 cells per condition and quantified the DDX3X distribution in cells. We first confirmed the re-localization of DDX3X in WT-infected cells (Figure 4.4). However, we did not observe this phenotype in the kinase-dead mutant infected cells as most cells did not exhibit any nuclear rim staining. Upon quantification, we found that the kinase activity of pUS3 significantly (*p=0.001*) impacted the redistribution of DDX3X to the INM (Figure 4.5). In those experiments, we also noted that the size of the VP5 foci, indicative of capsid accumulations, differed between the two conditions, with larger foci in the WT condition. For further analysis, we therefore quantified the VP5 phenotypes into the following groups: i) diffuse nuclear, ii) nucleo-cytoplasmic, iii) small nuclear aggregates, iv) mid-sized nuclear (<2 μm) and large nuclear (2-4 μm). We found the following differences in these forms (Figure 4.6). The diffuse nuclear phenotype was mostly seen (*p=0.04*) with WT-condition as compared to the mutant strain while the Nucleo-cytoplasmic phenotype was similar to the WT-condition (*p=0.08*). Not a single large nuclear bleb/aggregate was seen in the kinase-mutant infected cells, while approximately 10-15% WT-infected cells show large VP5 aggregates (2-4 μm) at the nuclear periphery (*p=0.002*). However, medium-sized nuclear foci (up to 2 μm) were extensively seen in the mutant-infected cells as compared to WT-infected cells (*p=0.021*).

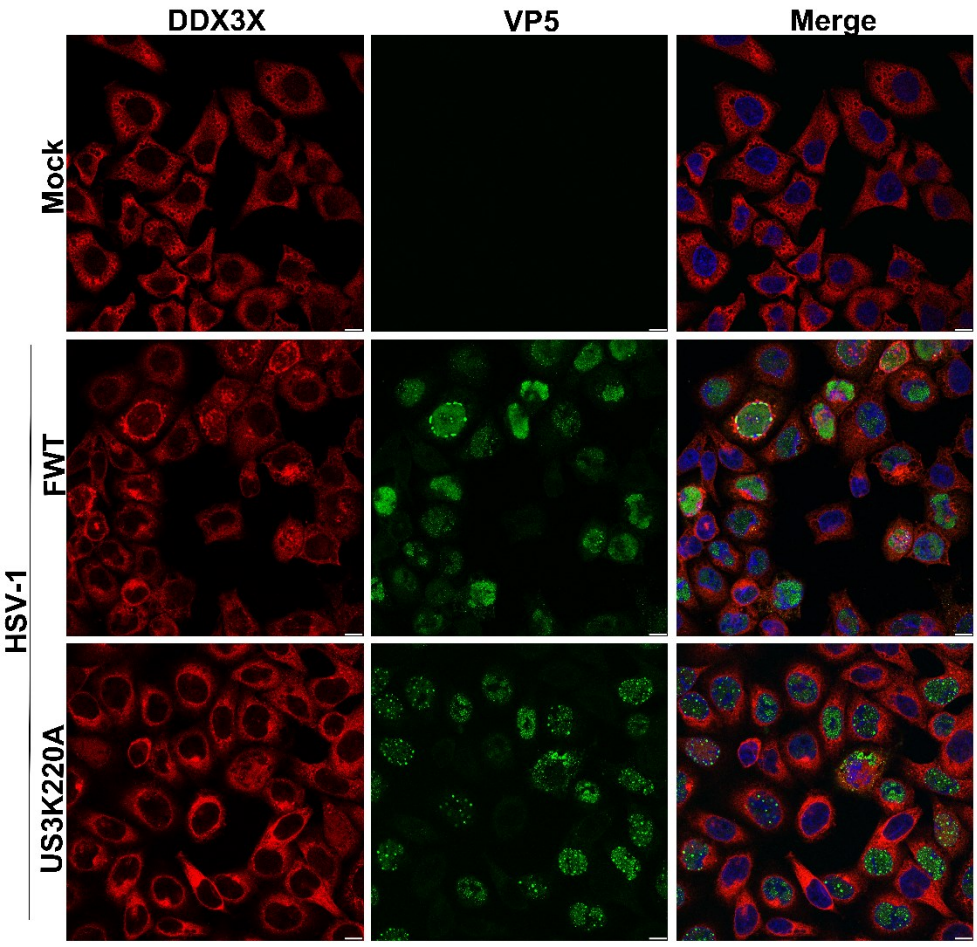

Figure 4.4: Effect of phosphorylation on DDX3X INM re-localization

HeLa cells grown on coverslips were infected with HSV-1 (F) WT and US3K220A at a MOI of 5, harvested 11 hpi, and fixed with 4% PFA. They were then immunostained with R648, an antibody recognizing DDX3X (1:200) or an anti-VP5 (1:100) viral capsid antibodies and visualized on a Leica SP8-DLS CLSM (Blue: Hoechst 33342; Green: VP5; Red: DDX3X). The white scale bar is 10 µm. The experiment was performed 3 times and led to the same results.

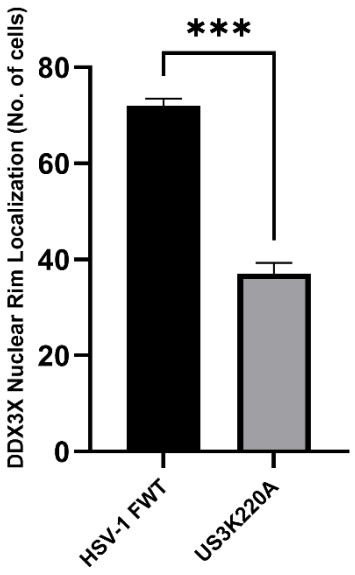

Figure 4.5: DDX3X INM re-localization

For each condition, 200 cells were analyzed on LAS X Software to quantify DDX3X nuclear localization. The graph bars represent statistical means and SEM. Bilateral Student's *t-test* was performed, ****p < 0.001*. The graph is representative of 3 independent experiments.

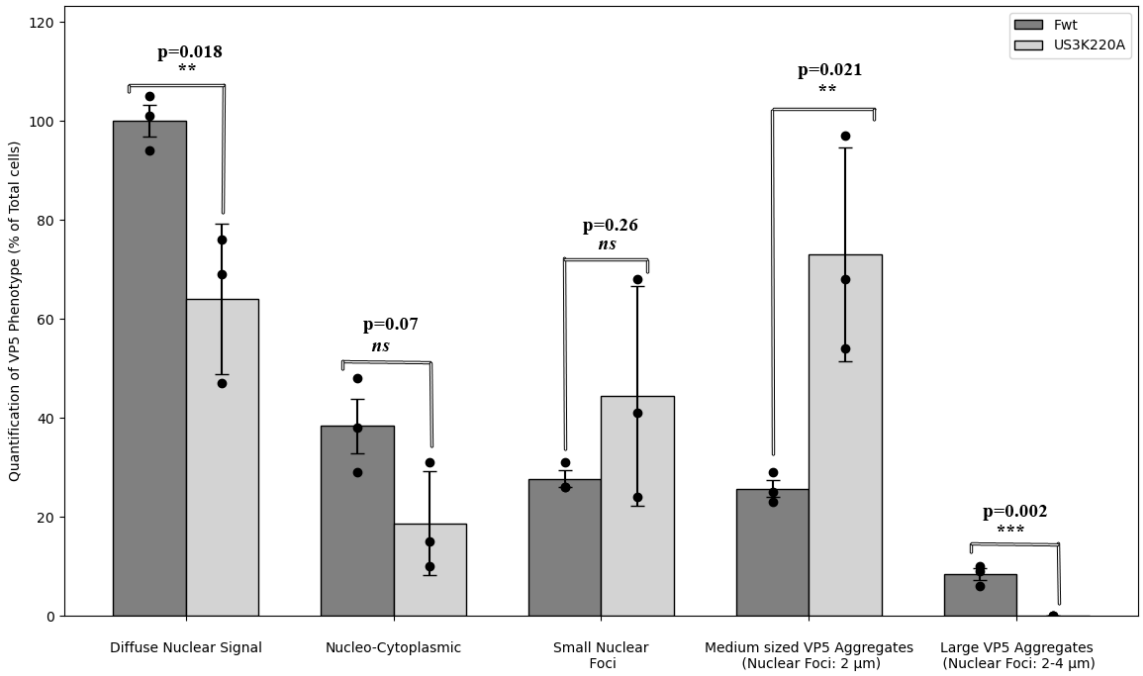

Figure 4.6: Quantification of VP5 Phenotype

Two hundred cells from each condition were randomly selected on LAS X software to quantify VP5 phenotype. The black bars represent the WT condition while the grey bars represent the kinase

mutant condition. The graph bars are representative of statistical means and SEM. The Nested *t-test* was performed on Python 3.8.5 (NumPy, SciPy, and Matplotlib libraries), ***p < 0.02, ns*: non-significant. The graph is a representative average of 3 independent experiments.

4.3 DDX3X interacts with exogenously expressed pUL31

We previously reported that DDX3X interacts with pUL31 (142), but those experiments were done with DDX3X-bound affinity chromatography columns and whole viral cell lysates that also contain other viral proteins. To specifically address whether DDX3X interacts directly with pUL31, we resorted to the CV31 cell line (Vero cells complementary expressing HSV-1 pUL31). To first confirm the normal expression of DDX3X in this complimentary cell line, we infected Vero and CV31 cells with HSV-1 (F) WT for 12 hours and confirmed DDX3X expression through western blotting (Figure 4.7). We found these cells normally express DDX3X as normal Vero cells and could be used for our experiments. Next, to probe the DDX3X interaction with pUL31, we immunostained them for DDX3X and pUL31 and visualized them by confocal microscopy. The data confirmed the presence of pUL31 in the complementary cell line and its absence in Vero cells (Figure 4.8). We then quantified the DDX3X-pUL31 co-localization using the PCC and MCC co-localization tools (Figure 4.9). The PCC value of 0.7 suggested that both proteins were indeed co-localized, albeit only partially. By the MCC method upon using a Costes automated threshold setting, the values were 0.6 (M1) and 0.8 (M2) respectively (Figure 4.9). M1 indicates the proportion of DDX3X that overlaps with pUL31 and M2 the opposite. Both quantification methodologies confirmed a partial co-localization of DDX3X with HSV-1 pUL31, suggesting that DDX3X does interact with pUL31 in the absence of other viral components in agreement with our previous Co-IP assay (142).

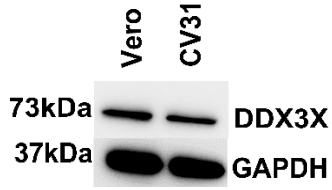

Figure 4.7: DDX3X expression in CV31 cells

Vero and CV31 cells, infected with HSV-1 (F) WT at a MOI of 5, were harvested at 12 hpi in RIPA lysis buffer. Thirty-five micrograms of proteins were loaded on a 5-20% SDS gradient gel and immunoblotted (i) overnight with the monoclonal mouse anti-DDX3X R648 antibody (1:1000; expected mw of 73 kDa) and (ii) mouse anti-GAPDH (1:10000; expected mw of 37 kDa). The blots were visualized with a ChemiDoc. The figure represents a single experiment.

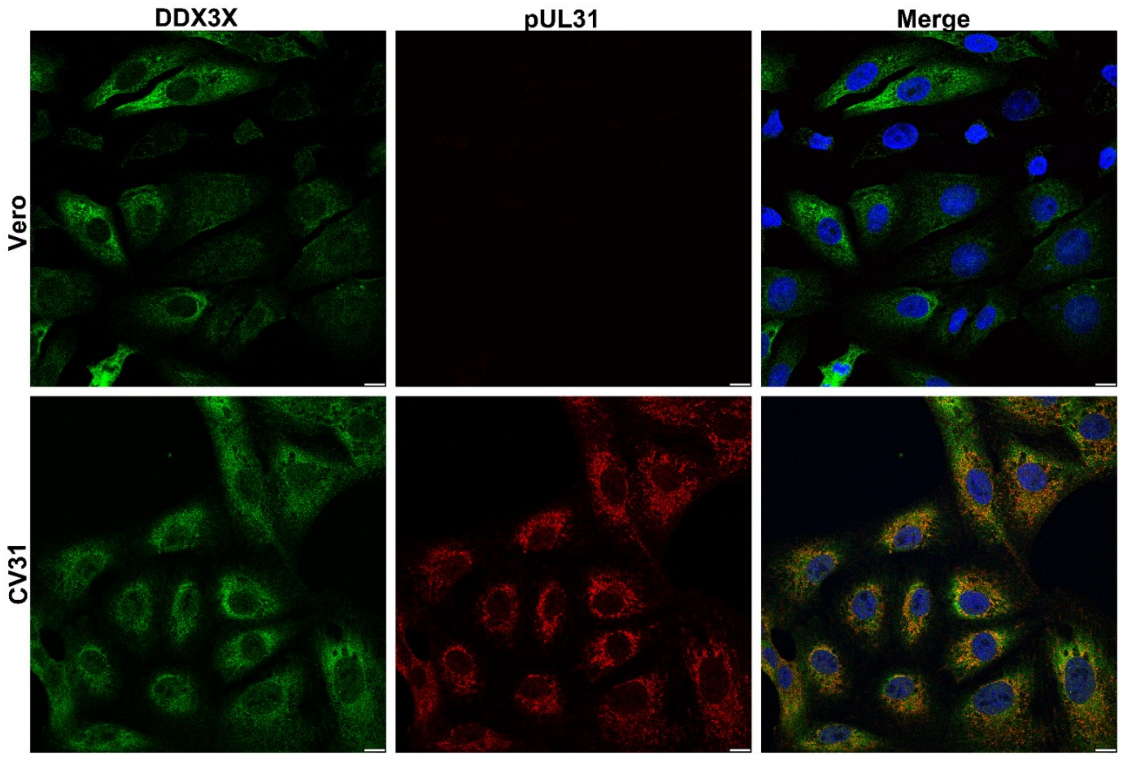

Figure 4.8: DDX3X co-localizes with pUL31

Vero and CV31 cells grown on coverslips were fixed, then immunostained with R648/anti-DDX3X (1:200) and anti-pUL31 (1:200) antibodies and visualized by confocal microscopy (Blue: Hoechst 33342; Green: DDX3X; and Red: pUL31). The grey scale bars represent 10 µm. The figure represents 3 independent experiments.

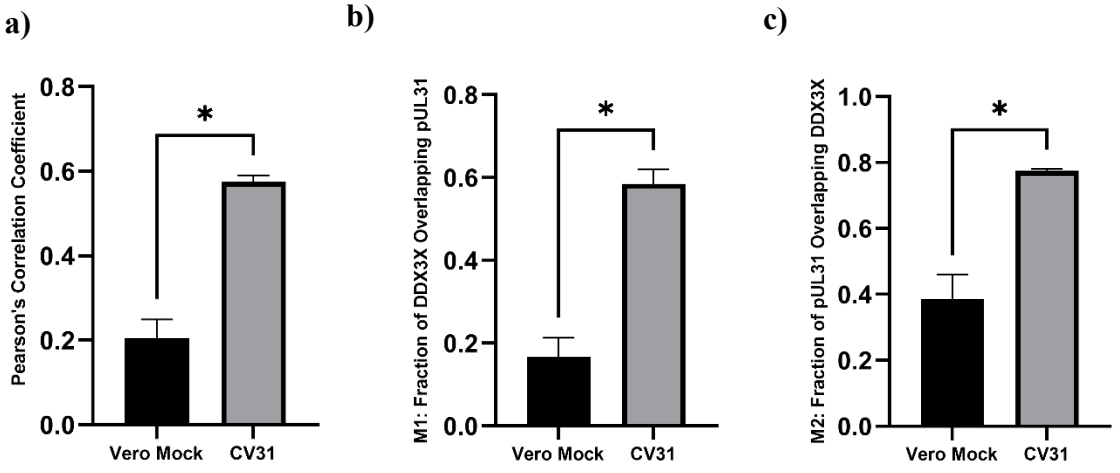

Figure 4.9: DDX3X co-localizes with pUL31

Ten images from each condition were randomly selected, and co-localization was measured using (a) PCC (b, c) MCC (M1 & M2), with the ImageJ JACoP plugin. The graph bars are representative

of statistical means and SEM. The independent Student's *t-test* was performed, *p < 0.05. The graphs are representative average of 3 independent experiments.

4.4 DDX3X also interacts with endogenously expressed pUL34

As our lab previously found DDX3X interaction with the NEC was pUL31 dependent (142), we investigated if pUL34 also interacts with DDX3X. To this end, we first transiently transfected pUL34 plasmid (pRR1238) in 143B cells for 48 hours, prepared cell lysates, and confirmed pUL34 expression through Western blotting. The data revealed an expression similar to that seen during an infection (Figure 4.10). Next, we transfected 143B and HEK293T cells (repeated twice in each cell line) with pUL34 plasmid (pRR1238) for 24 hours. We chose these two cell lines with proven greater transfection efficiencies to confirm our findings. The results (Figure 4.11) and quantification by PCC (0.75) and MCC (M2: 0.9) (Figure 4.12) confirmed a strong co-localization exists between these two proteins in the pUL34-positive cells.

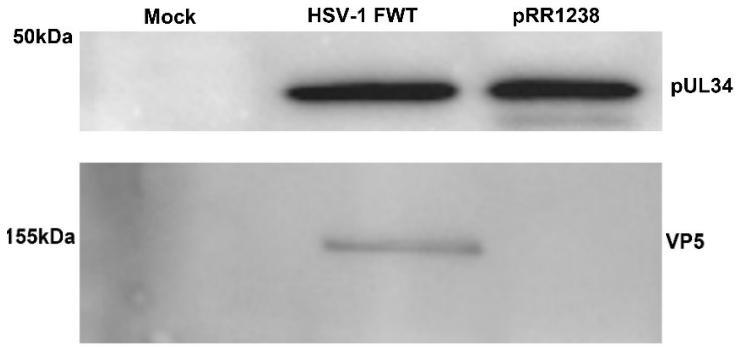

Figure 4.10: pRR1238 expression in 143B cells

pRR1238 (pUL34) plasmid (1.5 µg/well) was transiently transfected in 143B cells. The cells were harvested 48 hours post-transfection. Forty micrograms of total lysates were loaded on a 5-20% SDS gradient gel and immunoblotted (a) with rabbit anti-pUL34 antibody (1:2000) and (b) mouse anti-VP5 as a control for the infection (1:2000). The figure represents a single experiment.

A

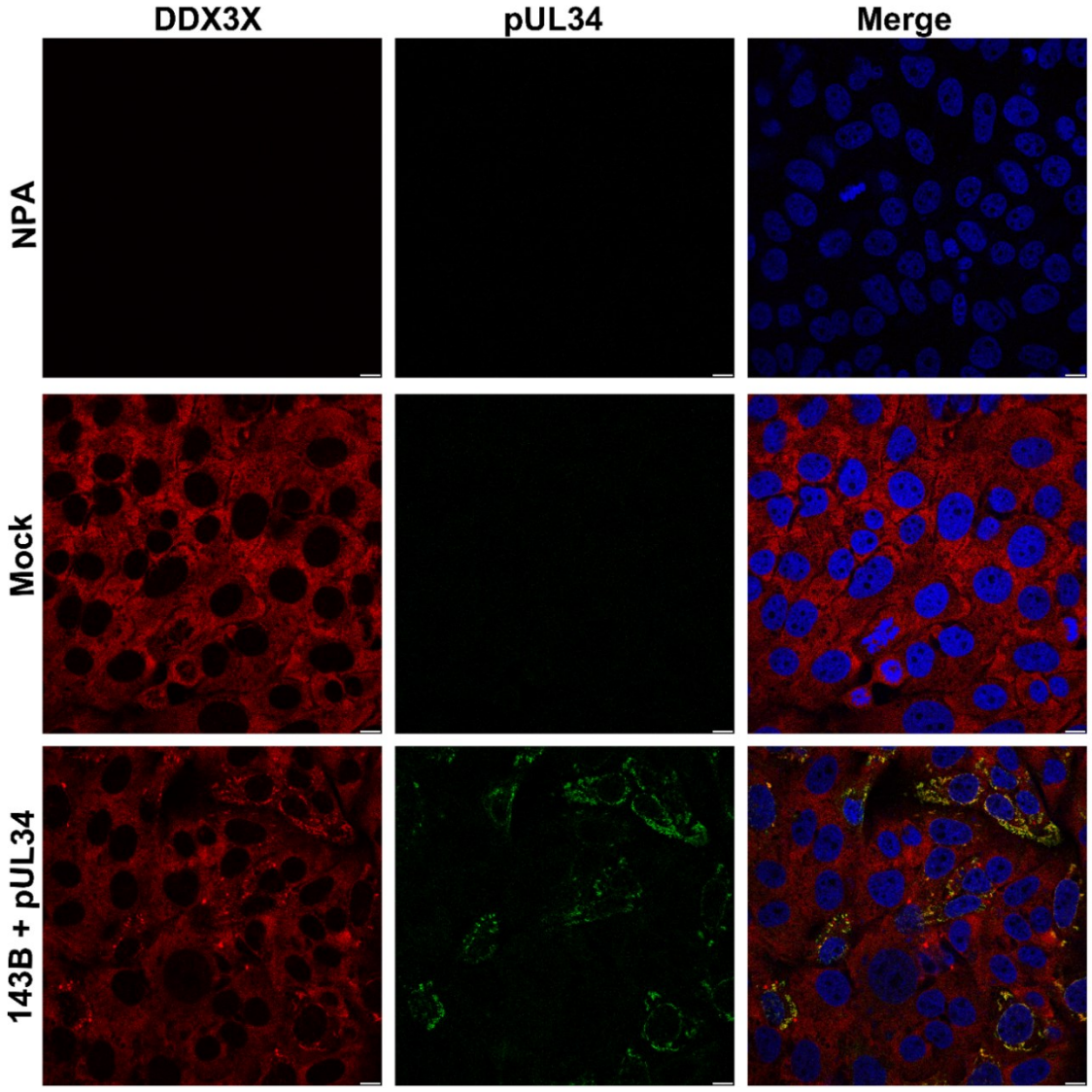

B

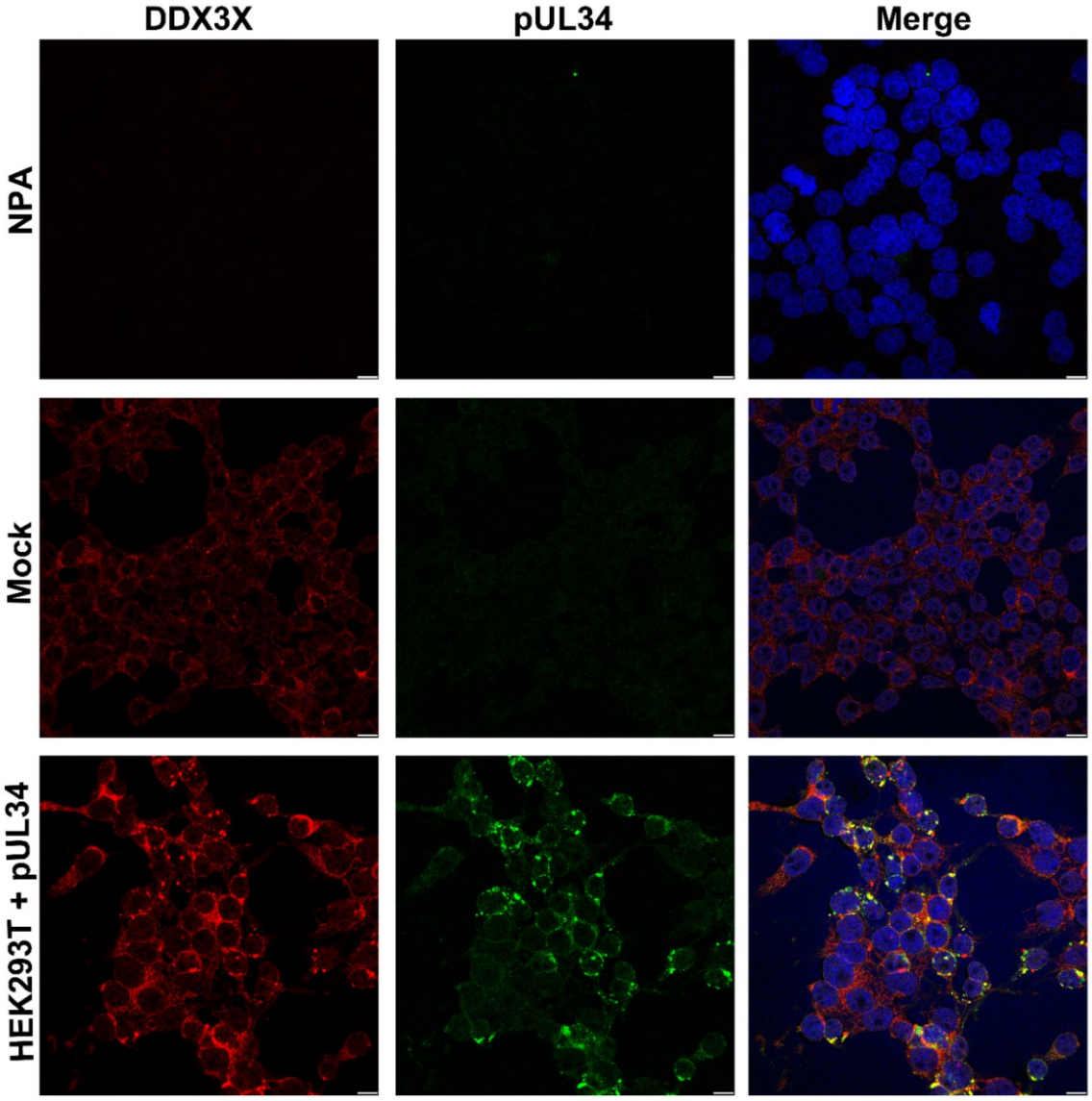

Figure 4.11: DDX3X interaction with HSV-1 pUL34

(a) 143B cells and (b) HEK293T cells were transiently transfected with pRR1238 (pUL34) plasmid for 24 hours. Fixed cells were immunostained with R648/anti-DDX3X (1:200) and anti-pUL34 (1:1000) antibodies and visualized by confocal microscopy (Blue: Hoechst 33342; Green: pUL34; and Red: DDX3X). The grey scale bars represent 10 μm and yellow in the merge channel shows co-localization. The experiment was repeated 4 times (twice in each cell line) with similar results.

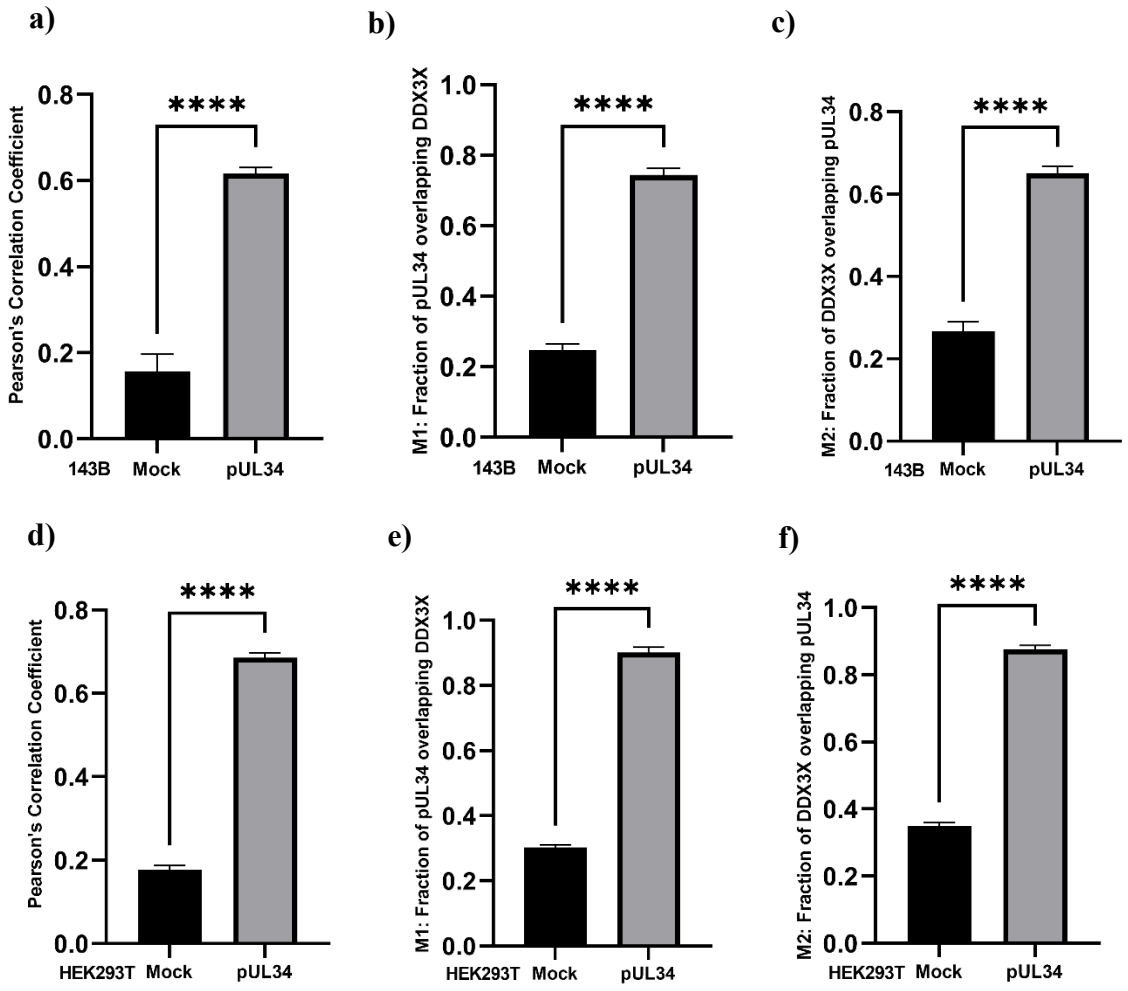

Figure 4.12: Quantification of DDX3X interaction with pUL34

pRR1238 (pUL34 plasmid) was transiently transfected in 143B (panels a-c) and HEK293T cells (panels d-f). Thirty pUL34-positive transfected cells were selected randomly for each condition and co-localization was measured using PCC (panels a and d) or MCC (panels b, c, e, and f) with the ImageJ JACoP plugin. The graph bars are representative of statistical means and SEM. The independent Student's *t-test* were performed on GraphPad Prism (version 9), ****$p < 0.0001$. The graphs are representative of an average of 4 (twice in each cell line) independent experiments.

4.5 DDX3X interaction with NEC

As we found that DDX3X interacts separately with both exogenously expressed pUL34 and pUL31, we investigated whether these interactions are altered in the presence of both NEC components and in the absence of other viral proteins. We therefore co-transfected 143B cells with pRR1238 (pUL34) and pRR1334 (pUL31). The cells were fixed 24 hours post-transfection, immunostained and monitored by confocal microscopy. As expected, DDX3X did interact with the NEC and, interestingly, there was a strong co-localization signal (Figure 4.13). We also

confirmed this interaction in HEK293T cells. Interestingly, the DDX3X co-localization with the NEC was similar to that observed in the presence of a full set of viral proteins as seen during a WT (F) infection of HeLa cells (Figure 4.14). We measured DDX3X interaction with both components of NEC when they were transfected alone or co-transfected together (intact NEC) (Figure 4.15). NEC formation has an additive effect on its interaction with DDX3X. DDX3X interaction with pUL31 was improved, however, this was non-significant (*p=non-significant*). Interestingly, DDX3X interaction with pUL34 was significantly (*p=0.04*) improved in the presence of an intact NEC (Figures 4.14 and 4.15). However, when compared with WT-infected cells in the presence of different viral proteins, the interaction was non-significantly higher in infected cells as compared to both transfected cell lines (Figures 4.16 and 4.17).

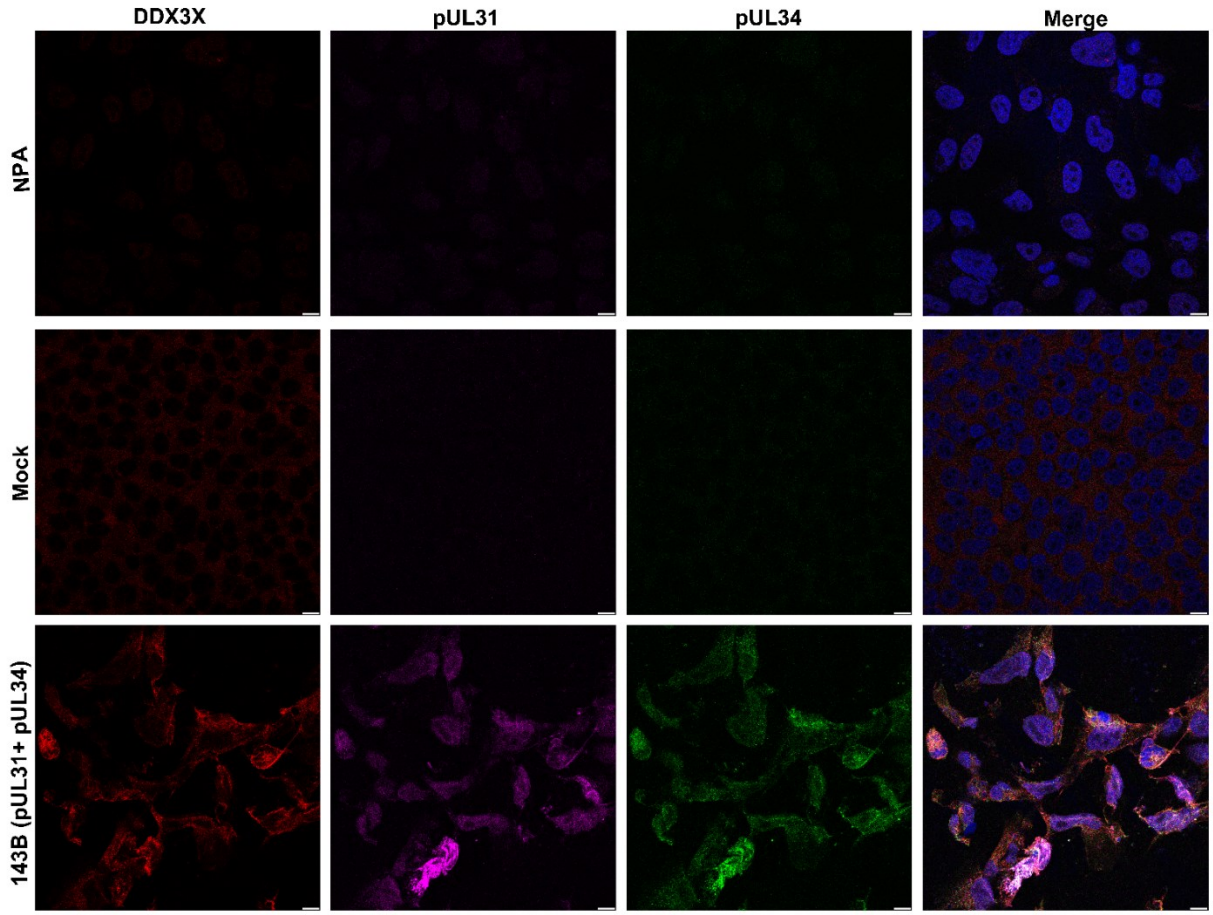

Figure 4.13: DDX3X co-localizes with both components of NEC (co-transfected pUL31 and pUL34 plasmids) in 143B cells

pRR1238 (pUL34) and pRR1334 (pUL31) plasmids were co-transfected in 143B cells, the samples were fixed 24 hours post-transfection and immunostained with rabbit anti-DDX3X (1:200), anti-

pUL31 (1:200), and anti-pUL34 (1:1000) antibodies, and visualized by confocal microscopy (Blue: Hoechst 33342; Green: pUL34; Red: DDX3X; and Magenta: pUL31). The grey scale bars represent 10 µm. The experiment was performed 2 times with similar results.

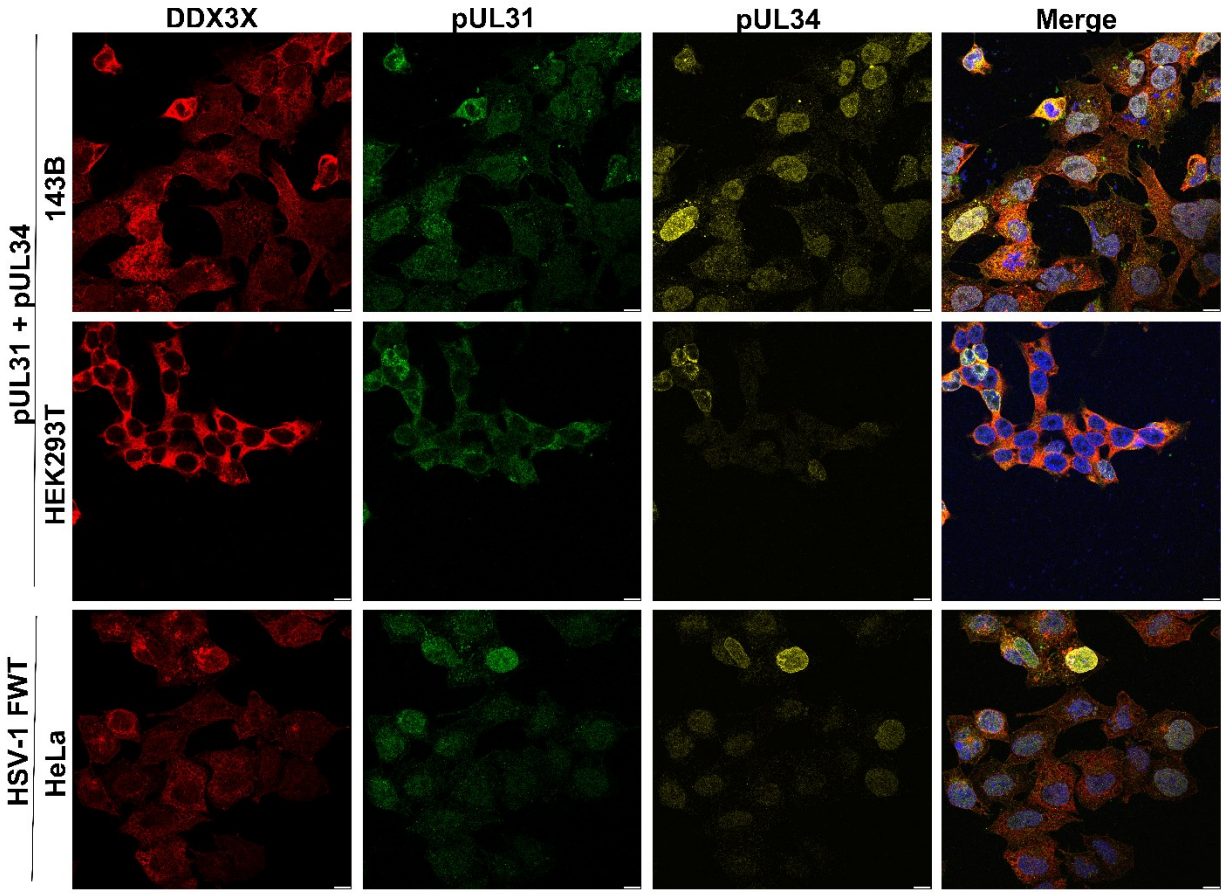

Figure 4.14: DDX3X co-localizes with NEC in transfected and infected cells

pRR1238 (pUL34) and pRR1334 (pUL31) plasmids were co-transfected in a) 143B cells and b) HEK293T cells for 24 hours, while HeLa cells were infected with HSV-1 (F) for 11 hours. The cells were immunostained with rabbit anti-DDX3X (1:200), rat anti-pUL31 (1:200), and chicken anti-pUL34 (1:1000) antibodies and visualized by confocal microscopy (Blue: Hoechst 33342; Green: pUL31; Red: DDX3X; and Brown: pUL31). The grey scale bars represent 10 µm. This figure represents a single experiment.

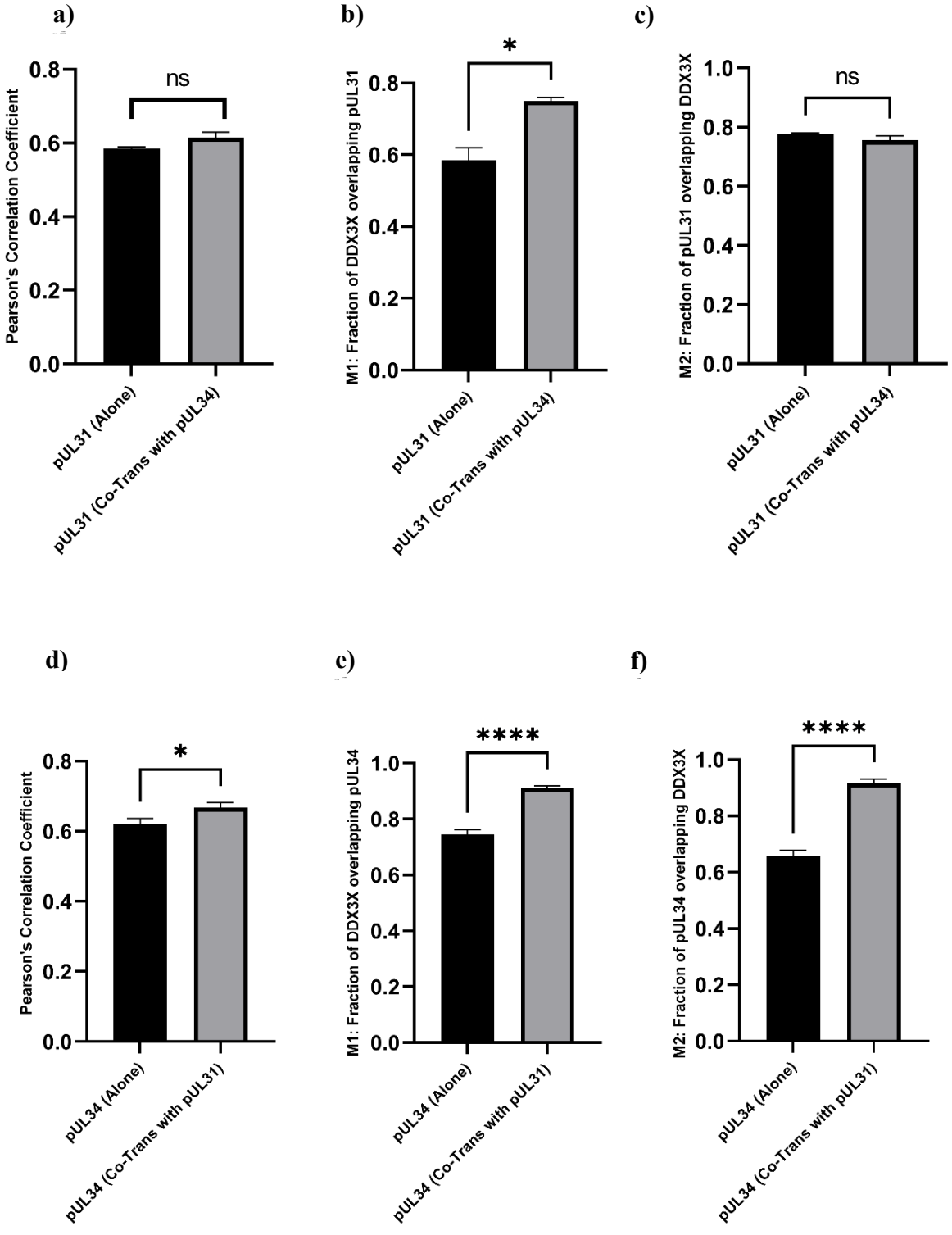
a)
b)
c)
d)
e)
f)
Pearson's Correlation Coefficient
M1: Fraction of DDX3X overlapping pUL31
M2: Fraction of pUL31 overlapping DDX3X
M1: Fraction of DDX3X overlapping pUL34
M2: Fraction of pUL34 overlapping DDX3X
ns
*
****
pUL31 (Alone)
pUL31 (Co-Trans with pUL34)
pUL34 (Alone)
pUL34 (Co-Trans with pUL31)
0.0
0.2
0.4
0.6
0.8
1.0

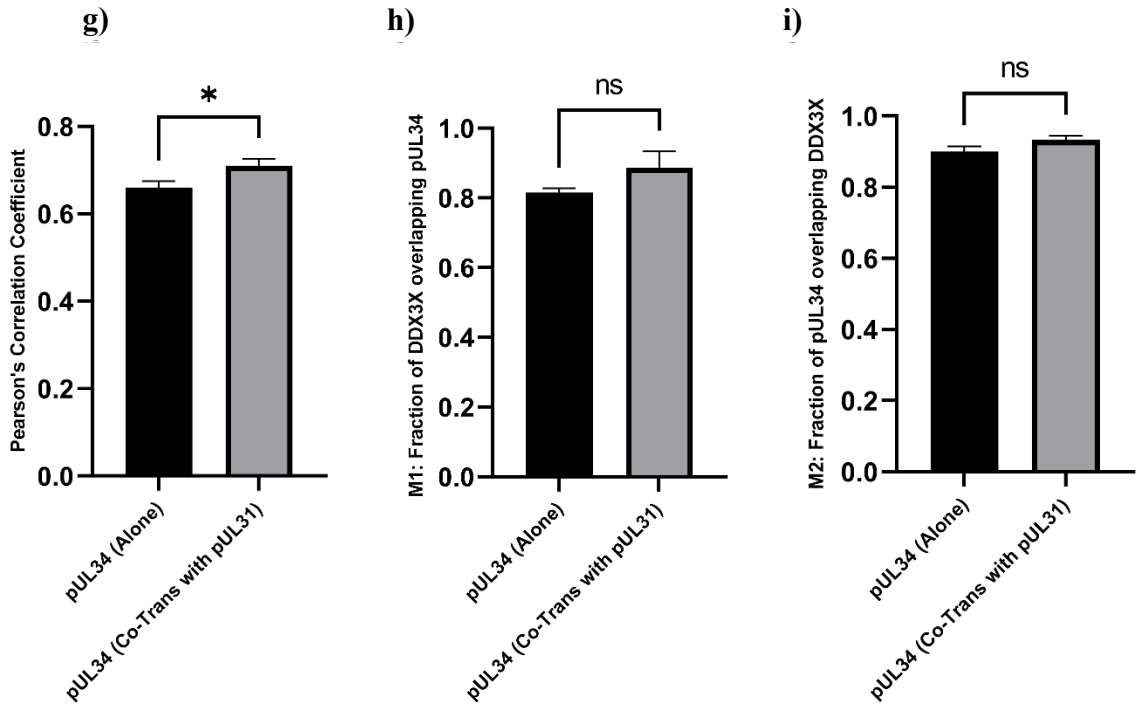

Figure 4.15: Quantification of DDX3X co-localization with NEC components

pRR1238 (pUL34) and pRR1334 (pUL31) plasmids were transiently transfected or co-transfected in 143B (panels a-f) and HEK293T cells (panels g-i). Twenty transfected cells were selected randomly for each condition, and the co-localization was measured using PCC (panels a, d, and g) or MCC (panels b, c, e, f, h, and I). The graph bars are representative of statistical means and SEM. The independent Student's *t-test* were performed with the above single experiment using GraphPad Prism (version 9), *$p < 0.03$, ****$p < 0.0001$, and *ns*: non-significant.

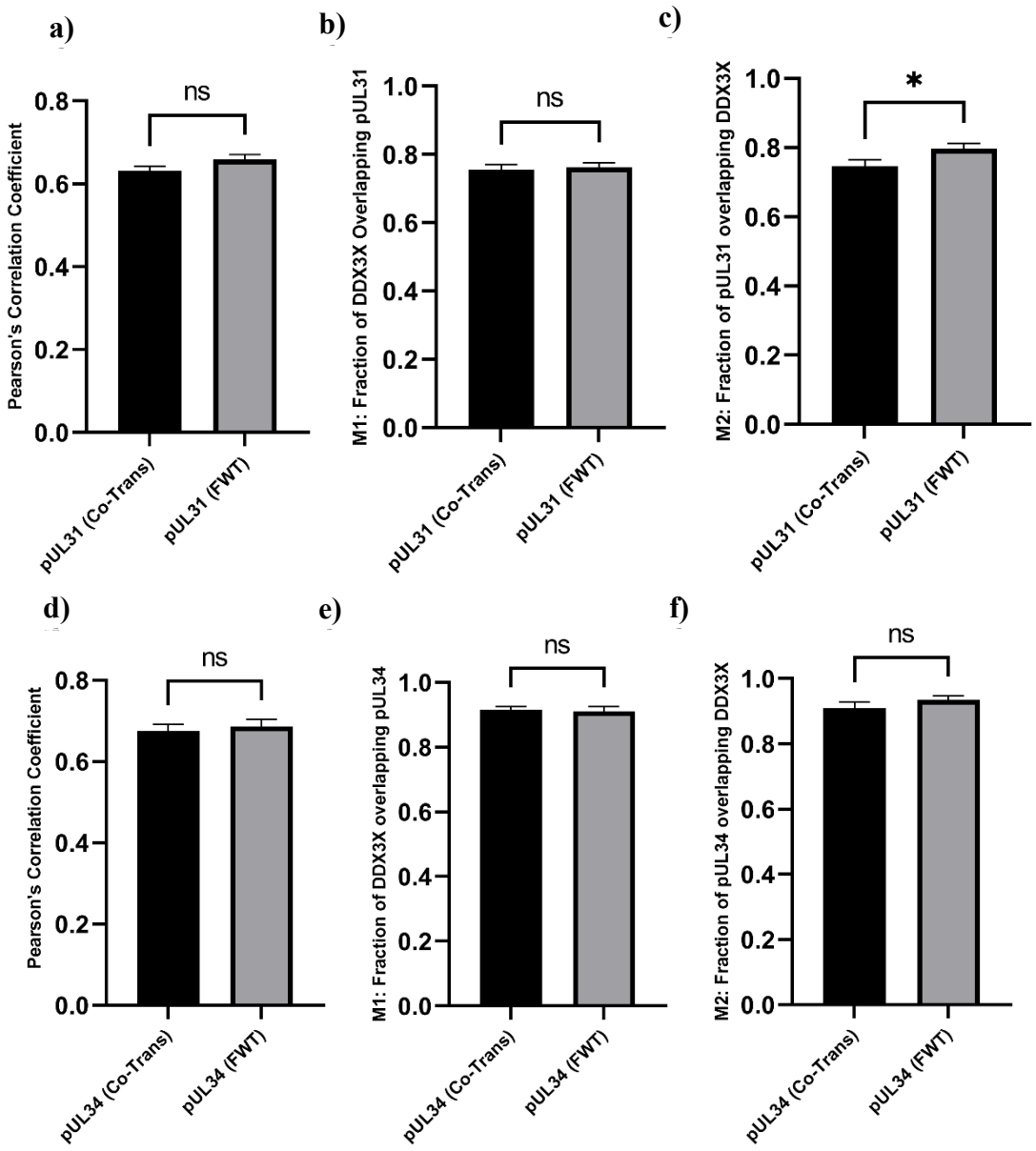

Figure 4.16: Comparing co-localization in co-transfected 143B and WT-infected HeLa cells

pRR1238 (pUL34) and pRR1334 (pUL31) plasmids were transiently co-transfected in 143B cells for 24 hours, while HeLa cells were infected with HSV-1 (F) for 11 hours. Twenty transfected and infected cells were selected randomly for each condition i.e., pUL31 (panels a-c) and pUL34 (panels d-f), and the co-localization was measured using PCC (panels a and d) or MCC (panels b, c, e, and f) and compared using ImageJ. The graph bars are representative of statistical means and SEM. The independent Student's *t-test* were performed with the above single experiment using GraphPad Prism (version 9), $*p < 0.03$, and *ns*: non-significant. The data represents a single experiment.

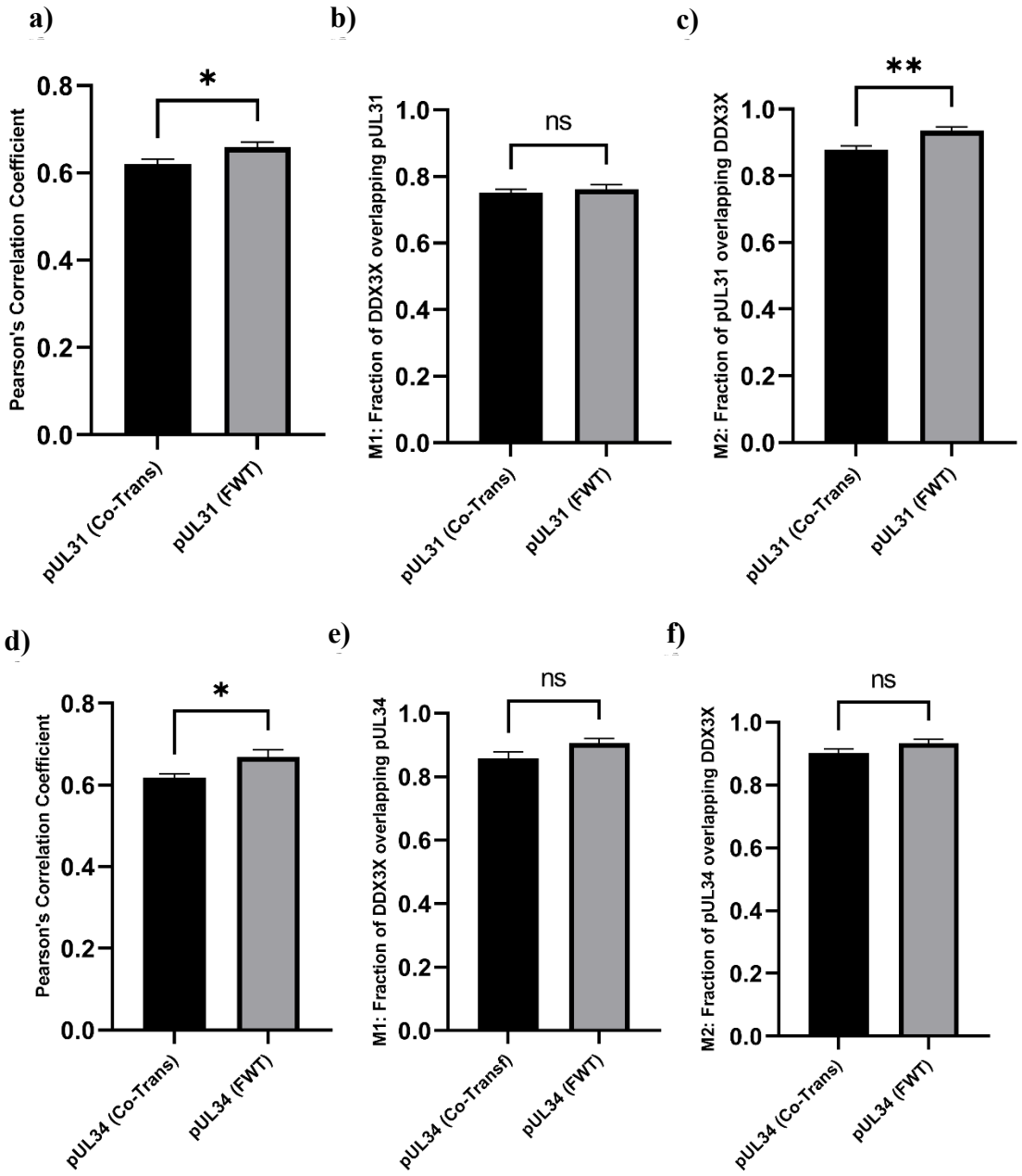

Figure 4.17: Comparing co-localization in co-transfected HEK293T and WT-infected HeLa cells

pRR1238 (pUL34) and pRR1334 (pUL31) plasmids were transiently co-transfected in HEK293T cells for 24 hours, while HeLa cells were infected with HSV-1 (F) for 11 hours. Twenty transfected and infected cells were selected randomly for each condition i.e., pUL31 (panels a-c) and pUL34 (panels d-f), and the co-localization was measured using PCC (panels a and d) or MCC (panels b, c, e, and f), and compared using ImageJ. The graph bars are representative of statistical means and SEM. The independent Student's *t-test* were performed with the above single experiment using GraphPad Prism (version 9), $*p < 0.02$, $**p < 0.001$, and *ns*: non-significant. The data represents a single experiment.

4.6 Impact of pUS3 phosphorylation on DDX3X interaction with pUL31

HSV-1 pUL31 is a nucleo-phosphoprotein and a substrate of pUS3. Furthermore, the phosphorylation of both pUL31 and pUL34 is important for their interaction, correct NEC positioning and nuclear egress (110). In the absence of the pUS3 kinase activity, the NEC is misplaced at the INM and leads to the accumulation of perinuclear virions in the INM herniations (145). Previously, we had shown that DDX3X nuclear localization is dependent of the presence of the NEC (142), but it was unclear if the interaction of DDX3X with the NEC is phospho-dependent. To address this issue, we infected HEK293 Flp-In GS-DDX3X cells (cells overexpressing a protein G-tagged version of DDX3X) with WT and K220A virus for 24 hours and did Co-IP. As seen in Figure 4.18, pUL31 was co-immunoprecipitated along DDX3X in the K220A sample with an intensity comparable to that in the WT infection condition. This was confirmed by quantification of these data (Figure 4.19). This suggested that the DDX3X interaction with pUL31 is independent of pUS3 phosphorylation. In other words, our results showed that DDX3X does not require intact NEC for its interaction and coming to INM.

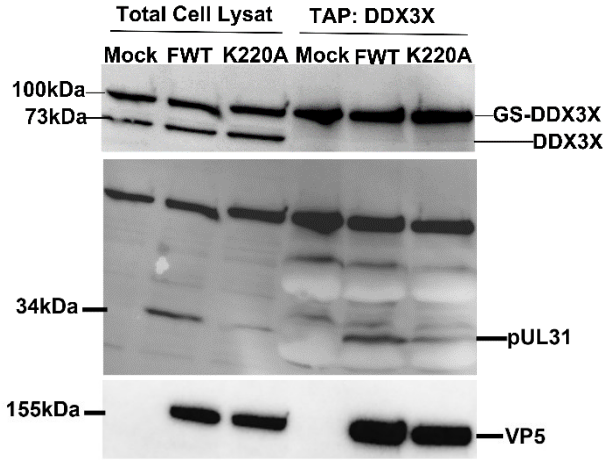

Figure 4.18: Impact of phosphorylation on DDX3X interaction with pUL31

HEK293 Flp-In GS-DDX3X cells, infected with HSV-1 (F) WT and US3K220A at a MOI of 5, were harvested at 12 hpi on ice in RIPA lysis buffer. For IP, 1 mL of lysate was incubated overnight with 50 µL IgG Sepharose Fast Flow (50% slurry) at 4°C. The beads were harvested and subjected to WB with the designated antibodies after being rinsed once with 1 mL lysis buffer (150 mM NaCl) and twice with buffer containing 500 mM NaCl. The experiment was performed 3 times.

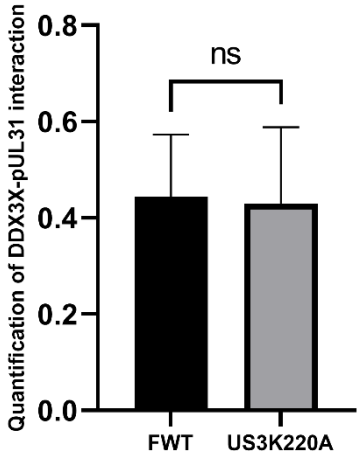

Figure 4.19: Quantification of DDX3X-pUL31 interaction

To quantify and compare the gene expression of US3K220A with HSV-1 F (WT) in both cell lysate and IP portion, immunoblot was quantified using ImageJ. The graph bars are representative of the statistical mean and SEM. The independent Student's *t-test* was performed, *ns: non-significant*. The graph is a representative average of 3 independent experiments.

4.7 PCBP1 interacts with the NEC

PCBP1 is mostly involved in RNA metabolism and acts as a proviral host factor. Our lab first identified PCBP1 among 7 other host proteins specifically present at C-capsids (330). Preliminary work in our lab suggests that PCBP1 is required for HSV-1 viral infection. However, the role of PCBP1 during viral egress and the selection of C-capsids is still enigmatic. Taking advantage of the availability of pUL31 and pUL34 mammalian expression vectors, we first transfected pUL34 in 143B cells for 24 hours. After fixation and permeabilization, we immunostained the cells with indicated antibodies and checked the PCBP1 localization in the pUL34 positive cells (Figure 4.20). Quantification of these images indicates that PCBP1 did not co-localize with pUL34 according to the PCC (< 0.5/ Figure 4. 20). Initially, MCC values with Costes automated threshold setting were odd given the high background in the un-transfected cells. Therefore, we used manual threshold settings and repeated the analysis, which confirmed the lack of interaction between PCBP1 and pUL34. In contrast, when we transfected the pUL31 plasmid in the same cell line, we found that PCBP1 co-localized with that protein (PCC > 0.65/ Figures 4.22-4.23).

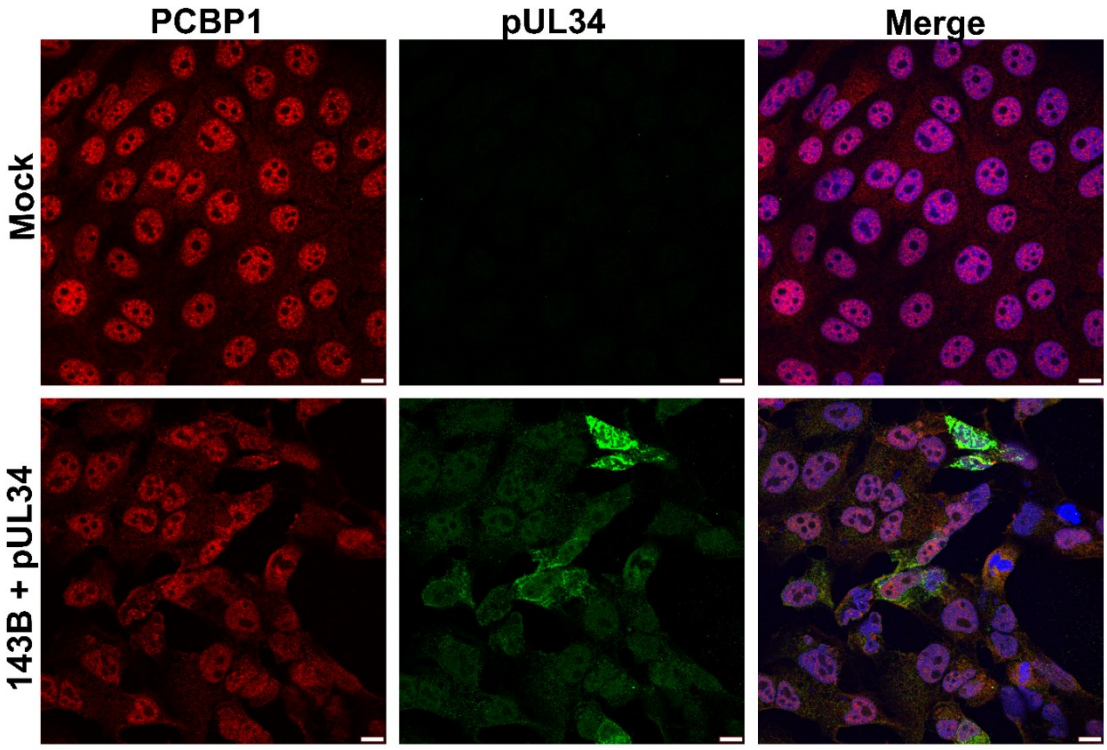

Figure 4.20: PCBP1 co-localization with HSV-1 pUL34

143B cells were transiently transfected with pRR1238 (pUL34) plasmid and fixed 24 hours post-transfection. Cells were immunostained with anti-PCBP1 (1:200) and anti-pUL34 (1:1000) antibodies, mounted on slides, and observed by confocal microscopy (Blue: Hoechst 33342; Green: pUL34; and Red: PCBP1). The white scale bars represent 10 µm. The figure represents a single experiment.

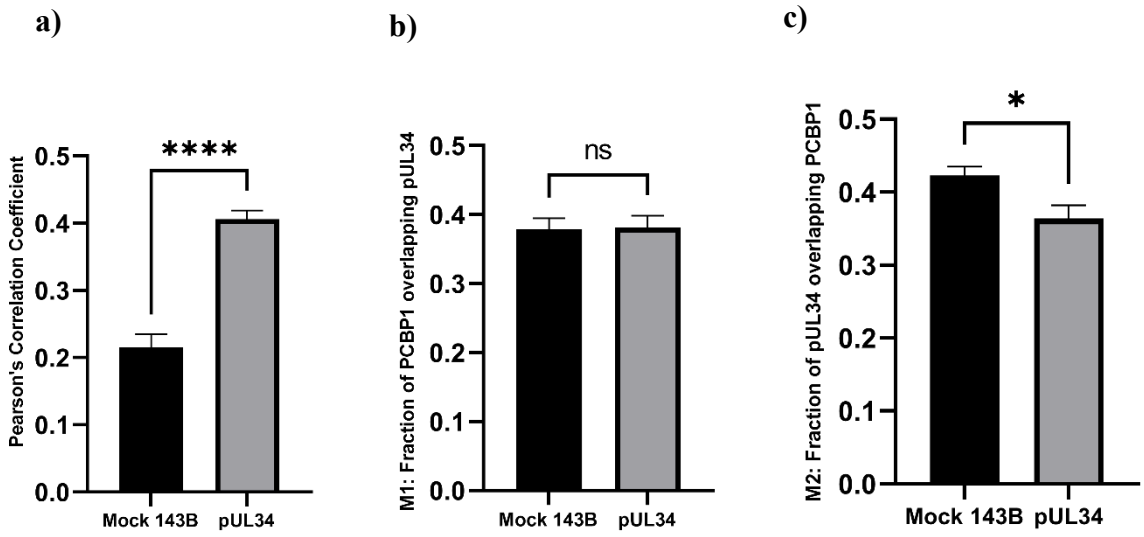

Figure 4.21: Measuring co-localization of PCBP1 with pUL34

Thirty transfected cells were randomly selected from the above conditions and co-localization was measured using (a) Pearson's correlation coefficient and (b, c) Mander's correlation coefficient with the ImageJ JACoP plugin. The graph bars are representative of statistical means and SEM. The two-tailed *t-test* was performed on GraphPad Prism, ***p< 0.0001*, **p< 0.05, ns:* non-significant. These quantifications are from a single experiment.

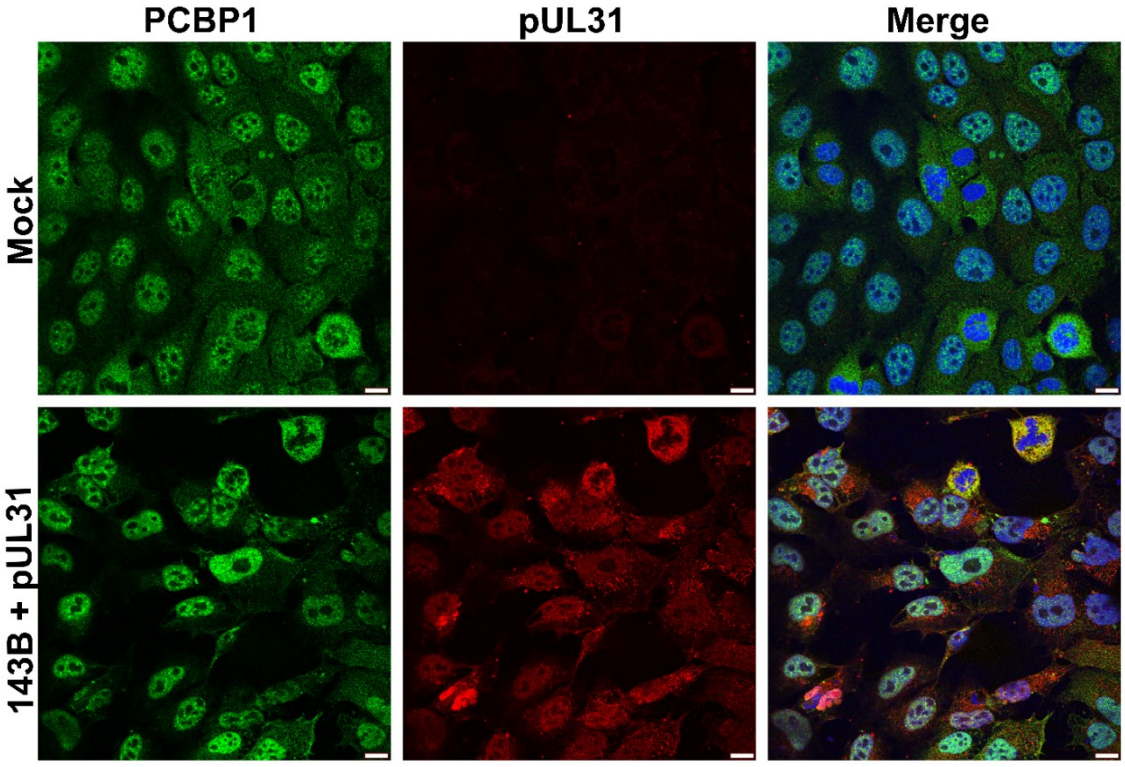

Figure 4.22: PCBP1 co-localization with HSV-1 pUL31

143B cells, transfected with pRR1334 plasmid (1.5 µg), were fixed 24 hpi, immunostained with anti-PCBP1 (1:200) and anti-pUL31 (1:200) antibodies, and examined by confocal microscopy (Blue: Hoechst 33342; Green: PCBP1; and Red: pUL31). The white scale bars represent 10 µm. The figure is representative of 2 independent experiments.

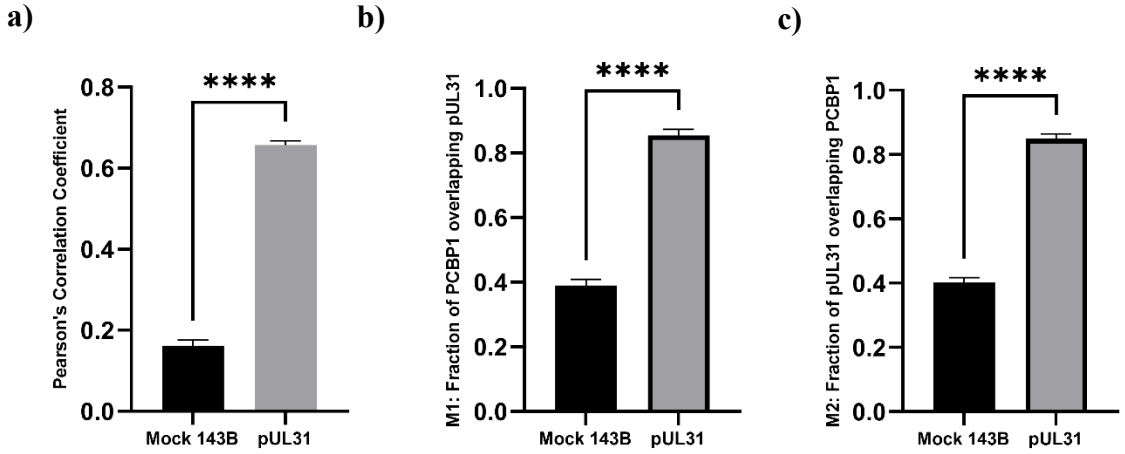

Figure 4.23: Co-localization of PCBP1 with HSV-1 pUL31

Thirty transfected cells from the above confocal images were quantified from each condition randomly selected on LASX software. The co-localization was measured using (a) PCC (b, c) MCC (M1 & M2), with the ImageJ JACoP plugin. The graph bars are representative of statistical means and SEM. The independent Student's *t-test* was performed with ****$p < 0.0001$. The data is representative of 2 independent experiments.

4.8 PCBP1 interaction with DDX3X late in the infection

So far, we found that PCBP1 interacts with pUL31 and very poorly, if at all, with pUL34. This is an interesting scenario as pUL31 also interacts with DDX3X and is involved in DDX3X recruitment to the INM and the formation of the large capsid aggregates at the nuclear periphery. It is thus conceivable that the PCBP1 found on C-capsids bridges them to the NEC via DDX3X (142), in turn explaining their selective egress. This scenario is further corroborated by a reported interaction between DDX3X and PCBP1 (356). To evaluate this in the context of HSV-1 infected cells, we infected HeLa cells with HSV-1 WT (F) virus for 11 hours and confirmed the interaction between PCBP1 and DDX3X by fluorescence microscopy. Here we used VP22 as a marker of infection to distinguish the infected cells from normal cells as the VP5 antibody is from the same species as the PCBP1 antibody. As seen in Figures 4.24 and 4.25, both proteins showed partial co-localization at that time. Most interestingly, PCBP1 was accumulated in a ring-like configuration around the nucleus (in roughly 15% of the infected cells), where it interacted with DDX3X. Interestingly, no such co-localization took place at early times points (Figures 4.26, 4.27).

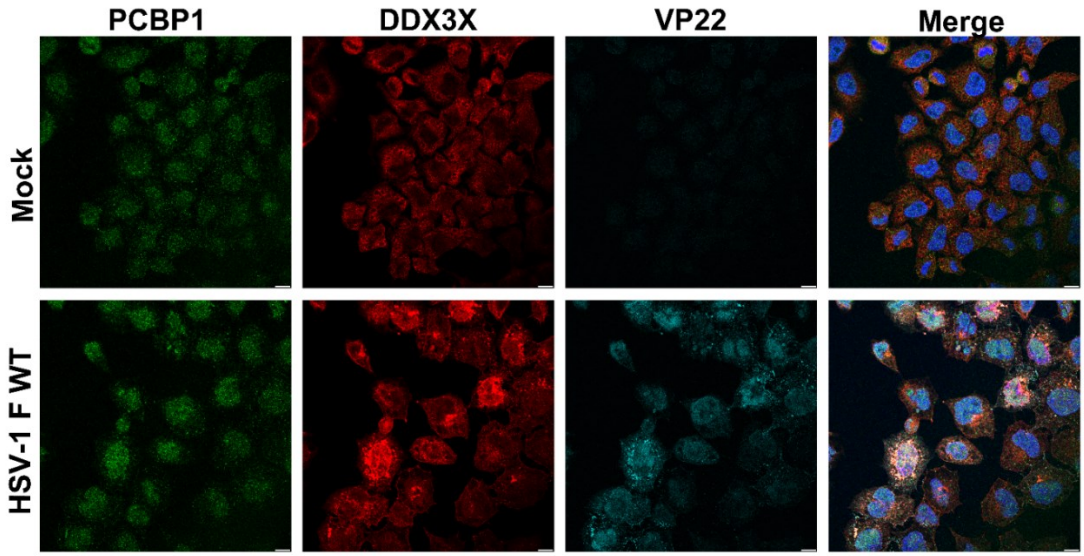

Figure 4.24: PCBP1 co-localization with DDX3X in HeLa cells 11 hpi

HeLa cells, infected with HSV-1 (F) at an MOI of 5, were fixed at 11 hpi. The cells were immunostained with mouse anti-hnRNP E1/PCBP1 (1:100), chicken anti-VP22 (1:200), and R648/anti-DDX3X (1:200) antibodies and monitored by confocal microscopy (Blue: Hoechst 33342; Green: PCBP1; Red: DDX3X; and Cyan: VP22). The grey scale bars represent 10 µm. The figure is representative of 2 independent experiments.

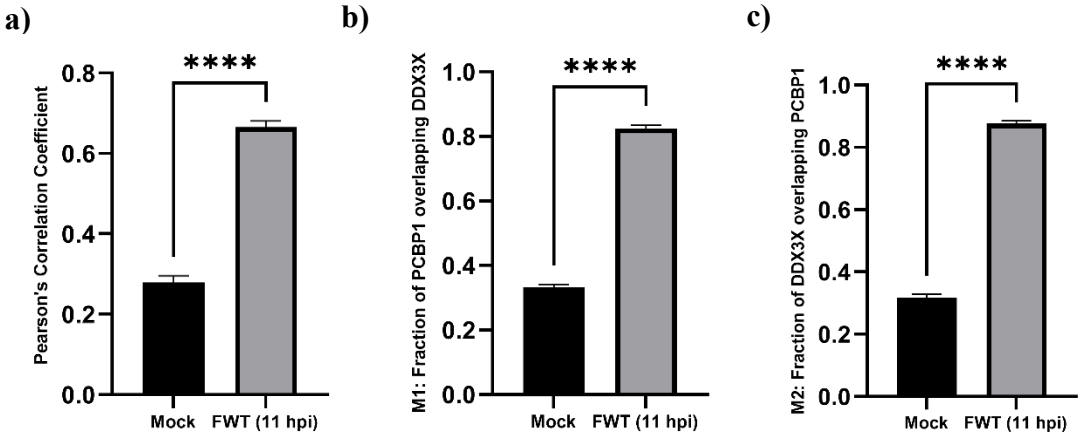

Figure 4.25: PCBP1-DDX3X co-localization measurement at 11 hpi

Thirty infected cells were randomly selected on LASX software and co-localization was measured using (a) PCC and (b) MCC (M1 & M2) with the ImageJ JACoP plugin. The graph bars are representative of statistical means and SEM. The bilateral Student's *t-test* was performed using GraphPad Prism software (version 9), ****$p < 0.001$. The data is representative of 2 independent experiments.

A) 2 hpi

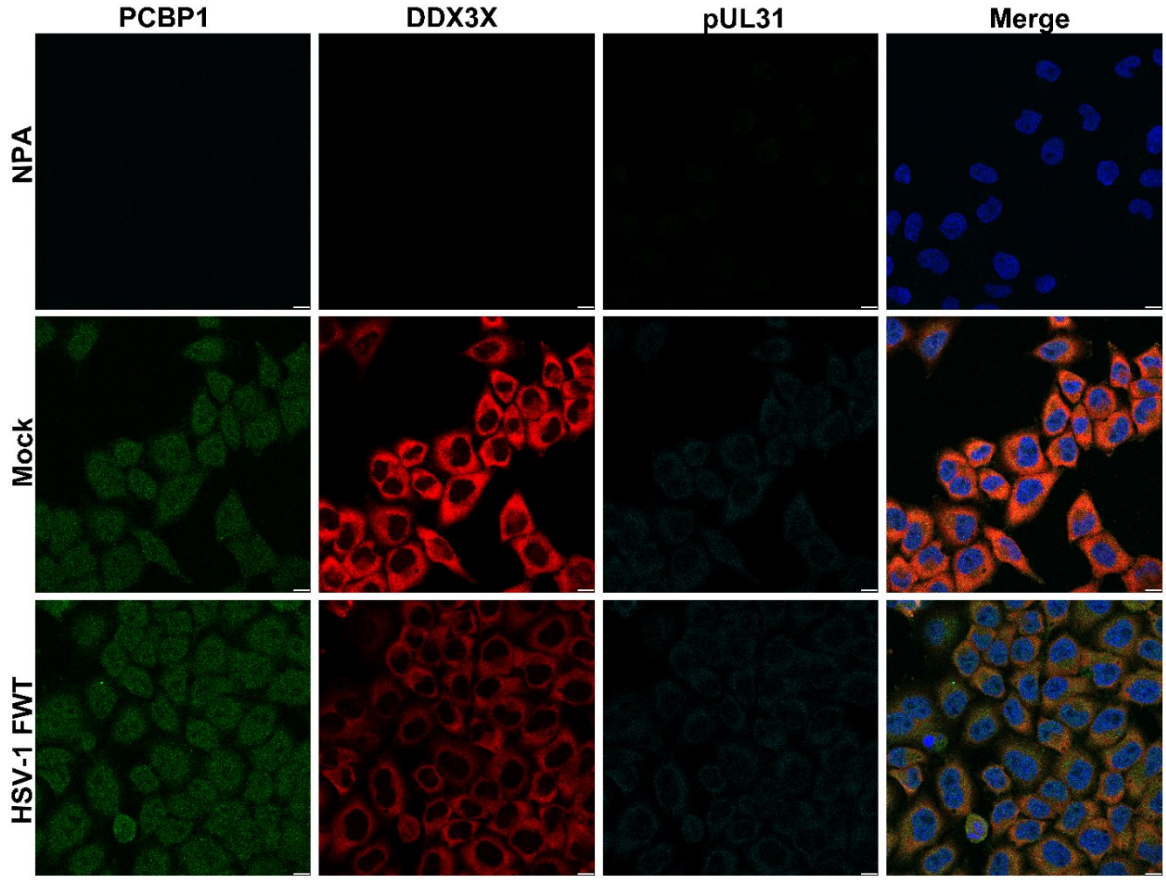

B) 4 hpi

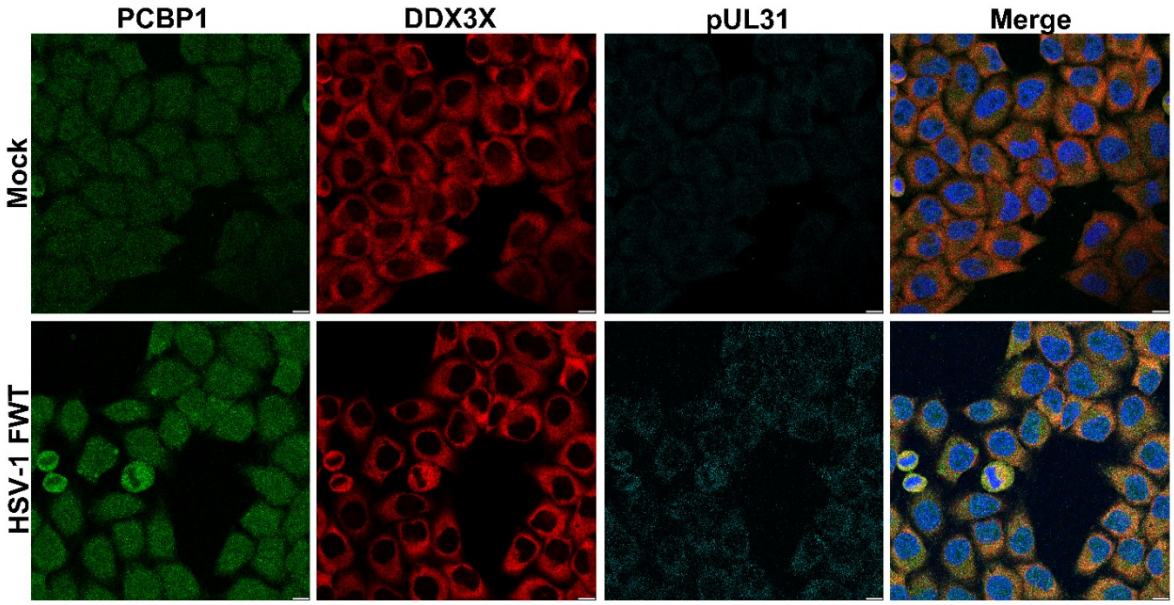

Figure 4.26: DDX3X co-localization with PCBP1 at different time intervals

HeLa cells, grown on coverslips, were either Mock treated or infected with HSV-1 (F) WT at an MOI of 5. Infected cells were fixed (a) 2 and (b) 4 hpi and immunostained with mouse anti-hnRNP E1/PCBP1 (1:100), rat anti-pUL31 (1:200), R648/anti-DDX3X (1:200) antibodies and examined by confocal microscopy (Blue: Hoechst 33342; Green: PCBP1; Red: DDX3X; and Cyan: pUL31). The white scale bars represent 10 µm. The figure represents a single experiment.

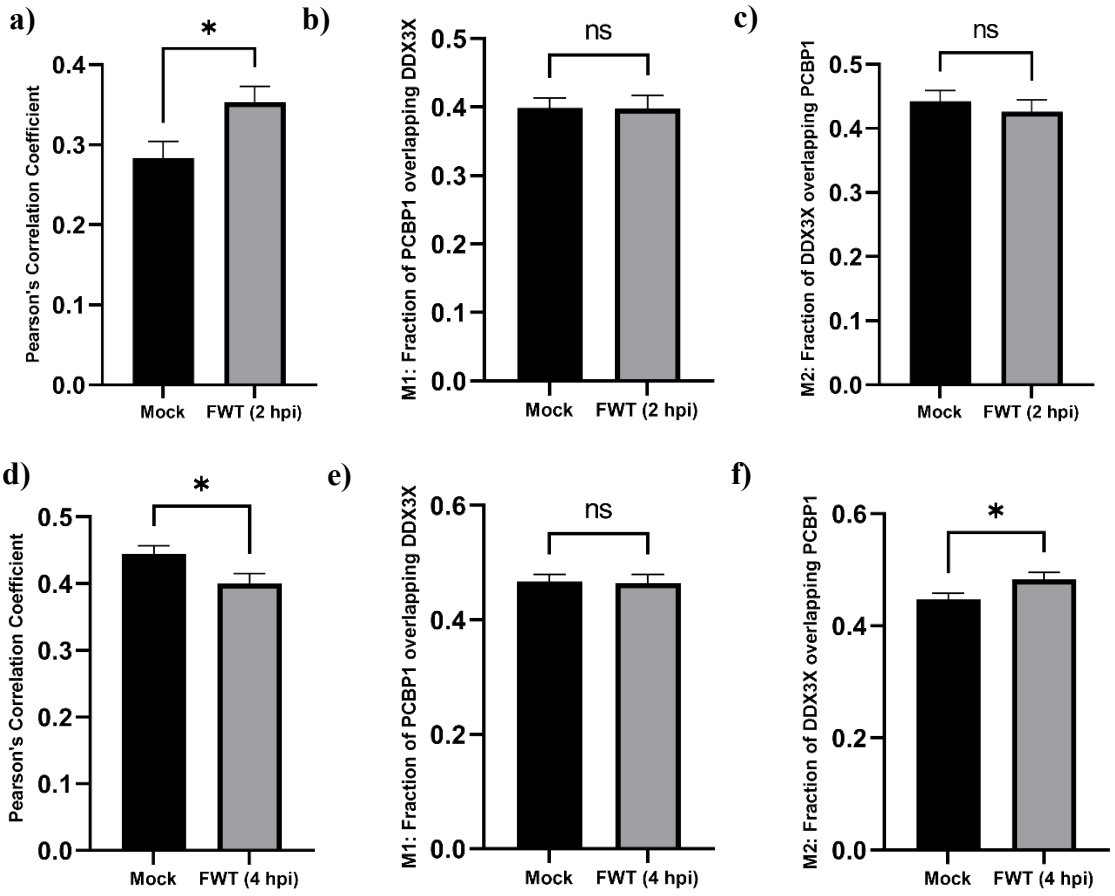

Figure 4.27: PCBP1-DDX3X co-localization measurement at 2 and 4 hpi

Thirty cells were randomly selected on LASX software from 2, and 4 hpi conditions, and co-localization was measured using (a) Pearson's correlation coefficient and (b) Mander's correlation coefficient with the ImageJ JACoP plugin. The graph bars are representative of statistical means and SEM. The independent Student's *t-test* was performed on GraphPad Prism software (version 9), *$p < 0.017$, *ns*: non-significant. The data is representative of a single experiment.

4.9 PCBP1 interaction with DDX3X is dependent on an active pUS3

It is noteworthy that HSV-1 pUS3 phosphorylates PAK1 to inhibit apoptosis (357), which in turn phosphorylates PCBP1 on the Thr-60 and Thr-127 positions. This phosphorylation results in PCBP1 increasing nuclear retention in nuclear speckles around the INM (296). It is, thus possible that pUS3 directly phosphorylates PCBP1 to change its subcellular localization. To

confirm this hypothesis, we infected HeLa cells with WT (F) and dead kinase mutant (US3K220A) and surprisingly did not see any PCBP1 nuclear rim phenotype in cells infected with this mutant virus (Figure 4.26). Moreover, phosphorylation significantly impacts (*p=0.01*) DDX3X interaction with PCBP1 (Figures 4.28-4.29).

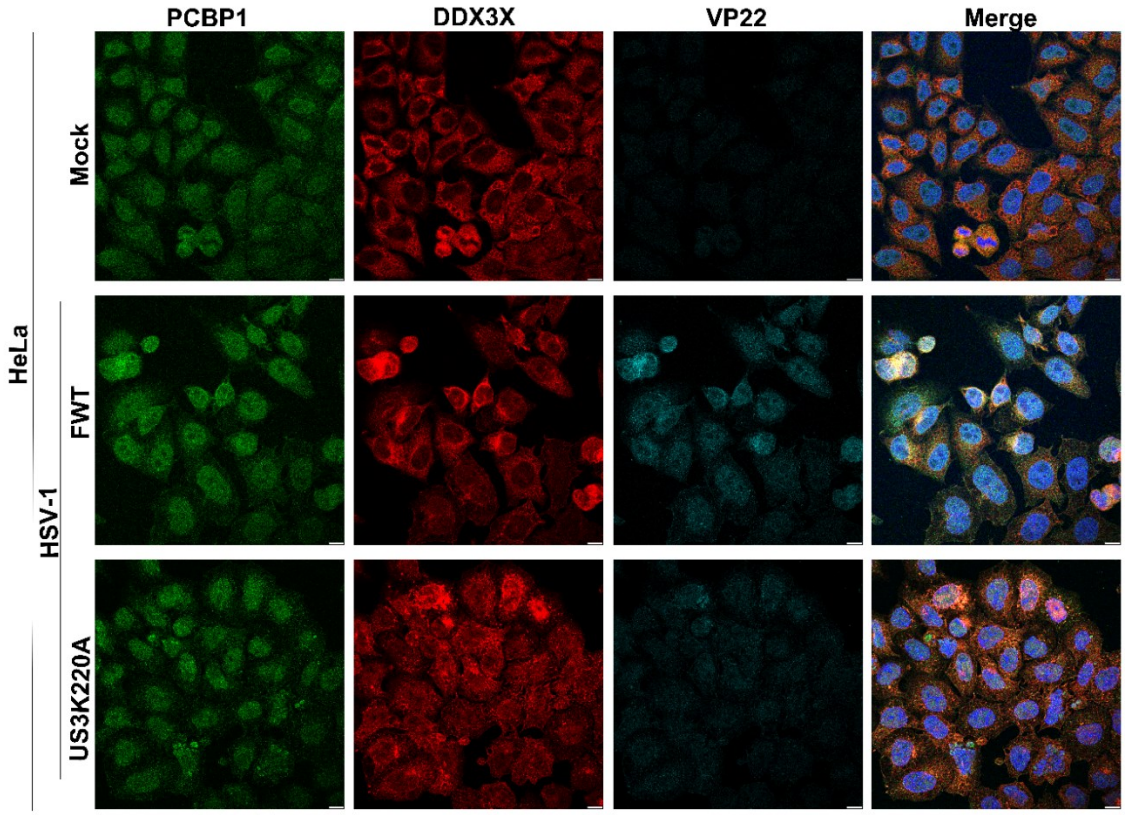

Figure 4.28: Impact of phosphorylation on DDX3X co-localization with PCBP1

HeLa cells, on coverslips, were infected with HSV-1 (F) WT and US3K220A at an MOI of 5. Once fixed at 11 hpi, the cells were immunostained with mouse anti-hnRNP E1/PCBP1 (1:100), chicken anti-VP22 (1:200), R648/anti-DDX3X (1:200) antibodies and subjected to confocal microscopy (Blue: Hoechst 33342; Green: PCBP1; Red: DDX3X; and Cyan: VP22). The grey scale bars represent 10 µm. The experiment was performed once.

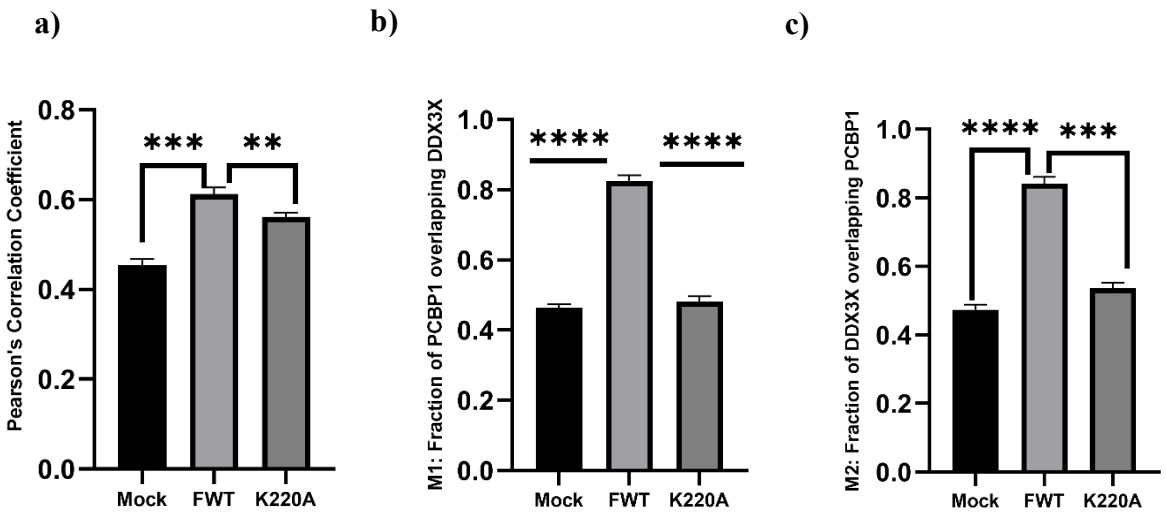

Figure 4.29: Measuring the impact of phosphorylation on DDX3X co-localization with PCBP1

Twenty cells were randomly selected on LASX software from 3 conditions and co-localization was measured using (a) Pearson's correlation coefficient and (b) Mander's correlation coefficient with the ImageJ JACoP plugin. The graph bars are representative of statistical means and SEM. The One-way Analysis of variance (ANOVA) test was performed on GraphPad Prism software (version 9), $**p < 0.02$. The data is representative of a single experiment.

Chapter 5: Discussion

Due to continuous co-evolution, virus-host interactions are complex dynamic relationships. Different host cells directly contribute to the detection, surveillance, and elimination of viral pathogens, which interact with these cellular factors and have adopted diverse sophisticated strategies to evade the body's immune defense (358). A deep understanding of host-pathogen interactomes is critical for studying fundamental mechanisms governing immunity and infection and developing novel host-directed preventative or therapeutic antiviral drug targets. Host-directed therapy is a recent concept to identify global host factors essential for the replication and pathology of common viruses for the development of broad-spectrum pan-viral therapies (359). Recent studies pinpoint DDX3X as a common host protein that could be used for developing broad-spectrum pan-viral therapeutic agents (245).

C-capsids contain mature HSV-1 DNA and preferentially escape out of the nucleus. The exact reason for this selection is still enigmatic. An initial model suggested that the CVSC plays a prominent role in capsid selection, since it was believed to be unique to those capsids (360). This has since been repudiated since this complex also coats A and B nuclear capsids, albeit C-capsids contain four times more CVSC proteins than other capsid types (361). This hints that different viral and host protein interactions are likely involved. The core subject of this study is two host proteins, i.e., DDX3X and PCBP1, with respect to the preferential escape of HSV-1 C-capsids out of the nucleus. DDX3X is an important host protein involved in different aspects of RNA metabolism and gene expression (362). Since its discovery, the proviral and antiviral roles of DDX3X in different viral infections have been extensively studied. DDX3X is widely implicated in the pathogenesis and productive life cycles of RNA (363) as well as DNA viruses (364). Mature virions of DNA viruses incorporate DDX3X, including HBV, HCMV, and PRV (365, 366). Previously, our lab found that the tegument of mature HSV-1 virion incorporates 49 distinct host cellular proteins including DDX3X (55). A subsequent study identified DDX3X as a critical host protein in HSV-1 infectivity, with the knockdown of either cellular or viral pool of the protein significantly reducing viral yields (54). We also demonstrated DDX3X requirements for HSV-1 replication and optimal gene expression (54, 367). Finally, capsid nuclear egress at the nuclear periphery is DDX3X dependent (142), which indicates the role of DDX3X in the selective egress of C-capsids. The present study identifies the significance of viral kinase (pUS3) activity in re-

localizing DDX3X to the inner nuclear rim and its importance in the formation of nuclear capsid blebs. It also demonstrates the DXX3X interaction with both NEC components as well as with PCBP1, which could explain its important role in the selective egress of C-capsids.

Previous co-IP analyses showed an interaction between pUL31 with the DDX3X C-terminus, but this was done in the context of a full NEC and a full complement of other viral proteins (142). The question was therefore if DDX3X can independently bind pUL31, requires both NEC components or the interaction is dependent on those other viral proteins. Here we found that DDX3X co-localizes with pUL31 (Figures 4.8 and 4.9) and pUL34 (Figures 4.11 and 4.12) separately when transfected alone in the absence of pUS3 or other viral partners. It is interesting that DDX3X best interacts with an intact NEC (Figures 4.13-4.14), where both viral proteins are present. Moreover, the presence of both NEC components had the highest co-localization with DDX3X (Figure 4.15 – 4.17). It is perhaps not surprising as NEC recruits various cellular proteins to help in the smooth egress of nuclear capsids (120) and its interaction with DDX3X also facilitates the selective egress of mature C-capsids. Oddly, pUL34 was not among the 15 interacting partners of DDX3X identified by mass spectrometry (142). However, pUL34's presence at the nuclear periphery is dependent on C-capsids, whose presence, in turn, is dependent on DDX3X (142). This situation could indicate the complex interaction of pUL34 with DDX3X at the INM and its putative role in the selection of C-capsids coming for egress.

pUS3 is a ser/thr viral kinase that phosphorylates pUL31 and pUL34. This phosphorylation is required to properly position NEC, for primary envelopment, and subsequent nuclear egress (132). We initially thought DDX3X interacted with pUL31 at the INM after the formation of an intact NEC (pUL31 and pUL34) with pUS3 phosphorylating both components. Our results confirmed the significant impact of pUS3 phosphorylation on DDX3X localization to the INM. However, it is interesting that our findings show a non-significant impact of the pUS3 kinase activity on DDX3X interaction with pUL31 by co-IP. This could lead to a situation where pUL31 indirectly interacts with DDX3X through pUL34 at the INM or pUL31 interacts with DDX3X at places other than the INM. This requires further analysis. However, it would be interesting to decipher the possible DDX3X interaction with pUL47, a protein already discovered to interact with NEC and pUS3 and also detected on primary enveloped virions (117).

The subcellular localization of DDX3X is important as it is often correlated with disease progression and tumorigenesis (209). We found that pUS3 phosphorylation significantly impacts DDX3X re-localization to the INM late during infection (Figure 4.5). This is an interesting finding as we showed the non-significant effect of phosphorylation on DDX3X interaction with pUL31, which is thought to capture DDX3X at the INM (142). DDX3X is a known substrate of host kinases as TBK1 phosphorylation activates DDX3X-mediated IFN-β transcription (219). pUS3 can phosphorylate host cellular proteins, including PKA, PKC, vdUTPase, TSC2, lamin A/C, and KIF3A (368). pUS3 may thus also phosphorylate DDX3X, which may directly or indirectly be responsible for its re-localization to the INM.

DDX3X co-localizes with perinuclear aggregates, thought to be C-capsids coming for egress, as they co-localize with VP5, a major capsid protein (142). For statistical ease, we divided these nuclear blebs into two categories, i.e., i) large blebs of 2-4 μm and ii) medium-sized blebs up to 2 μm. Mutating the kinase activity of pUS3 significantly affected these VP5 phenotypes. We did not see any large (2-4 μm) aggregates in US3K220A-infected cells, though we observed these aggregates in more than 15% of WT-infected cells. However, the smaller nuclear aggregates were much more abundant with the viral mutant. Interestingly, knocking down pUS3 causes INM herniations (118), so this increase could be due to the small number of capsids trapped in these herniations.

PCBP1 is a KH domain host protein with a variable role in RNA metabolism and viral gene expression. Different proteins from the KH-domain family have been found to modulate herpesviruses. For instance, hnRNP K is essential for HSV-1 propagation by interacting with ICP27 (369). It also interacts with CK2ß and IE2 of HHV-6 (370), and the KSHV ORF57 to modulate IRES-mediated translation. Our lab previously found PCBP1 specifically present on C-capsid as compared to other types, which could indicate its involvement in selective egress (330). However, its mechanism of action has been elusive. An interesting aspect is that its iron channeling properties may be responsible for the proviral effect of PCBP1. Iron is required for the normal function of the ribonucleotide reductase enzyme encoded by the members of *Orthoherpesviridae* (371). PCBP1 is an iron chaperone that can transport cytosolic ferrous ions to different enzymes, including ferritin and DOHH (372). The requirement of iron is also evident from an *in vitro* study where the addition of 2,2, bipyridyl (BIP), a ferrous ion chelator, inhibits viral genome replication

and causes a 50% reduction in HSV-1 titers (373). However, it is difficult to envision how this ion channel activity drives the fully assembled viral capsid across the nuclear envelope. The present work suggests an alternative and appealing mechanism where PCBP1 may bridge the nuclear C-capsids to the NEC through DDX3X.

Recent data showed PCBP1 interacts with DDX3X (356), has a nucleocytoplasmic distribution in normal cells, and is predominately localized to cytoplasm. We first confirmed by co-immunofluorescence a PCBP1 interaction with DDX3X at 11 hpi (Figures 4.24 and 4.25). We found a unique PCBP1 phenotype in infected cells, where in almost 15% of infected cells, PCBP1 concentrates in a ring-like configuration around the INM (Figure 4.23). This was quite exciting as PCBP1 is already found on C-capsids. Phosphorylation of PCBP1 by mitogen-induced p21-activated kinase 1 (Pak1) on Thr-60 and Thr-127 increases its nuclear retention (296), and HSV-1 pUS3 phosphorylates PAK1 to inhibit apoptosis (357). It is quite possible that pUS3 directly phosphorylates PCBP1 or indirectly through PAK1 and brings it to the INM at a specific time when nuclear capsids are coming for egress. This is also evident from Figure 4.29, where phosphorylation significantly impacts PCBP1's interaction with DDX3X. This could also be related to PCBP1's selective presence on C-capsids. Being a tail-anchored protein, pUL34 was likely a possible interacting partner of PCBP1 as it recruits not only pUL31 to the INM but also is required for membrane scission and its presence on INM is capsid dependent (145). However, we did not find a strong co-localization signal between PCBP1 and pUL34. In contrast, we found a PCBP1 interaction with pUL31. This could indicate a scenario where DDX3X, via its interaction with PCBP1 and NEC, indirectly plays an important role in selecting C-capsids. Moreover, pUS3 also interacts with pUL47, which is already implicated in nuclear egress (117). It is conceivable that pUS3-directed phosphorylation brings PCBP1 to the INM late during infection, where it is selectively loaded on C-capsids and helps in their preferential egress via its interaction with DDX3X. It will be interesting in the future to know when exactly the PCBP1 is recruited to C-capsids, if DDX3X also interacts with pUL47, and if this is involved in the selection of content specific to C-capsids. Overall, the above results pointed towards a model where pUL31 through DDX3X is involved in PCBP1 selection on C-capsids and DDX3X interaction with PCBP1 facilitates the preferential egress of HSV-1 C-capsids only late during the infection when capsids are coming for egress. Albeit hypothetical, this model is interesting since DDX3X is central to these PPIs.

Biologically, proteins hardly ever operate as solitary species, and it is estimated that approximately 80% of proteins function as complexes (374). Several *in vitro* techniques to study PPIs include protein arrays, co-IP, WB, tandem affinity purification, NMR spectroscopy, proteomics, X-ray crystallography, yeast two-hybrid assays, affinity chromatography, and IF microscopy. In the latter case, there are different and unfortunately complex approaches to quantify co-localization between two proteins, including PCC (Pearson's correlation coefficient) (375), ICCS (376), intensity correlation quotient (qualitative) (377), and MCC (Mander's correlation coefficient) (378). Throughout this study, we used two methods, i.e., PCC and MCC, with Coste's automated threshold setting in JACoP/ImageJ to measure the co-localization between fluorophores. PCC, a proven correlation metric, was first introduced by Galton in the 19th century, and is extensively applied for measuring co-localization. It measures the deviation from the mean intensities of both fluorescently labeled channels at each pixel/data set and recorded between -1 to +1. A null value means no linear correlation, while the degree of co-localization increases with increasing value towards +1 (perfect positive linear correlation), and -1 indicates "perfect anti-correlation". However, the PCC is insensitive to differences in "signal to noise" (SNR) as it considers the deviation from the mean (375). Mander instead proposed a new model where the scale ranges between "0" (no-colocalization) to "1" (perfect colocalization), and splits into two, i.e., M1 and M2, both measuring the fraction of intensities of the respective counterparts (i.e., protein 1 vs protein 2). MCC considers absolute intensities. However, it is greatly affected by the poor signal intensity or noise ratios between corresponding channels. For MCC, the most difficult problem is usually to define an absolute threshold for both channels without affecting the results. To address this problem, we used the Coste's automated threshold setting available in the JACoP plugin in our co-localization quantification. Nevertheless, its efficiency is hard to predict and absolute statements should be considered carefully (378, 379). Hence, correlations are perhaps best evaluated by computing both the Manders and Pearson coefficients. However, as pointed above, their efficiency in quantifying PPI/co-localization is subject to debate. Moreover, co-localization is the quantification of two different phenomena, i.e., i) co-occurrence which measures the spatial overlap of two fluorophores, and ii) correlation which measures the degree of relationship between overlapped signals (380). Co-occurrence usually measures the physiochemical similarities between interacting proteins, i.e., partitioning based on hydrophobic or hydrophilic interactions. On the other hand, correlation measures direct or indirect interaction

between corresponding fluorophores and is of more biological significance (381). Correlation and co-occurrence seem unrelated and give unique, distinctive features of co-localization. *Costes et al.,* 2004 (382) and *Aaron et al.,* 2019 (383) have proposed MCC as a hybrid technique to measure both correlation and co-occurrence. Despite being used for the last 27 years, the interpretation of MCC is still being argued widely (380, 384). Although both coefficients are mathematically similar (385), however, they differ in their accuracy of measuring co-localization when coupled with visual bias. We found PCC easy to predict without any need to pre-process the image, insensitive to changes in the gain, pixel intensities, background (signal offset), and only gave positive values when there was clear 'color overlay' indicating co-localization of two signals. On the other hand, MCC was sometimes hard to predict when coupled with visual bias, increased with increasing offset, favored high-intensity pixel combinations, and downplayed low-intensity pixel combinations. Based on above mentioned facts, we found PCC more efficient and superior to MCC in quantifying co-localization. For instance, sometimes we did not see an overlap, but MCC suggested false positive interaction. In that scenario, we had to manually adjust the threshold settings, which is counter intuitive and prone to user's bias. In the end, our data support a co-localization of DDX3X with pUL31, pUL34, and PCBP1.

It should be noted that our study is primarily based on confocal microscopy in most of our experiments, which only monitor co-localization of proteins. To infer physical interactions, these phenotypes should be confirmed with sensitive PPI methods like co-immunoprecipitation or affinity purification. Another limitation of this study was the unequal number of repeats among experiments. This is especially critical when we probed the PCBP1 interaction with DDX3X at different time intervals and its relation with active pUS3 activity, which was only done once. Clearly such experiments should be repeated with the same experimental conditions to confirm these phenotypes.

Chapter 6: Conclusion

Viruses are obligate intracellular pathogens and contenders of the next human pandemic. In the last century, humans have faced several viral pandemics with the loss of millions of precious human lives. Host-pathogen interactomes are a fascinating part of cell biology and a necessary aspect of understanding the underlying mechanisms of the evolution of successful viruses. Despite the discovery of herpesviruses since the 20th century, we are still behind in determining the host and viral factors involved in the productive life cycle of *Orthoherpesviridae*. Moreover, the precise mechanism of HSV-1 nuclear egress is still enigmatic and subject to continuous scientific research. However, with the increasing scientific efforts coupled with modern technology, we are at the cusp of solving this century-old puzzle.

Our labs found DDX3X among the 49 other host proteins incorporated into the HSV-1 tegument layer (54). We next reported DDX3X's importance in optimal gene expression and productive life cycle of HSV-1 and established its interaction with pUL31 (142). Through confocal microscopy and co-IP analyses, we now find that DDX3X interacts with both pUL31 and pUL34 individually. Our results also demonstrate the optimal DDX3X interaction with the intact NEC but that this interaction is not impacted by the pUS3 kinase activity. This represents a scenario where one of both NEC proteins may individually bring DDX3X to the INM, where the formation of the NEC could be important for DDX3X to play its role in the selective egress of C-capsids. Moreover, DDX3X also interacts with PCBP1, which may also modulate the preferential egress of C-capsids. This study is a step forward in mapping the complex multiple host-protein interactions with viral partners and elucidating their possible role in the enigmatic selective escape of HSV-1 C-capsids.

Chapter 7: Bibliography

1. Wildy P. 1973. Herpes: history and classification, vol 1, p 1-25. Academic Press New York 1:1-25.
2. Gatherer D, Depledge DP, Hartley CA, Szpara ML, Vaz PK, Benkő M, Brandt CR, Bryant NA, Dastjerdi A, Doszpoly A. 2021. ICTV virus taxonomy profile: Herpesviridae 2021. Journal of General Virology 102:001673.
3. Davison AJ. 2002. Evolution of the herpesviruses. Veterinary microbiology 86:69-88.
4. McGeoch DJ, Gatherer D. 2005. Integrating reptilian herpesviruses into the family herpesviridae. Journal of virology 79:725-731.
5. Singh N, Tscharke DC. 2020. Herpes simplex virus latency is noisier the closer we look. Journal of virology 94:10.1128/jvi. 01701-19.
6. Lau J, Balasubramaniam R. 2023. Oral Herpes Simplex Virus Infections. Sexually Transmissible Oral Diseases:p159-167.
7. AlMukdad S, Harfouche M, Farooqui US, Aldos L, Abu-Raddad LJ. 2023. Epidemiology of herpes simplex virus type 1 and genital herpes in Australia and New Zealand: Systematic review, meta-analyses, and meta-regressions. Epidemiology & Infection:1-23.
8. Mertz GJ, Rosenthal SL, Stanberry LR. 2003. Is herpes simplex virus type 1 (HSV-1) now more common than HSV-2 in first episodes of genital herpes? Sexually transmitted diseases 30(10):801-802.
9. Philipone E, Yoon AJ, Philipone E, Yoon AJ. 2017. Oral Ulcers. Oral Pathology in the Pediatric Patient: A Clinical Guide to the Diagnosis and Treatment of Mucosal Lesions:33-60.
10. Babu A, Malathi L, Kasthuri M, Jimson S. 2017. Ulcerative lesions of the oral cavity–an overview. Biomedical and Pharmacology Journal 10(1):401-405.
11. Olkhovska O, Kirsanova T, Zarkova T, Kucherenko O, Tatarkina A. 2014. Herpes viral infections in children: manual for practical lessons for the V–VI year students, Kharkiv National Medical University (Ukraine).
12. Hammad WAB, Konje JC. 2021. Herpes simplex virus infection in pregnancy–An update. European Journal of Obstetrics & Gynecology and Reproductive Biology 259:38-45.
13. Stone J, Looker KJ, Silhol R, Turner KME, Hayes R, Coetzee J, Baral S, Schwartz S, Mayaud P, Gottlieb S. 2023. The population impact of herpes simplex virus type 2 (HSV-

2) vaccination on the incidence of HSV-2, HIV and genital ulcer disease in South Africa: a mathematical modelling study. EBioMedicine 90:104530.

14. Greenwood R. 2014. Herpesvirus Infections. Viruses, Immunity, and Mental Disorders:65.
15. Organization WH. Globally, an estimated two-thirds of the population under 50 are infected with herpes simplex virus type 1; 2015.
16. Chang JY, Balch C, Puccio J, Oh HS. 2023. A Narrative Review of Alternative Symptomatic Treatments for Herpes Simplex Virus. Viruses 15:1314.
17. McCormick I, James C, Welton NJ, Mayaud P, Turner KME, Gottlieb SL, Foster A, Looker KJ. 2022. Incidence of herpes simplex virus keratitis and other ocular disease: Global review and estimates. Ophthalmic epidemiology 29:353-362.
18. James C, Harfouche M, Welton NJ, Turner KM, Abu-Raddad LJ, Gottlieb SL, Looker KJ. 2020. Herpes simplex virus: global infection prevalence and incidence estimates, 2016. Bulletin of the World Health Organization 98:315.
19. Bhatta AK, Keyal U, Liu Y, Gellen E. 2018. Vertical transmission of herpes simplex virus: an update. JDDG: Journal der Deutschen Dermatologischen Gesellschaft 16:685-692.
20. Looker KJ, Johnston C, Welton NJ, James C, Vickerman P, Turner KM, Boily M-C, Gottlieb SL. 2020. The global and regional burden of genital ulcer disease due to herpes simplex virus: a natural history modelling study. BMJ global health 5(3):e001875.
21. Auriti C, De Rose DU, Santisi A, Martini L, Piersigilli F, Bersani I, Ronchetti MP, Caforio L. 2021. Pregnancy and viral infections: Mechanisms of fetal damage, diagnosis and prevention of neonatal adverse outcomes from cytomegalovirus to SARS-CoV-2 and Zika virus. Biochimica et Biophysica Acta (BBA)-Molecular Basis of Disease 1867:166198.
22. Burrel S, Boutolleau D, Ryu D, Agut H, Merkel K, Leendertz FH, Calvignac-Spencer S. 2017. Ancient recombination events between human herpes simplex viruses. Molecular biology and evolution 34:1713-1721.
23. Pfaff F, Groth M, Sauerbrei A, Zell R. 2016. Genotyping of herpes simplex virus type 1 by whole-genome sequencing. Journal of General Virology 97:2732-2741.
24. Forni D, Pontremoli C, Clerici M, Pozzoli U, Cagliani R, Sironi M. 2020. Recent out-of-Africa migration of human herpes simplex viruses. Molecular Biology and Evolution 37:1259-1271.

25. Kolb AW, Ané C, Brandt CR. 2013. Using HSV-1 genome phylogenetics to track past human migrations. PloS one 8(10):e76267.
26. Tweedy J, Spyrou MA, Pearson M, Lassner D, Kuhl U, Gompels UA. 2016. Complete genome sequence of germline chromosomally integrated human herpesvirus 6A and analyses integration sites define a new human endogenous virus with potential to reactivate as an emerging infection. Viruses 8(1):19.
27. Alandijany T. 2019. Host intrinsic and innate intracellular immunity during herpes simplex virus type 1 (HSV-1) infection. Frontiers in microbiology 10:2611.
28. Boeren M, Meysman P, Laukens K, Ponsaerts P, Ogunjimi B, Delputte P. 2022. T cell immunity in HSV-1-and VZV-infected neural ganglia. Trends in Microbiology 31:51-61.
29. Kurt-Jones EA, Chan M, Zhou S, Wang J, Reed G, Bronson R, Arnold MM, Knipe DM, Finberg RW. 2004. Herpes simplex virus 1 interaction with Toll-like receptor 2 contributes to lethal encephalitis. Proceedings of the National Academy of Sciences 101:1315-1320.
30. Zhang S-Y, Jouanguy E, Ugolini S, Smahi A, Elain Gl, Romero P, Segal D, Sancho-Shimizu V, Lorenzo L, Puel A. 2007. TLR3 deficiency in patients with herpes simplex encephalitis. science 317:1522-1527.
31. Malmgaard L, Melchjorsen J, Bowie AG, Mogensen SC, Paludan SR. 2004. Viral activation of macrophages through TLR-dependent and-independent pathways. The Journal of Immunology 173(11):6890-6898.
32. Melchjorsen J, Rintahaka J, Søby S, Horan KA, Poltajainen A, Østergaard L, Paludan SR, Matikainen S. 2010. Early innate recognition of herpes simplex virus in human primary macrophages is mediated via the MDA5/MAVS-dependent and MDA5/MAVS/RNA polymerase III-independent pathways. Journal of virology 84:11350-11358.
33. Mossman KL, Macgregor PF, Rozmus JJ, Goryachev AB, Edwards AM, Smiley JR. 2001. Herpes simplex virus triggers and then disarms a host antiviral response. Journal of virology 75:750-758.
34. van Gent M, Chiang JJ, Muppala S, Chiang C, Azab W, Kattenhorn L, Knipe DM, Osterrieder N, Gack MU. 2022. The US3 kinase of herpes simplex virus phosphorylates the RNA sensor RIG-I to suppress innate immunity. Journal of Virology 96:e01510-21.

35. Zhao J, Zeng Y, Xu S, Chen J, Shen G, Yu C, Knipe D, Yuan W, Peng J, Xu W. 2016. A viral deamidase targets the helicase domain of RIG-I to block RNA-induced activation. Cell host & microbe 20:770-784.
36. Yao X-D, Rosenthal KL. 2011. Herpes simplex virus type 2 virion host shutoff protein suppresses innate dsRNA antiviral pathways in human vaginal epithelial cells. Journal of general virology 92:1981-1993.
37. Yuan H, You J, You H, Zheng C. 2018. Herpes simplex virus 1 UL36USP antagonizes type I interferon-mediated antiviral innate immunity. Journal of Virology 92:10.1128/jvi. 01161-18.
38. Li Z, Feng Z, Fang Z, Chen J, Chen W, Liang W, Chen Q. 2023. Herpes simplex virus type I glycoprotein L evades host antiviral innate immunity by abrogating the nuclear translocation of phosphorylated NF-κB sub-unit p65. Frontiers in Microbiology 14:1178249.
39. Chee AV, Roizman B. 2004. Herpes simplex virus 1 gene products occlude the interferon signaling pathway at multiple sites. Journal of virology 78:4185-4196.
40. Johnson KE, Knipe DM. 2010. Herpes simplex virus-1 infection causes the secretion of a type I interferon-antagonizing protein and inhibits signaling at or before Jak-1 activation. Virology 396:21-29.
41. Velusamy T. 2020. Role of herpes simplex virus 1 protein ICP47 in antigen presentation and pathogenesisThe Australian National University (Australia):2400693967.
42. Jenks JA, Goodwin ML, Permar SR. 2019. The roles of host and viral antibody Fc receptors in herpes simplex virus (HSV) and human cytomegalovirus (HCMV) infections and immunity. Frontiers in immunology 10:2110.
43. Gianopulos KA, Komala Sari T, Weed DJ, Pritchard SM, Nicola AV. 2022. Conformational changes in herpes simplex virus glycoprotein C. Journal of Virology 96:e00163-22.
44. Liu F, Zhou ZH. 2007. Comparative virion structures of human herpesviruses. Human herpesviruses: biology, therapy, and immunoprophylaxis, Chapter 3, Cambridge University Press (UK):NBK47399.
45. Heming JD, Conway JF, Homa FL. 2017. Herpesvirus capsid assembly and DNA packaging. Cell biology of herpes viruses:119-142.

46. Argnani R, Lufino M, Manservigi M, Manservigi R. 2005. Replication-competent herpes simplex vectors: design and applications. Gene therapy 12:S170-S177.
47. Roizman B. 1996. Herpes simplex viruses and their replication. Fields virology 1:2231-2295.
48. Watson G, Xu W, Reed A, Babra B, Putman T, Wick E, Wechsler S, Rohrmann G, Jin L. 2012. Sequence and comparative analysis of the genome of HSV-1 strain McKrae. Virology 433:528-537.
49. Lehman I, Boehmer PE. 1999. Replication of herpes simplex virus DNA. Journal of Biological Chemistry 274:28059-28062.
50. Bauer DW, Huffman JB, Homa FL, Evilevitch A. 2013. Herpes virus genome, the pressure is on. Journal of the American Chemical Society 135:11216-11221.
51. Newcomb WW, Trus BL, Booy FP, Steven AC, Wall JS, Brown JC. 1993. Structure of the herpes simplex virus capsid molecular composition of the pentons and the triplexes. Journal of molecular biology 232:499-511.
52. Okoye ME, Sexton GL, Huang E, McCaffery JM, Desai P. 2006. Functional analysis of the triplex proteins (VP19C and VP23) of herpes simplex virus type 1. Journal of virology 80:929-940.
53. Snijder J, Radtke K, Anderson F, Scholtes L, Corradini E, Baines J, Heck AJ, Wuite GJ, Sodeik B, Roos WH. 2017. Vertex-specific proteins pUL17 and pUL25 mechanically reinforce herpes simplex virus capsids. Journal of virology 91:10.1128/jvi. 00123-17.
54. Stegen C, Yakova Y, Henaff D, Nadjar J, Duron J, Lippé R. 2013. Analysis of virion-incorporated host proteins required for herpes simplex virus type 1 infection through a RNA interference screen. PloS one 8:e53276.
55. Loret S, Guay G, Lippé R. 2008. Comprehensive characterization of extracellular herpes simplex virus type 1 virions. Journal of virology 82:8605-8618.
56. Radtke K, Kieneke D, Wolfstein A, Michael K, Steffen W, Scholz T, Karger A, Sodeik B. 2010. Plus-and minus-end directed microtubule motors bind simultaneously to herpes simplex virus capsids using different inner tegument structures. PLoS pathogens 6:e1000991.

57. Liashkovich I, Hafezi W, Kühn JM, Oberleithner H, Shahin V. 2011. Nuclear delivery mechanism of herpes simplex virus type 1 genome. Journal of Molecular Recognition 24:414-421.
58. Hagglund R, Roizman B. 2004. Role of ICP0 in the strategy of conquest of the host cell by herpes simplex virus 1. Journal of virology 78:2169-2178.
59. Mbong EF, Woodley L, Dunkerley E, Schrimpf JE, Morrison LA, Duffy C. 2012. Deletion of the herpes simplex virus 1 UL49 gene results in mRNA and protein translation defects that are complemented by secondary mutations in UL41. Journal of virology 86:12351-12361.
60. Yang L, Wang M, Cheng A, Yang Q, Wu Y, Jia R, Liu M, Zhu D, Chen S, Zhang S. 2019. Innate immune evasion of alphaherpesvirus tegument proteins. Frontiers in immunology 10:2196.
61. Henaff D, Rémillard-Labrosse G, Loret S, Lippé R. 2013. Analysis of the early steps of herpes simplex virus 1 capsid tegumentation. Journal of virology 87:4895-4906.
62. Owen D. 2018. Investigating the structure and function of HSV-1 tegument proteins: UL7 and UL51. University of Cambridge (UK):26007.
63. Ebert K. 2015. Characterising the relationship between the herpes simplex virus tegument proteins VP22 and vhs.Imperial College London (UK):42885
64. Gianni T, Amasio M, Campadelli-Fiume G. 2009. Herpes simplex virus gD forms distinct complexes with fusion executors gB and gH/gL in part through the C-terminal profusion domain. Journal of Biological Chemistry 284:17370-17382.
65. Jambunathan N, Clark CM, Musarrat F, Chouljenko VN, Rudd J, Kousoulas KG. 2021. Two sides to every story: herpes simplex type-1 viral glycoproteins gB, gD, gH/gL, gK, and cellular receptors function as key players in membrane fusion. Viruses 13:1849.
66. Dogrammatzis C, Waisner H, Kalamvoki M. 2020. “Non-essential” proteins of HSV-1 with essential roles in vivo: a comprehensive review. Viruses 13:17.
67. Hollinshead M, Johns HL, Sayers CL, Gonzalez-Lopez C, Smith GL, Elliott G. 2012. Endocytic tubules regulated by Rab GTPases 5 and 11 are used for envelopment of herpes simplex virus. The EMBO journal 31:4204-4220.

68. Turcotte S, Letellier J, Lippé R. 2005. Herpes simplex virus type 1 capsids transit by the trans-Golgi network, where viral glycoproteins accumulate independently of capsid egress. Journal of virology 79:8847-8860.
69. Kumar SP, Chandy ML, Shanavas M, Khan S, Suresh K. 2016. Pathogenesis and life cycle of herpes simplex virus infection-stages of primary, latency and recurrence. Journal of Oral and Maxillofacial Surgery, Medicine, and Pathology 28:350-353.
70. Dollery SJ, Delboy MG, Nicola AV. 2010. Low pH-induced conformational change in herpes simplex virus glycoprotein B. Journal of virology 84:3759-3766.
71. O'Donnell CD, Kovacs M, Akhtar J, Valyi-Nagy T, Shukla D. 2010. Expanding the role of 3-O sulfated heparan sulfate in herpes simplex virus type-1 entry. Virology 397:389-398.
72. Montgomery RI, Warner MS, Lum BJ, Spear PG. 1996. Herpes simplex virus-1 entry into cells mediated by a novel member of the TNF/NGF receptor family. Cell 87:427-436.
73. Agelidis AM, Shukla D. 2015. Cell entry mechanisms of HSV: what we have learned in recent years. Future virology 10:1145-1154.
74. Newcomb WW, Booy FP, Brown JC. 2007. Uncoating the herpes simplex virus genome. Journal of molecular biology 370:633-642.
75. Brandariz-Nuñez A, Liu T, Du T, Evilevitch A. 2019. Pressure-driven release of viral genome into a host nucleus is a mechanism leading to herpes infection. Elife 8:e47212.
76. Gruffat H, Marchione R, Manet E. 2016. Herpesvirus late gene expression: a viral-specific pre-initiation complex is key. Frontiers in microbiology 7:869.
77. Ding X, Neumann DM, Zhu L. 2022. Host factors associated with either VP16 or VP16-induced complex differentially affect HSV-1 lytic infection. Reviews in Medical Virology 32:e2394.
78. Everett RD, Sourvinos G, Leiper C, Clements JB, Orr A. 2004. Formation of nuclear foci of the herpes simplex virus type 1 regulatory protein ICP4 at early times of infection: localization, dynamics, recruitment of ICP27, and evidence for the de novo induction of ND10-like complexes. Journal of virology 78:1903-1917.
79. Dremel SE, Didychuk AL. Better late than never: A unique strategy for late gene transcription in the beta-and gammaherpesviruses 146: 57-69.

80. Burkham J, Coen DM, Weller SK. 1998. ND10 protein PML is recruited to herpes simplex virus type 1 prereplicative sites and replication compartments in the presence of viral DNA polymerase. Journal of virology 72:10100-10107.
81. Chen I-HB, Sciabica KS, Sandri-Goldin RM. 2002. ICP27 interacts with the RNA export factor Aly/REF to direct herpes simplex virus type 1 intronless mRNAs to the TAP export pathway. Journal of virology 76:12877-12889.
82. Friedel CC, Whisnant AW, Djakovic L, Rutkowski AJ, Friedl M-S, Kluge M, Williamson JC, Sai S, Vidal RO, Sauer S. 2021. Dissecting herpes simplex virus 1-induced host shutoff at the RNA level. Journal of Virology 95:10.1128/jvi. 01399-20.
83. Summers BC, Leib DA. 2002. Herpes simplex virus type 1 origins of DNA replication play no role in the regulation of flanking promoters. Journal of virology 76:7020-7029.
84. Biron KK. 2007. Candidate anti-herpesviral drugs; mechanisms of action and resistance. Human Herpesviruses: Biology, Therapy, and Immunoprophylaxis, Chapter 68, Cambridge University Press (UK):NBK47396.
85. Schildgen O, Gräper S, Blümel J, Külshammer M, Matz B. 2019. Temperature-sensitive origin-binding protein as a tool for investigations of herpes simplex virus activities in vivo. Journal of General Virology 100:105-117.
86. Weller SK, Kuchta RD. 2013. The DNA helicase–primase complex as a target for herpes viral infection. Expert opinion on therapeutic targets 17:1119-1132.
87. Packard JE, Dembowski JA. 2021. HSV-1 DNA replication—coordinated regulation by viral and cellular factors. Viruses 13:2015.
88. Dembowski JA, Dremel SE, DeLuca NA. 2017. Replication-coupled recruitment of viral and cellular factors to herpes simplex virus type 1 replication forks for the maintenance and expression of viral genomes. PLoS pathogens 13:e1006166.
89. Weisshart K, Chow CS, Coen DM. 1999. Herpes simplex virus processivity factor UL42 imparts increased DNA-binding specificity to the viral DNA polymerase and decreased dissociation from primer-template without reducing the elongation rate. Journal of virology 73:55-66.
90. Weller SK, Coen DM. 2012. Herpes simplex viruses: mechanisms of DNA replication. Cold Spring Harbor perspectives in biology 4:a013011.

91. Ibáñez FJ, Farías MA, Gonzalez-Troncoso MP, Corrales N, Duarte LF, Retamal-Díaz A, González PA. 2018. Experimental dissection of the lytic replication cycles of herpes simplex viruses in vitro. Frontiers in Microbiology 9:2406.
92. Tandon R, Mocarski ES, Conway JF. 2015. The A, B, Cs of herpesvirus capsids. Viruses 7:899-914.
93. Newcomb WW, Trus BL, Cheng N, Steven AC, Sheaffer AK, Tenney DJ, Weller SK, Brown JC. 2000. Isolation of herpes simplex virus procapsids from cells infected with a protease-deficient mutant virus. Journal of virology 74:1663-1673.
94. Sherman G, Bachenheimer SL. 1988. Characterization of intranuclear capsids made by ts morphogenic mutants of HSV-1. Virology 163:471-480.
95. Newcomb WW, Homa FL, Thomsen DR, Booy FP, Trus BL, Steven AC, Spencer JV, Brown JC. 1996. Assembly of the herpes simplex virus capsid: characterization of intermediates observed during cell-free capsid formation. Journal of molecular biology 263:432-446.
96. Sheaffer AK, Newcomb WW, Gao M, Yu D, Weller SK, Brown JC, Tenney DJ. 2001. Herpes simplex virus DNA cleavage and packaging proteins associate with the procapsid prior to its maturation. Journal of Virology 75:687-698.
97. McNab AR, Desai P, Person S, Roof LL, Thomsen DR, Newcomb WW, Brown JC, Homa FL. 1998. The product of the herpes simplex virus type 1 UL25 gene is required for encapsidation but not for cleavage of replicated viral DNA. Journal of virology 72:1060-1070.
98. Freeman KG, Huffman JB, Homa FL, Evilevitch A. 2021. UL25 capsid binding facilitates mechanical maturation of the Herpesvirus capsid and allows retention of pressurized DNA. Journal of Virology 95:10.1128/jvi. 00755-21.
99. Huet A, Huffman JB, Conway JF, Homa FL. 2020. Role of the herpes simplex virus CVSC proteins at the capsid portal vertex. Journal of Virology 94:10.1128/jvi. 01534-20.
100. Thomas EC, Bossert M, Banfield BW. 2022. The herpes simplex virus tegument protein pUL21 is required for viral genome retention within capsids. Plos Pathogens 18:e1010969.
101. Panté N, Kann M. 2002. Nuclear pore complex is able to transport macromolecules with diameters of~ 39 nm. Molecular biology of the cell 13:425-434.

102. Campadelli-Fiume G, Farabegoli F, Di Gaeta S, Roizman B. 1991. Origin of unenveloped capsids in the cytoplasm of cells infected with herpes simplex virus 1. Journal of virology 65:1589-1595.
103. Norrild B, Virtanen I, Pedersen B, Pereira L. 1983. Requirements for transport of HSV-1 glycoproteins to the cell surface membrane of human fibroblasts and Vero cells. Archives of virology 77:155-166.
104. Wild P, Engels M, Senn C, Tobler K, Ziegler U, Schraner EM, Loepfe E, Ackermann M, Mueller M, Walther P. 2005. Impairment of nuclear pores in bovine herpesvirus 1-infected MDBK cells. Journal of virology 79:1071-1083.
105. Mettenleiter TC, Müller F, Granzow H, Klupp BG. 2013. The way out: what we know and do not know about herpesvirus nuclear egress. Cellular microbiology 15:170-178.
106. Stackpole CW. 1969. Herpes-type virus of the frog renal adenocarcinoma: I. Virus development in tumor transplants maintained at low temperature. Journal of virology 4:75-93.
107. Draganova EB, Zhang J, Zhou ZH, Heldwein EE. 2020. Structural basis for capsid recruitment and coat formation during HSV-1 nuclear egress. Elife 9:e56627.
108. Draganova EB, Wang H, Wu M, Liao S, Vu A, Gonzalez-Del Pino G, Zhou ZH, Roller RJ, Heldwein K. 2023. The universal suppressor mutation in the HSV-1 nuclear egress complex restores membrane budding defects by stabilizing the oligomeric lattice. bioRxiv:2023.06. 22.546118.
109. Ungricht R, Kutay U. 2017. Mechanisms and functions of nuclear envelope remodelling. Nature Reviews molecular cell biology 18:229-245.
110. Reynolds AE, Wills EG, Roller RJ, Ryckman BJ, Baines JD. 2002. Ultrastructural localization of the herpes simplex virus type 1 UL31, UL34, and US3 proteins suggests specific roles in primary envelopment and egress of nucleocapsids. Journal of virology 76:8939-8952.
111. Marschall M, Häge S, Conrad M, Alkhashrom S, Kicuntod J, Schweininger J, Kriegel M, Lösing J, Tillmanns J, Neipel F. 2020. Nuclear egress complexes of HCMV and other herpesviruses: Solving the puzzle of sequence coevolution, conserved structures and subfamily-spanning binding properties. Viruses 12:683.

112. Fuchs W, Klupp BG, Granzow H, Osterrieder N, Mettenleiter TC. 2002. The interacting UL31 and UL34 gene products of pseudorabies virus are involved in egress from the host-cell nucleus and represent components of primary enveloped but not mature virions. Journal of virology 76:364-378.
113. Klupp BG, Granzow H, Fuchs W, Keil GM, Finke S, Mettenleiter TC. 2007. Vesicle formation from the nuclear membrane is induced by coexpression of two conserved herpesvirus proteins. Proceedings of the National Academy of Sciences 104:7241-7246.
114. Masoud Bahnamiri M, Roller RJ. 2023. DISTINCT ROLES OF VIRAL US3 AND UL13 PROTEIN KINASES IN HERPES VIRUS SIMPLEX TYPE 1 (HSV-1) NUCLEAR EGRESS. bioRxiv:2023.03. 20.533584.
115. Reynolds AE, Ryckman BJ, Baines JD, Zhou Y, Liang L, Roller RJ. 2001. UL31 and UL34 proteins of herpes simplex virus type 1 form a complex that accumulates at the nuclear rim and is required for envelopment of nucleocapsids. Journal of virology 75:8803-8817.
116. Adlakha M, Livingston CM, Bezsonova I, Weller SK. 2020. The herpes simplex virus 1 immediate early protein ICP22 is a functional mimic of a cellular J protein. Journal of Virology 94:10.1128/jvi. 01564-19.
117. Liu Z, Kato A, Shindo K, Noda T, Sagara H, Kawaoka Y, Arii J, Kawaguchi Y. 2014. Herpes simplex virus 1 UL47 interacts with viral nuclear egress factors UL31, UL34, and Us3 and regulates viral nuclear egress. Journal of virology 88:4657-4667.
118. Gao J, Finnen RL, Sherry MR, Le Sage V, Banfield BW. 2020. Differentiating the roles of UL16, UL21, and Us3 in the nuclear egress of herpes simplex virus capsids. Journal of virology 94:10.1128/jvi. 00738-20.
119. Funk C, Marques da Silveira e Santos D, Ott M, Raschbichler V, Bailer SM. 2021. The HSV1 tail-anchored membrane protein pUL34 contains a basic motif that supports active transport to the inner nuclear membrane prior to formation of the nuclear egress complex. Viruses 13:1544.
120. Bigalke JM, Heuser T, Nicastro D, Heldwein EE. 2014. Membrane deformation and scission by the HSV-1 nuclear egress complex. Nature communications 5:4131.
121. Funk C, Ott M, Raschbichler V, Nagel C-H, Binz A, Sodeik B, Bauerfeind R, Bailer SM. 2015. The herpes simplex virus protein pUL31 escorts nucleocapsids to sites of nuclear egress, a process coordinated by its N-terminal domain. PLoS pathogens 11:e1004957.

122. Park R, Baines JD. 2006. Herpes simplex virus type 1 infection induces activation and recruitment of protein kinase C to the nuclear membrane and increased phosphorylation of lamin B. Journal of virology 80:494-504.
123. Hagen C, Dent KC, Zeev-Ben-Mordehai T, Grange M, Bosse JB, Whittle C, Klupp BG, Siebert CA, Vasishtan D, Bäuerlein FJ. 2015. Structural basis of vesicle formation at the inner nuclear membrane. Cell 163:1692-1701.
124. Bigalke J, Heldwein E. 2017. Have NEC coat, will travel: structural basis of membrane budding during nuclear egress in herpesviruses. Advances in virus research 97:107-141.
125. Thorsen MK, Draganova EB, Heldwein EE. 2022. The nuclear egress complex of Epstein-Barr virus buds membranes through an oligomerization-driven mechanism. PLoS Pathogens 18:e1010623.
126. Zeev-Ben-Mordehai T, Weberruß M, Lorenz M, Cheleski J, Hellberg T, Whittle C, El Omari K, Vasishtan D, Dent KC, Harlos K. 2015. Crystal structure of the herpesvirus nuclear egress complex provides insights into inner nuclear membrane remodeling. Cell reports 13:2645-2652.
127. Holm L, Rosenstrï¿ ½m Pi. 2010. Dali server: conservation mapping in 3D. Nucleic acids research 38:W545-W549.
128. Blaho JA, Mitchell C, Roizman B. 1994. An amino acid sequence shared by the herpes simplex virus 1 alpha regulatory proteins 0, 4, 22, and 27 predicts the nucleotidylylation of the UL21, UL31, UL47, and UL49 gene products. Journal of Biological Chemistry 269:17401-17410.
129. Schnee M, Ruzsics Z, Bubeck A, Koszinowski UH. 2006. Common and Specific Properties of Herpesvirus UL34/UL31 Protein Family Members Revealed by Protein ComplementationAssay. Journal of virology 80:11658-11666.
130. Milbradt J, Auerochs S, Sevvana M, Muller YA, Sticht H, Marschall M. 2012. Specific residues of a conserved domain in the N terminus of the human cytomegalovirus pUL50 protein determine its intranuclear interaction with pUL53. Journal of Biological Chemistry 287:24004-24016.
131. Li M. 2016. Mingsheng Cai, Daixiong Chen, Zhancheng Zeng, Hang Yang, Si Jiang, Xiaowei Li, Jingying Mai, Tao Peng &. Arch Virol 161:2379-2385.

132. Mou F, Wills E, Baines JD. 2009. Phosphorylation of the UL31 protein of herpes simplex virus 1 by the US3-encoded kinase regulates localization of the nuclear envelopment complex and egress of nucleocapsids. Journal of virology 83:5181-5191.
133. Banfield BW. 2019. Beyond the NEC: modulation of herpes simplex virus nuclear egress by viral and cellular components. Current Clinical Microbiology Reports 6:1-9.
134. Wills E, Mou F, Baines JD. 2009. The UL31 and UL34 gene products of herpes simplex virus 1 are required for optimal localization of viral glycoproteins D and M to the inner nuclear membranes of infected cells. Journal of virology 83:4800-4809.
135. Roberts KL, Baines JD. 2011. UL31 of herpes simplex virus 1 is necessary for optimal NF-κB activation and expression of viral gene products. Journal of virology 85:4947-4953.
136. Dembowski JA, DeLuca NA. 2015. Selective recruitment of nuclear factors to productively replicating herpes simplex virus genomes. PLoS pathogens 11:e1004939.
137. Granato M, Feederle R, Farina A, Gonnella R, Santarelli R, Hub B, Faggioni A, Delecluse H-J. 2008. Deletion of Epstein-Barr virus BFLF2 leads to impaired viral DNA packaging and primary egress as well as to the production of defective viral particles. Journal of virology 82:4042-4051.
138. Popa M, Ruzsics Z, Lötzerich M, Dölken L, Buser C, Walther P, Koszinowski UH. 2010. Dominant negative mutants of the murine cytomegalovirus M53 gene block nuclear egress and inhibit capsid maturation. Journal of virology 84:9035-9046.
139. Chang YE, Van Sant C, Krug PW, Sears AE, Roizman B. 1997. The null mutant of the U (L) 31 gene of herpes simplex virus 1: construction and phenotype in infected cells. Journal of virology 71:8307-8315.
140. Liang L, Tanaka M, Kawaguchi Y, Baines JD. 2004. Cell lines that support replication of a novel herpes simplex virus 1 UL31 deletion mutant can properly target UL34 protein to the nuclear rim in the absence of UL31. Virology 329:68-76.
141. Leelawong M, Guo D, Smith GA. 2011. A physical link between the pseudorabies virus capsid and the nuclear egress complex. Journal of virology 85:11675-11684.
142. Khadivjam B, Bonneil É, Thibault P, Lippé R. 2023. RNA helicase DDX3X modulates herpes simplex virus 1 nuclear egress. Communications Biology 6:134.

143. Klupp BG, Granzow H, Mettenleiter TC. 2000. Primary envelopment of pseudorabies virus at the nuclear membrane requires the UL34 gene product. Journal of virology 74:10063-10073.
144. Roller RJ, Bjerke SL, Haugo AC, Hanson S. 2010. Analysis of a charge cluster mutation of herpes simplex virus type 1 UL34 and its extragenic suppressor suggests a novel interaction between pUL34 and pUL31 that is necessary for membrane curvature around capsids. Journal of virology 84:3921-3934.
145. Bigalke JM, Heldwein EE. 2015. Structural basis of membrane budding by the nuclear egress complex of herpesviruses. The EMBO journal 34:2921-2936.
146. Roller RJ, Zhou Y, Schnetzer R, Ferguson J, DeSalvo D. 2000. Herpes simplex virus type 1 UL34 gene product is required for viral envelopment. Journal of virology 74:117-129.
147. Leach N, Bjerke SL, Christensen DK, Bouchard JM, Mou F, Park R, Baines J, Haraguchi T, Roller RJ. 2007. Emerin is hyperphosphorylated and redistributed in herpes simplex virus type 1-infected cells in a manner dependent on both UL34 and US3. Journal of virology 81:10792-10803.
148. Scott ES, O'Hare P. 2001. Fate of the inner nuclear membrane protein lamin B receptor and nuclear lamins in herpes simplex virus type 1 infection. Journal of virology 75:8818-8830.
149. Rönfeldt S, Franzke K, Hölper JE, Klupp BG, Mettenleiter TC. 2020. Mutational functional analysis of the Pseudorabies virus nuclear egress complex-nucleocapsid interaction. Journal of virology 94:10.1128/jvi. 01910-19.
150. Hellberg T, Paßvogel L, Schulz KS, Klupp BG, Mettenleiter TC. 2016. Nuclear egress of herpesviruses: the prototypic vesicular nucleocytoplasmic transport. Advances in virus research 94:81-140.
151. Haugo AC, Szpara ML, Parsons L, Enquist LW, Roller RJ. 2011. Herpes simplex virus 1 pUL34 plays a critical role in cell-to-cell spread of virus in addition to its role in virus replication. Journal of virology 85:7203-7215.
152. Frame MC, Purves FC, McGEOCH DJ, Marsden HS, Leader DP. 1987. Identification of the herpes simplex virus protein kinase as the product of viral gene US3. Journal of General Virology 68:2699-2704.

153. Li L, Li Z, Wang E, Yang R, Xiao Y, Han H, Lang F, Li X, Xia Y, Gao F. 2016. Herpes simplex virus 1 infection of tree shrews differs from that of mice in the severity of acute infection and viral transcription in the peripheral nervous system. Journal of virology 90:790-804.
154. Bahnamiri MM, Roller RJ. 2023. Distinct Roles of Viral US3 and UL13 Protein KINASES in Herpes Virus Simplex Type 1 (HSV-1) Nuclear Egress. bioRxiv.
155. Mou F, Forest T, Baines JD. 2007. US3 of herpes simplex virus type 1 encodes a promiscuous protein kinase that phosphorylates and alters localization of lamin A/C in infected cells. Journal of virology 81:6459-6470.
156. Yu X, He S. 2016. The interplay between human herpes simplex virus infection and the apoptosis and necroptosis cell death pathways. Virology journal 13:1-8.
157. Naghavi MH, Gundersen GG, Walsh D. 2013. Plus-end tracking proteins, CLASPs, and a viral Akt mimic regulate herpesvirus-induced stable microtubule formation and virus spread. Proceedings of the National Academy of Sciences 110:18268-18273.
158. Musarrat F, Chouljenko V, Kousoulas KG. 2021. Cellular and Viral Determinants of Herpes Simplex Virus 1 Entry and Intracellular Transport toward the Nuclei of Infected Cells. Journal of virology 95:10.1128/jvi. 02434-20.
159. Walters MS, Kinchington PR, Banfield BW, Silverstein S. 2010. Hyperphosphorylation of histone deacetylase 2 by alphaherpesvirus US3 kinases. Journal of virology 84:9666-9676.
160. Kato A, Tsuda S, Liu Z, Kozuka-Hata H, Oyama M, Kawaguchi Y. 2014. Herpes simplex virus 1 protein kinase Us3 phosphorylates viral dUTPase and regulates its catalytic activity in infected cells. Journal of virology 88:655-666.
161. Hirohata Y, Arii J, Liu Z, Shindo K, Oyama M, Kozuka-Hata H, Sagara H, Kato A, Kawaguchi Y. 2015. Herpes simplex virus 1 recruits CD98 heavy chain and β1 integrin to the nuclear membrane for viral de-envelopment. Journal of virology 89:7799-7812.
162. Poon AP, Gu H, Roizman B. 2006. ICP0 and the US3 protein kinase of herpes simplex virus 1 independently block histone deacetylation to enable gene expression. Proceedings of the National Academy of Sciences 103:9993-9998.
163. David AT, Baghian A, Foster T, Chouljenko V, Kousoulas K. 2008. The herpes simplex virus type 1 (HSV-1) glycoprotein K (gK) is essential for viral corneal spread and neuroinvasiveness. Current eye research 33:455-467.

164. Kato A, Yamamoto M, Ohno T, Kodaira H, Nishiyama Y, Kawaguchi Y. 2005. Identification of proteins phosphorylated directly by the Us3 protein kinase encoded by herpes simplex virus 1. Journal of virology 79:9325-9331.
165. Hirvonen J. 2020. Modification of Lamin A/C affects chromatin distribution in HSV-1 infected cells. University of Jyvaskyla (Finland):202006265128.
166. Kato A, Liu Z, Minowa A, Imai T, Tanaka M, Sugimoto K, Nishiyama Y, Arii J, Kawaguchi Y. 2011. Herpes simplex virus 1 protein kinase Us3 and major tegument protein UL47 reciprocally regulate their subcellular localization in infected cells. Journal of virology 85:9599-9613.
167. Brahim Belhaouari D, Pires De Souza GA, Lamb DC, Kelly SL, Goldstone JV, Stegeman JJ, Colson P, La Scola B, Aherfi S. 2022. Metabolic arsenal of giant viruses: Host hijack or self-use? Elife 11:e78674.
168. Banerjee A, Kulkarni S, Mukherjee A. 2020. Herpes simplex virus: the hostile guest that takes over your home. Frontiers in microbiology 11:733.
169. Jankowsky E, Fairman-Williams ME. 2010. An introduction to RNA helicases: superfamilies, families, and major themes. RNA helicases 19:1-31.
170. Linder P, Fuller-Pace FV. 2013. Looking back on the birth of DEAD-box RNA helicases. Biochimica et Biophysica Acta (BBA)-Gene Regulatory Mechanisms 1829:750-755.
171. Venkataramanan S, Gadek M, Calviello L, Wilkins K, Floor SN. 2021. DDX3X and DDX3Y are redundant in protein synthesis. Rna 27:1577-1588.
172. Schmid S, Linder P. 1992. D-E-A-D protein family of putative RNA helicases. Molecular microbiology 6:283-291.
173. Linder P, Jankowsky E. 2011. From unwinding to clamping—the DEAD box RNA helicase family. Nature reviews Molecular cell biology 12:505-516.
174. Sharma D, Jankowsky E. 2014. The Ded1/DDX3 subfamily of DEAD-box RNA helicases. Critical reviews in biochemistry and molecular biology 49:343-360.
175. Franca R, Belfiore A, Spadari S, Maga G. 2007. Human DEAD-box ATPase DDX3 shows a relaxed nucleoside substrate specificity. Proteins: Structure, Function, and Bioinformatics 67:1128-1137.

176. Park S, Lee S-G, Kim Y, Song K. 1998. Assignment1 of a human putative RNA helicase gene, DDX3, to human X chromosome bands p11. 3→ p11. 23. Cytogenetics and cell genetics 81:178-179.
177. Sekiguchi T, Iida H, Fukumura J, Nishimoto T. 2004. Human DDX3Y, the Y-encoded isoform of RNA helicase DDX3, rescues a hamster temperature-sensitive ET24 mutant cell line with a DDX3X mutation. Experimental cell research 300:213-222.
178. Matsumura T, Endo T, Isotani A, Ogawa M, Ikawa M. 2019. An azoospermic factor gene, Ddx3y and its paralog, Ddx3x are dispensable in germ cells for male fertility. Journal of Reproduction and Development 65:121-128.
179. Fieremans N, Van Esch H, Holvoet M, Van Goethem G, Devriendt K, Rosello M, Mayo S, Martinez F, Jhangiani S, Muzny DM. 2016. Identification of intellectual disability genes in female patients with a skewed X-inactivation pattern. Human mutation 37:804-811.
180. Rosner A, Rinkevich B. 2007. The DDX3 subfamily of the DEAD box helicases: divergent roles as unveiled by studying different organisms and in vitro assays. Current medicinal chemistry 14:2517-2525.
181. Jankowsky A, Guenther U-P, Jankowsky E. 2010. The RNA helicase database. Nucleic acids research 39:D338-D341.
182. Sharma D, Putnam AA, Jankowsky E. 2017. Biochemical differences and similarities between the DEAD-Box helicase orthologs DDX3X and Ded1p. Journal of molecular biology 429:3730-3742.
183. Johnstone O, Deuring R, Bock R, Linder P, Fuller MT, Lasko P. 2005. Belle is a Drosophila DEAD-box protein required for viability and in the germ line. Developmental biology 277:92-101.
184. Chang T-C, Liu W-S. 2010. The molecular evolution of PL10 homologs. BMC evolutionary biology 10:1-12.
185. Padmanabhan PK, Ferreira GR, Zghidi-Abouzid O, Oliveira C, Dumas C, Mariz FC, Papadopoulou B. 2021. Genetic depletion of the RNA helicase DDX3 leads to impaired elongation of translating ribosomes triggering co-translational quality control of newly synthesized polypeptides. Nucleic Acids Research 49:9459-9478.

186. Vogt PH, Ditton H-J, Kamp C, Zimmer J. 2007. Structure and function of AZFa locus in human spermatogenesis, The Y chromosome and male germ cell biology in health and diseases. World Scientific: p 91-125.
187. Kotov AA, Olenkina OM, Godneeva BK, Adashev VE, Olenina LV. 2017. Progress in understanding the molecular functions of DDX3Y (DBY) in male germ cell development and maintenance. Bioscience trends 11:46-53.
188. Högbom M, Collins R, van den Berg S, Jenvert R-M, Karlberg T, Kotenyova T, Flores A, Hedestam GBK, Schiavone LH. 2007. Crystal structure of conserved domains 1 and 2 of the human DEAD-box helicase DDX3X in complex with the mononucleotide AMP. Journal of molecular biology 372:150-159.
189. Bohnsack KE, Yi S, Venus S, Jankowsky E, Bohnsack MT. 2023. Cellular functions of eukaryotic RNA helicases and their links to human diseases. Nature Reviews Molecular Cell Biology 24(10):749-769.
190. Mo J, Liang H, Su C, Li P, Chen J, Zhang B. 2021. DDX3X: structure, physiologic functions and cancer. Molecular cancer 20:1-20.
191. Lattmann S, Giri B, Vaughn JP, Akman SA, Nagamine Y. 2010. Role of the amino terminal RHAU-specific motif in the recognition and resolution of guanine quadruplex-RNA by the DEAH-box RNA helicase RHAU. Nucleic acids research 38:6219-6233.
192. Hall M, Beiko R. 2018. RNA Remodeling Proteins. Springer Science and Business Media LLC:113-129.
193. Valentin-Vega YA, Wang Y-D, Parker M, Patmore DM, Kanagaraj A, Moore J, Rusch M, Finkelstein D, Ellison DW, Gilbertson RJ. 2016. Cancer-associated DDX3X mutations drive stress granule assembly and impair global translation. Scientific reports 6:25996.
194. de Bisschop G, Ameur M, Ulryck N, Benattia F, Ponchon L, Sargueil B, Chamond N. 2019. HIV-1 gRNA, a biological substrate, uncovers the potency of DDX3X biochemical activity. Biochimie 164:83-94.
195. Shen H, Yanas A, Owens MC, Zhang C, Fritsch C, Fare CM, Copley KE, Shorter J, Goldman YE, Liu KF. 2022. Sexually dimorphic RNA helicases DDX3X and DDX3Y differentially regulate RNA metabolism through phase separation. Molecular Cell 82:2588-2603.

196. Merz C, Urlaub H, Will CL, Lührmann R. 2007. Protein composition of human mRNPs spliced in vitro and differential requirements for mRNP protein recruitment. Rna 13:116-128.
197. Hoye ML, Calviello L, Poff AJ, Ejimogu N-E, Newman CR, Montgomery MD, Ou J, Floor SN, Silver DL. 2022. Aberrant cortical development is driven by impaired cell cycle and translational control in a DDX3X syndrome model. Elife 11:e78203.
198. Che Q, Wang W, Duan P, Fang F, Liu C, Zhou T, Li H, Xiong C, Zhao K. 2019. Downregulation of miR-322 promotes apoptosis of GC-2 cell by targeting Ddx3x. Reproductive biology and endocrinology 17:1-9.
199. Choi H, Kwon J, Cho MS, Sun Y, Zheng X, Wang J, Bouker KB, Casey JL, Atkins MB, Toretsky J. 2021. Targeting DDX3X triggers antitumor immunity via a dsRNA-mediated tumor-intrinsic type I interferon response. Cancer research 81:3607-3620.
200. Ojha J, Secreto CR, Rabe KG, Van Dyke DL, Kortum KM, Slager SL, Shanafelt TD, Fonseca R, Kay NE, Braggio E. 2015. Identification of recurrent truncated DDX3X mutations in chronic lymphocytic leukaemia. British journal of haematology 169:445.
201. Khadivjam B, Stegen C, Hogue-Racine M-A, El Bilali N, Döhner K, Sodeik B, Lippé R. 2017. The ATP-dependent RNA helicase DDX3X modulates herpes simplex virus 1 gene expression. Journal of virology 91:10.1128/jvi. 02411-16.
202. Good AL, Haemmerle MW, Oguh AU, Doliba NM, Stoffers DA. 2019. Metabolic stress activates an ERK/hnRNPK/DDX3X pathway in pancreatic β cells. Molecular Metabolism 26:45-56.
203. Chen C-Y, Chan C-H, Chen C-M, Tsai Y-S, Tsai T-Y, Wu Lee Y-H, You L-R. 2016. Targeted inactivation of murine Ddx3x: essential roles of Ddx3x in placentation and embryogenesis. Human molecular genetics 25:2905-2922.
204. Ng-Cordell E, Kolesnik-Taylor A, O'Brien S, Astle D, Scerif G, Baker K. 2022. Social and emotional characteristics of girls and young women with DDX3X-associated intellectual disability: a descriptive and comparative study. Journal of Autism and Developmental Disorders 53:3208-19.
205. Chan C-H, Chen C-M, Lee Y-HW, You L-R. 2019. DNA damage, liver injury, and tumorigenesis: consequences of DDX3X loss. Molecular Cancer Research 17:555-566.

206. Brennan R, Haap-Hoff A, Gu L, Gautier V, Long A, Schröder M. 2018. Investigating nucleo-cytoplasmic shuttling of the human DEAD-box helicase DDX3. European Journal of Cell Biology 97:501-511.
207. Lai M-C, Lee Y-HW, Tarn W-Y. 2008. The DEAD-box RNA helicase DDX3 associates with export messenger ribonucleoproteins as well astip-associated protein and participates in translational control. Molecular biology of the cell 19:3847-3858.
208. Chen Q, Liu Q, Dezhi L, Wang D, Chen H, Xiao S, Fang L. 2014. Molecular cloning, functional characterization and antiviral activity of porcine DDX3X. Biochemical and Biophysical Research Communications 443:1169-1175.
209. Heerma van Voss MR, Vesuna F, Bol GM, Meeldijk J, Raman A, Offerhaus GJ, Buerger H, Patel AH, Van Der Wall E, Van Diest PJ. 2017. Nuclear DDX3 expression predicts poor outcome in colorectal and breast cancer. OncoTargets and therapy:3501-3513.
210. Chao C-H, Chen C-M, Cheng P-L, Shih J-W, Tsou A-P, Wu Lee Y-H. 2006. DDX3, a DEAD box RNA helicase with tumor growth–suppressive property and transcriptional regulation activity of the p21waf1/cip1 promoter, is a candidate tumor suppressor. Cancer research 66:6579-6588.
211. Chen W-J, Wang W-T, Tsai T-Y, Li H-K, Lee Y-HW. 2017. DDX3 localizes to the centrosome and prevents multipolar mitosis by epigenetically and translationally modulating p53 expression. Scientific reports 7:9411.
212. Shih J-W, Wang W-T, Tsai T-Y, Kuo C-Y, Li H-K, Wu Lee Y-H. 2012. Critical roles of RNA helicase DDX3 and its interactions with eIF4E/PABP1 in stress granule assembly and stress response. Biochemical Journal 441:119-129.
213. Calviello L, Venkataramanan S, Rogowski KJ, Wyler E, Wilkins K, Tejura M, Thai B, Krol J, Filipowicz W, Landthaler M. 2021. DDX3 depletion represses translation of mRNAs with complex 5′ UTRs. Nucleic acids research 49:5336-5350.
214. Oh S, Flynn RA, Floor SN, Purzner J, Martin L, Do BT, Schubert S, Vaka D, Morrissy S, Li Y. 2016. Medulloblastoma-associated DDX3 variant selectively alters the translational response to stress. Oncotarget 7:28169.
215. Soto-Rifo R, Ohlmann T. 2013. The role of the DEAD-box RNA helicase DDX3 in mRNA metabolism. Wiley Interdisciplinary Reviews: RNA 4:369-385.

216. Yang F, Fang E, Mei H, Chen Y, Li H, Li D, Song H, Wang J, Hong M, Xiao W. 2019. Cis-acting circ-CTNNB1 promotes β-catenin signaling and cancer progression via DDX3-mediated transactivation of YY1. Cancer research 79:557-571.
217. Khan AQ, Kuttikrishnan S, Siveen KS, Prabhu KS, Shanmugakonar M, Al-Naemi HA, Haris M, Dermime S, Uddin S. RAS-mediated oncogenic signaling pathways in human malignancies 54: p 1-13.
218. Heaton SM, Atkinson SC, Sweeney MN, Yang SN, Jans DA, Borg NA. 2019. Exportin-1-dependent nuclear export of DEAD-box helicase DDX3X is central to its role in antiviral immunity. Cells 8:1181.
219. Soulat D, Bürckstümmer T, Westermayer S, Goncalves A, Bauch A, Stefanovic A, Hantschel O, Bennett KL, Decker T, Superti-Furga G. 2008. The DEAD-box helicase DDX3X is a critical component of the TANK-binding kinase 1-dependent innate immune response. The EMBO journal 27:2135-2146.
220. Saikruang W, Ang Yan Ping L, Abe H, Kasumba DM, Kato H, Fujita T. 2022. The RNA helicase DDX3 promotes IFNB transcription via enhancing IRF-3/p300 holocomplex binding to the IFNB promoter. Scientific Reports 12:3967.
221. Mamiya N. 1999. Hepatitis C virus core protein interacts with a human DEAD box protein DDX3. J Biol Chem 274:14751-15756.
222. Deckert J, Hartmuth K, Boehringer D, Behzadnia N, Will CL, Kastner B, Stark H, Urlaub H, Luhrmann R. 2006. Protein composition and electron microscopy structure of affinity-purified human spliceosomal B complexes isolated under physiological conditions. Molecular and cellular biology 26(14):5528-5543.
223. Fröhlich A, Rojas-Araya B, Pereira-Montecinos C, Dellarossa A, Toro-Ascuy D, Prades-Pérez Y, García-de-Gracia F, Garcés-Alday A, Rubilar PS, Valiente-Echeverría F. 2016. DEAD-box RNA helicase DDX3 connects CRM1-dependent nuclear export and translation of the HIV-1 unspliced mRNA through its N-terminal domain. Biochimica et Biophysica Acta (BBA)-Gene Regulatory Mechanisms 1859:719-730.
224. Katahira J. 2015. Nuclear export of messenger RNA. Genes 6:163-184.
225. Naji S, Ambrus G, Cimermančič P, Reyes JR, Johnson JR, Filbrandt R, Huber MD, Vesely P, Krogan NJ, Yates JR. 2012. Host cell interactome of HIV-1 Rev includes RNA helicases

involved in multiple facets of virus production. Molecular & Cellular Proteomics 11(4):015313.

226. Lee C-S, Dias AP, Jedrychowski M, Patel AH, Hsu JL, Reed R. 2008. Human DDX3 functions in translation and interacts with the translation initiation factor eIF3. Nucleic acids research 36:4708-4718.

227. Copsey AC, Cooper S, Parker R, Lineham E, Lapworth C, Jallad D, Sweet S, Morley SJ. 2017. The helicase, DDX3X, interacts with poly (A)-binding protein 1 (PABP1) and caprin-1 at the leading edge of migrating fibroblasts and is required for efficient cell spreading. Biochemical Journal 474:3109-3120.

228. Kanai Y, Dohmae N, Hirokawa N. 2004. Kinesin transports RNA: isolation and characterization of an RNA-transporting granule. Neuron 43:513-525.

229. Elvira G, Wasiak S, Blandford V, Tong X-K, Serrano A, Fan X, del Rayo Sanchez-Carbente M, Servant F, Bell AW, Boismenu D. 2006. Characterization of an RNA granule from developing brain. Molecular & cellular proteomics 5:635-651.

230. Merrick WC. 2004. Cap-dependent and cap-independent translation in eukaryotic systems. Gene 332:1-11.

231. Eng SJCB. 2016. Investigating the role of FMRP, CYFIP1 and DDX3X in the processes of mRNA localisation and translation within mesenchymal cells.University of Sussex (UK).

232. Soto-Rifo R, Rubilar PS, Limousin T, De Breyne S, Decimo D, Ohlmann T. 2012. DEAD-box protein DDX3 associates with eIF4F to promote translation of selected mRNAs. The EMBO journal 31:3745-3756.

233. Chen H-H, Yu H-I, Yang M-H, Tarn W-Y. 2018. DDX3 activates CBC-eIF3–mediated translation of uORF-containing oncogenic mRNAs to promote metastasis in HNSCC. Cancer research 78:4512-4523.

234. Geissler R, Golbik RP, Behrens S-E. 2012. The DEAD-box helicase DDX3 supports the assembly of functional 80S ribosomes. Nucleic acids research 40:4998-5011.

235. Han S, Sun S, Li P, Liu Q, Zhang Z, Dong H, Sun M, Wu W, Wang X, Guo H. 2020. Ribosomal protein L13 promotes IRES-driven translation of foot-and-mouth disease virus in a helicase DDX3-dependent manner. Journal of Virology 94:10.1128/jvi. 01679-19.

236. Cheng W, Wang S, Zhang Z, Morgens DW, Hayes LR, Lee S, Portz B, Xie Y, Nguyen BV, Haney MS. 2019. CRISPR-Cas9 screens identify the RNA helicase DDX3X as a repressor of C9ORF72 (GGGGCC) n repeat-associated non-AUG translation. Neuron 104:885-898.

237. He Y, Zhang D, Yang Y, Wang X, Zhao X, Zhang P, Zhu H, Xu N, Liang S. 2018. A double-edged function of DDX3, as an oncogene or tumor suppressor, in cancer progression. Oncology reports 39:883-892.

238. Hives M, Jurecekova J, Hives Holeckova K, Kliment J, Kmetova Sivonova M. 2023. The driving power of the cell cycle: cyclin-dependent kinases, cyclins and their inhibitors. Bratislava Medical Journal/Bratislavske Lekarske Listy 124:4.

239. Lai M-C, Chang W-C, Shieh S-Y, Tarn W-Y. 2010. DDX3 regulates cell growth through translational control of cyclin E1. Molecular and cellular biology 30:5444-5453.

240. Wu D-W, Liu W-S, Wang J, Chen C-Y, Cheng Y-W, Lee H. 2011. Reduced p21WAF1/CIP1 via Alteration of p53-DDX3 pathway is associated with poor relapse-free survival in early-stage human papillomavirus–associated lung cancer. Clinical Cancer Research 17:1895-1905.

241. Bol GM, Vesuna F, Xie M, Zeng J, Aziz K, Gandhi N, Levine A, Irving A, Korz D, Tantravedi S. 2015. Targeting DDX 3 with a small molecule inhibitor for lung cancer therapy. EMBO molecular medicine 7:648-669.

242. Cannizzaro E, Bannister AJ, Han N, Alendar A, Kouzarides T. 2018. DDX 3X RNA helicase affects breast cancer cell cycle progression by regulating expression of KLF 4. FEBS letters 592:2308-2322.

243. Li Q, Zhang P, Zhang C, Wang Y, Wan R, Yang Y, Guo X, Huo R, Lin M, Zhou Z. 2014. DDX3X regulates cell survival and cell cycle during mouse early embryonic development. Journal of biomedical research 28:282.

244. Chen H, Yu H, Cho W, Tarn W. 2015. DDX3 modulates cell adhesion and motility and cancer cell metastasis via Rac1-mediated signaling pathway. Oncogene 34:2790-2800.

245. Winnard Jr PT, Vesuna F, Raman V. 2021. Targeting host DEAD-box RNA helicase DDX3X for treating viral infections. Antiviral research 185:104994.

246. Marecki JC, Belachew B, Gao J, Raney KD. 2021. RNA helicases required for viral propagation in humans. The Enzymes 50:335-367.

247. Cavignac Y, Lieber D, Laib Sampaio K, Madlung J, Lamkemeyer T, Jahn G, Nordheim A, Sinzger C. 2015. The cellular proteins Grb2 and DDX3 are increased upon human cytomegalovirus infection and act in a proviral fashion. PLoS One 10:e0131614.
248. Wang H, Ryu W-S. 2010. Hepatitis B virus polymerase blocks pattern recognition receptor signaling via interaction with DDX3: implications for immune evasion. PLoS pathogens 6:e1000986.
249. Kalverda AP, Thompson GS, Vogel A, Schröder M, Bowie AG, Khan AR, Homans SW. 2009. Poxvirus K7 protein adopts a Bcl-2 fold: biochemical mapping of its interactions with human DEAD box RNA helicase DDX3. Journal of molecular biology 385:843-853.
250. Schmidt N, Lareau CA, Keshishian H, Ganskih S, Schneider C, Hennig T, Melanson R, Werner S, Wei Y, Zimmer M. 2021. The SARS-CoV-2 RNA–protein interactome in infected human cells. Nature microbiology 6:339-353.
251. Yang SN, Atkinson SC, Audsley MD, Heaton SM, Jans DA, Borg NA. 2020. RK-33 is a broad-spectrum antiviral agent that targets DEAD-box RNA helicase DDX3X. Cells 9:170.
252. Mamiya N, Worman HJ. 1999. Hepatitis C virus core protein binds to a DEAD box RNA helicase. Journal of Biological Chemistry 274:15751-15756.
253. Yasuda-Inoue M, Kuroki M, Ariumi Y. 2013. DDX3 RNA helicase is required for HIV-1 Tat function. Biochemical and biophysical research communications 441:607-611.
254. Loureiro ME, Zorzetto-Fernandes AL, Radoshitzky S, Chi X, Dallari S, Marooki N, Lèger P, Foscaldi S, Harjono V, Sharma S. 2018. DDX3 suppresses type I interferons and favors viral replication during Arenavirus infection. PLoS pathogens 14:e1007125.
255. Vashist S, Urena L, Chaudhry Y, Goodfellow I. 2012. Identification of RNA-protein interaction networks involved in the norovirus life cycle. Journal of virology 86:11977-11990.
256. Quaranta P, Lottini G, Chesi G, Contrafatto F, Russotto R, Macera L, Lai M, Spezia PG, Brai A, Botta M. 2020. DDX3 inhibitors show antiviral activity against positive-sense single-stranded RNA viruses but not against negative-sense single-stranded RNA viruses: The coxsackie B model. Antiviral Research 178:104750.
257. Su Y-S, Tsai A-H, Ho Y-F, Huang S-Y, Liu Y-C, Hwang L-H. 2018. Stimulation of the internal ribosome entry site (IRES)-dependent translation of enterovirus 71 by DDX3X RNA helicase and viral 2A and 3C proteases. Frontiers in Microbiology 9:1324.

258. Kumar S, Verma A, Yadav P, Dubey SK, Azhar EI, Maitra S, Dwivedi VD. 2022. Molecular pathogenesis of Japanese encephalitis and possible therapeutic strategies. Archives of Virology 167:1739-1762.
259. German J. 2013. Characterization of the West Nile virus pathogen associated molecular patterns. University of Maryland, College Park:3590618.
260. Nelson C, Mrozowich T, Gemmill DL, Park SM, Patel TR. 2021. Human DDX3X unwinds Japanese encephalitis and Zika viral 5′ terminal regions. International Journal of Molecular Sciences 22:413.
261. Li G, Feng T, Pan W, Shi X, Dai J. 2015. DEAD-box RNA helicase DDX3X inhibits DENV replication via regulating type one interferon pathway. Biochemical and biophysical research communications 456:327-332.
262. Thulasi Raman SN, Liu G, Pyo HM, Cui YC, Xu F, Ayalew LE, Tikoo SK, Zhou Y. 2016. DDX3 interacts with influenza A virus NS1 and NP proteins and exerts antiviral function through regulation of stress granule formation. Journal of virology 90:3661-3675.
263. Liu J, Huang X, Yu Y, Zhang J, Ni S, Hu Y, Huang Y, Qin Q. 2017. Fish DDX3X exerts antiviral function against grouper nervous necrosis virus infection. Fish & Shellfish Immunology 71:95-104.
264. Bei C, Zhang C, Wu H, Feng H, Zhang Y-A, Tu J. 2023. DDX3X Is Hijacked by Snakehead Vesiculovirus Phosphoprotein To Facilitate Virus Replication via Stabilization of the Phosphoprotein. Journal of Virology 97:e00035-23.
265. Vandelli A, Monti M, Milanetti E, Armaos A, Rupert J, Zacco E, Bechara E, Delli Ponti R, Tartaglia GG. 2020. Structural analysis of SARS-CoV-2 genome and predictions of the human interactome. Nucleic acids research 48:11270-11283.
266. Vesuna F, Akhrymuk I, Smith A, Winnard PT, Lin S-C, Panny L, Scharpf R, Kehn-Hall K, Raman V. 2022. RK-33, a small molecule inhibitor of host RNA helicase DDX3, suppresses multiple variants of SARS-CoV-2. Frontiers in Microbiology 13:959577.
267. Ciccosanti F, Di Rienzo M, Romagnoli A, Colavita F, Refolo G, Castilletti C, Agrati C, Brai A, Manetti F, Botta L. 2021. Proteomic analysis identifies the RNA helicase DDX3X as a host target against SARS-CoV-2 infection. Antiviral Research 190:105064.
268. Yedavalli VS, Neuveut C, Chi Y-h, Kleiman L, Jeang K-T. 2004. Requirement of DDX3 DEAD box RNA helicase for HIV-1 Rev-RRE export function. Cell 119:381-392.

269. Ariumi Y, Kuroki M, Abe K-i, Dansako H, Ikeda M, Wakita T, Kato N. 2007. DDX3 DEAD-box RNA helicase is required for hepatitis C virus RNA replication. Journal of virology 81:13922-13926.
270. Colpitts CC, El-Saghire H, Pochet N, Schuster C, Baumert TF. 2016. High-throughput approaches to unravel hepatitis C virus-host interactions. Virus research 218:18-24.
271. Li C, Ge L-l, Li P-p, Wang Y, Dai J-j, Sun M-x, Huang L, Shen Z-q, Hu X-c, Ishag H. 2014. Cellular DDX3 regulates Japanese encephalitis virus replication by interacting with viral un-translated regions. Virology 449:70-81.
272. Jazurek M, Ciesiolka A, Starega-Roslan J, Bilinska K, Krzyzosiak WJ. 2016. Identifying proteins that bind to specific RNAs-focus on simple repeat expansion diseases. Nucleic acids research 44:9050-9070.
273. Swanson MS, Dreyfuss G. 1988. Classification and purification of proteins of heterogeneous nuclear ribonucleoprotein particles by RNA-binding specificities. Molecular and cellular biology.
274. Geuens T, Bouhy D, Timmerman V. 2016. The hnRNP family: insights into their role in health and disease. Human genetics 135:851-867.
275. Bomsztyk K, Denisenko O, Ostrowski J. 2004. hnRNP K: one protein multiple processes. Bioessays 26:629-638.
276. Moran-Jones K, Wayman L, Kennedy DD, Reddel RR, Sara S, Snee MJ, Smith R. 2005. hnRNP A2, a potential ssDNA/RNA molecular adapter at the telomere. Nucleic acids research 33:486-496.
277. Jean-Philippe J, Paz S, Caputi M. 2013. hnRNP A1: the Swiss army knife of gene expression. International journal of molecular sciences 14:18999-19024.
278. Chen M, Zhang J, Manley JL. 2010. Turning on a fuel switch of cancer: hnRNP proteins regulate alternative splicing of pyruvate kinase mRNA. Cancer research 70:8977-8980.
279. Brennan C, Steitz* J. 2001. HuR and mRNA stability. Cellular and Molecular Life Sciences CMLS 58:266-277.
280. Lim I, Jung Y, Kim D-Y, Kim K-T. 2016. HnRNP Q has a suppressive role in the translation of mouse cryptochrome1. PloS one 11:e0159018.

281. Lu J, Gao F-H. 2017. The molecular mechanisms and the role of hnRNP K protein post-translational modification in DNA damage repair. Current Medicinal Chemistry 24:614-621.
282. Nazarov I, Bakhmet E, Tomilin A. 2019. KH-domain poly (C)-binding proteins as versatile regulators of multiple biological processes. Biochemistry (Moscow) 84:205-219.
283. Yuan C, Chen M, Cai X. 2021. Advances in poly (rC)-binding protein 2: Structure, molecular function, and roles in cancer. Biomedicine & Pharmacotherapy 139:111719.
284. Chaudhury A, Chander P, Howe PH. 2010. Heterogeneous nuclear ribonucleoproteins (hnRNPs) in cellular processes: Focus on hnRNP E1's multifunctional regulatory roles. Rna 16:1449-1462.
285. Wang Z, Qiu H, He J, Liu L, Xue W, Fox A, Tickner J, Xu J. 2020. The emerging roles of hnRNPK. Journal of cellular physiology 235:1995-2008.
286. Siomi H, Matunis MJ, Michael WM, Dreyfuss G. 1993. The pre-mRNA binding K protein contains a novel evolutionary conserved motif. Nucleic acids research 21:1193-1198.
287. Musco G, Stier G, Joseph C, Morelli MAC, Nilges M, Gibson TJ, Pastore A. 1996. Three-dimensional structure and stability of the KH domain: molecular insights into the fragile X syndrome. Cell 85:237-245.
288. Grishin NV. 2001. KH domain: one motif, two folds. Nucleic acids research 29:638-643.
289. Valverde R, Edwards L, Regan L. 2008. Structure and function of KH domains. The FEBS journal 275:2712-2726.
290. Wagener R, Aukema SM, Schlesner M, Haake A, Burkhardt B, Claviez A, Drexler HG, Hummel M, Kreuz M, Loeffler M. 2015. The PCBP1 gene encoding poly (rc) binding protein i is recurrently mutated in B urkitt lymphoma. Genes, Chromosomes and Cancer 54:555-564.
291. Bedard KM, Walter BL, Semler BL. 2004. Multimerization of poly (rC) binding protein 2 is required for translation initiation mediated by a viral IRES. Rna 10:1266-1276.
292. Walter BL, Parsley TB, Ehrenfeld E, Semler BL. 2002. Distinct poly (rC) binding protein KH domain determinants for poliovirus translation initiation and viral RNA replication. Journal of virology 76:12008-12022.
293. Makeyev AV, Liebhaber SA. 2002. The poly (C)-binding proteins: a multiplicity of functions and a search for mechanisms. Rna 8:265-278.

294. Ren C, Cho S-J, Jung Y-S, Chen X. 2014. DNA polymerase η is regulated by poly (rC)-binding protein 1 via mRNA stability. Biochemical Journal 464:377-386.
295. Chkheidze AN, Liebhaber SA. 2003. A novel set of nuclear localization signals determine distributions of the αCP RNA-binding proteins. Molecular and cellular biology 23:8405-8415.
296. Zhao H, Wei Z, Shen G, Chen Y, Hao X, Li S, Wang R. 2022. Poly (rC)-binding proteins as pleiotropic regulators in hematopoiesis and hematological malignancy. Frontiers in Oncology 12:1045797.
297. Berry AM, Flock KE, Loh HH, Ko JL. 2006. Molecular basis of cellular localization of poly C binding protein 1 in neuronal cells. Biochemical and biophysical research communications 349:1378-1386.
298. Tripathi V, Sixt KM, Gao S, Xu X, Huang J, Weigert R, Zhou M, Zhang YE. 2016. Direct regulation of alternative splicing by SMAD3 through PCBP1 is essential to the tumor-promoting role of TGF-β. Molecular cell 64:549-564.
299. Ilık İA, Aktaş T. 2022. Nuclear speckles: dynamic hubs of gene expression regulation. The FEBS Journal 289:7234-7245.
300. Habelhah H, Shah K, Huang L, Ostareck-Lederer A, Burlingame A, Shokat KM, Hentze MW, Ronai Ze. 2001. ERK phosphorylation drives cytoplasmic accumulation of hnRNP-K and inhibition of mRNA translation. Nature cell biology 3:325-330.
301. Ghanem LR, Chatterji P, Liebhaber SA. 2014. Specific enrichment of the RNA-binding proteins PCBP1 and PCBP2 in chief cells of the murine gastric mucosa. Gene Expression Patterns 14:78-87.
302. Nooren IM, Thornton JM. 2003. Diversity of protein–protein interactions. The EMBO journal 22:3486-3492.
303. Huo L, Shen C, Ju W, Zou J, Yan W, Brown WT, Zhong N. 2009. Identification of novel partner proteins of PCBP1. Beijing da xue xue bao Yi xue ban= Journal of Peking University Health Sciences 41:402-408.
304. Jiang J-n, Wu Y-y, Fang X-d, Ji F-j. 2020. EIF4E regulates STEAP1 expression in peritoneal metastasis. Journal of Cancer 11:990.
305. Choi HS, Song KY, Hwang CK, Kim CS, Law P-Y, Wei L-N, Loh HH. 2008. A proteomics approach for identification of single strand DNA-binding proteins involved in

transcriptional regulation of mouse μ opioid receptor gene. Molecular & cellular proteomics 7:1517-1529.

306. Sun Y, Jia X, Gao Q, Liu X, Hou L. 2017. The ubiquitin ligase UBE4A inhibits prostate cancer progression by targeting interleukin-like EMT inducer (ILEI). IUBMB life 69:16-21.

307. Ryu M-S, Zhang D, Protchenko O, Shakoury-Elizeh M, Philpott CC. 2017. PCBP1 and NCOA4 regulate erythroid iron storage and heme biosynthesis. The Journal of clinical investigation 127:1786-1797.

308. Boschi NM. 2014. The Role of Poly (c)-binding Proteins in the Post-transcriptional Control of Tyrosine Hydroxylase Mrna.University of Rochester:1638212277.

309. Thiele B-J, Doller A, Kähne T, Pregla R, Hetzer R, Regitz-Zagrosek V. 2004. RNA-binding proteins heterogeneous nuclear ribonucleoprotein A1, E1, and K are involved in post-transcriptional control of collagen I and III synthesis. Circulation research 95:1058-1066.

310. Skalweit A, Doller A, Huth A, Kähne T, Persson PB, Thiele B-J. 2003. Posttranscriptional control of renin synthesis: identification of proteins interacting with renin mRNA 3′-untranslated region. Circulation research 92:419-427.

311. Huang S-C, Zhang HS, Yu B, McMahon E, Nguyen DT, Yu FH, Ou AC, Ou JP, Benz Jr EJ. 2017. Protein 4.1 R exon 16 3′ splice site activation requires coordination among TIA1, Pcbp1, and RBM39 during terminal erythropoiesis. Molecular and Cellular Biology 37:e00446-16.

312. Thakur S, Nakamura T, Calin G, Russo A, Tamburrino JF, Shimizu M, Baldassarre G, Battista S, Fusco A, Wassell RP. 2003. Regulation of BRCA1 transcription by specific single-stranded DNA binding factors. Molecular and cellular biology 23:3774-3787.

313. Doyle GA, Sheng XR, Lin SS, Press DM, Grice DE, Buono RJ, Ferraro TN, Berrettini WH. 2007. Identification of five mouse μ-opioid receptor (MOR) gene (Oprm1) splice variants containing a newly identified alternatively spliced exon. Gene 395:98-107.

314. Wang D, Tawfik VL, Corder G, Low SA, Francois A, Basbaum AI, Scherrer G. 2018. Functional divergence of delta and mu opioid receptor organization in CNS pain circuits. Neuron 98:90-108.

315. Song KY, Choi HS, Law PY, Wei LN, Loh HH. 2017. Post-transcriptional regulation of the human mu-opioid receptor (MOR) by morphine-induced RNA binding proteins hnRNP K and PCBP1. Journal of cellular physiology 232:576-584.
316. Meng Q, Rayala SK, Gururaj AE, Talukder AH, O'Malley BW, Kumar R. 2007. Signaling-dependent and coordinated regulation of transcription, splicing, and translation resides in a single coregulator, PCBP1. Proceedings of the National Academy of Sciences 104:5866-5871.
317. Choi HS, Hwang CK, Song KY, Law P-Y, Wei L-N, Loh HH. 2009. Poly (C)-binding proteins as transcriptional regulators of gene expression. Biochemical and biophysical research communications 380:431-436.
318. Hollams EM, Giles KM, Thomson AM, Leedman PJ. 2002. MRNA stability and the control of gene expression: implications for human disease. Neurochemical research 27:957-980.
319. Chen C-YA, Shyu A-B. 1994. Selective degradation of early-response-gene mRNAs: functional analyses of sequence features of the AU-rich elements. Molecular and cellular biology 14:8471-8482.
320. Ji X, Humenik J, Liebhaber SA. 2019. A cytosine-rich splice regulatory determinant enforces functional processing of the human α-globin gene transcript. Blood, The Journal of the American Society of Hematology 133:2338-2347.
321. Conboy JG. 2019. α-Globin pre-mRNA splicing, revisited. Blood, The Journal of the American Society of Hematology 133:2250-2251.
322. Waggoner SA, Liebhaber SA. 2003. Regulation of α-globin mRNA stability. Experimental biology and medicine 228:387-395.
323. Ho JD, Robb GB, Tai SC, Turgeon PJ, Mawji IA, Man HJ, Marsden PA. 2013. Active stabilization of human endothelial nitric oxide synthase mRNA by hnRNP E1 protects against antisense RNA and microRNAs. Molecular and cellular biology 33:2029-2046.
324. Cho S-J, Jung Y-S, Chen X. 2013. Poly (C)-binding protein 1 regulates p63 expression through mRNA stability. PloS one 8:e71724.
325. Giles KM, Daly JM, Beveridge DJ, Thomson AM, Voon DC, Furneaux HM, Jazayeri JA, Leedman PJ. 2003. The 3′-untranslated region of p21WAF1 mRNA is a composite cis-

acting sequence bound by RNA-binding proteins from breast cancer cells, including HuR and poly (C)-binding protein. Journal of Biological Chemistry 278:2937-2946.

326. Luo Z, Dong X, Li Y, Zhang Q, Kim C, Song Y, Kang L, Liu Y, Wu K, Wu J. 2014. PolyC-binding protein 1 interacts with 5′-untranslated region of enterovirus 71 RNA in membrane-associated complex to facilitate viral replication. PLoS One 9:e87491.

327. Wang H, Vardy LA, Tan CP, Loo JM, Guo K, Li J, Lim SG, Zhou J, Chng WJ, Ng SB. 2010. PCBP1 suppresses the translation of metastasis-associated PRL-3 phosphatase. Cancer cell 18:52-62.

328. Zhang W, Shi H, Zhang M, Liu B, Mao S, Li L, Tong F, Liu G, Yang S, Wang H. 2016. Poly C binding protein 1 represses autophagy through downregulation of LC3B to promote tumor cell apoptosis in starvation. The International Journal of Biochemistry & Cell Biology 73:127-136.

329. Bates S, Ryan KM, Phillips AC, Vousden KH. 1998. Cell cycle arrest and DNA endoreduplication following p21Waf1/Cip1 expression. Oncogene 17:1691-1703.

330. El Bilali N, Khadivjam B, Bonneil E, Thibault P, Lippé R. 2021. Proteomics of Herpes Simplex Virus 1 Nuclear Capsids. Journal of Virology 95:10.1128/jvi. 01842-19.

331. Maric M. 2012. Identification of cellular factors involved in herpes simplex virus type 1 nuclear egress. The University of Iowa (USA):1095525082.

332. Cousineau S, Rheault M, Sagan S. 2022. Poly (rC)-Binding Protein 1 Limits Hepatitis C Virus Virion Assembly and Secretion. Viruses 14: 291.

333. Wang H, Li Y. 2019. Recent progress on functional genomics research of enterovirus 71. Virologica Sinica 34:9-21.

334. Sugimoto A, Abe Y, Watanabe T, Hosokawa K, Adachi J, Tomonaga T, Iwatani Y, Murata T, Fujimuro M. 2021. The FAT10 Posttranslational Modification Is Involved in Lytic Replication of Kaposi's Sarcoma-Associated Herpesvirus. Journal of Virology 95:10.1128/jvi. 02194-20.

335. Li D, Li S, Sun Y, Dong H, Li Y, Zhao B, Guo D, Weng C, Qiu H-J. 2013. Poly (C)-binding protein 1, a novel Npro-interacting protein involved in classical swine fever virus growth. Journal of virology 87:2072-2080.

336. Mole S. 2007. Regulation of splicing related SR proteins during the life cycle of human papillomavirus type 16. University of Glasgow (United Kingdom):1874575503.

337. Cousineau SE, Rheault M, Sagan SM. 2022. Poly (rC)-binding protein 1 limits hepatitis C virus virion assembly and secretion. Viruses 14:291.
338. Cousineau SE, Sagan SM. 2021. Poly (rC)-binding protein 1 limits hepatitis C virus assembly and egress. bioRxiv:2021.02. 28.433252.
339. McLaren M, Marsh K, Cochrane A. 2008. Modulating HIV-1 RNA processing and utilization. Front Biosci 13:5693-5707.
340. Zhao Q, Li J, Liang L, Huang S, Zhou C, Zhao Y, Wang Q, Zhou Y, Jiang L, Chen H. 2018. Interaction between influenza virus PA protein and host protein PCBP1. Scientia Agricultura Sinica 51:3389-3396.
341. Dinh PX. 2012. Roles of cellular proteins in replication of vesicular stomatitis virus. The University of Nebraska-Lincoln:1034586628.
342. Rodriguez LL, Arzt J. 2022. Picornaviridae. Veterinary Microbiology:533-542.
343. Bailey JM, Tapprich WE. 2007. Structure of the 5′ nontranslated region of the coxsackievirus b3 genome: chemical modification and comparative sequence analysis. Journal of virology 81:650-668.
344. Nishimura K, Ueda K, Guwanan E, Sakakibara S, Do E, Osaki E, Yada K, Okuno T, Yamanishi K. 2004. A posttranscriptional regulator of Kaposi's sarcoma-associated herpesvirus interacts with RNA-binding protein PCBP1 and controls gene expression through the IRES. Virology 325:364-378.
345. Alvarado-Hernandez B, Ma Y, Sharma NR, Majerciak V, Lobanov A, Cam M, Zhu J, Zheng Z-M. 2022. Protein-RNA interactome analysis reveals wide association of kaposi's sarcoma-associated herpesvirus ORF57 with host noncoding RNAs and polysomes. Journal of Virology 96:e01782-21.
346. Othman Z. 2014. Translational Control of Kaposi's Sarcoma Associated Herpesvirus (KSHV) vFLIP Expression. University of Surrey (United Kingdom):99513840902346.
347. Dinh PX, Beura LK, Panda D, Das A, Pattnaik AK. 2011. Antagonistic effects of cellular poly (C) binding proteins on vesicular stomatitis virus gene expression. Journal of virology 85:9459-9471.
348. Zheng Z-Z, Miao J, Zhao M, Tang M, Yeo AE, Yu H, Zhang J, Xia N-S. 2010. Role of heat-shock protein 90 in hepatitis E virus capsid trafficking. Journal of General Virology 91:1728-1736.

349. Pingale KD, Kanade GD, Karpe YA. 2020. Heterogeneous nuclear ribonucleoproteins participate in hepatitis E virus replication. Journal of molecular biology 432:2369-2387.
350. Song L, Mao R, Ding L, Tian Z, Zhang M, Wang J, Wang M, Lyu Y, Liu C, Feng M. 2022. hnRNP E1 regulates HPV16 oncogene expression and inhibits cervical cancerization. Frontiers in Oncology 12:905900.
351. Sokolowski M, Tan W, Jellne M, Schwartz S. 1998. mRNA instability elements in the human papillomavirus type 16 L2 coding region. Journal of virology 72:1504-1515.
352. Yu L, Majerciak V, Zheng Z-M. 2022. HPV16 and HPV18 genome structure, expression, and post-transcriptional regulation. International journal of molecular sciences 23:4943.
353. Zhou X, You F, Chen H, Jiang Z. 2012. Poly (C)-binding protein 1 (PCBP1) mediates housekeeping degradation of mitochondrial antiviral signaling (MAVS). Cell research 22:717-727.
354. Bolte S, Cordelières FP. 2006. A guided tour into subcellular colocalization analysis in light microscopy. Journal of microscopy 224:213-232.
355. Zhu S, Welsch RE, Matsudaira PT. A method to quantify co-localization in biological images, p 3887-3890.
356. Espinoza-Lewis RA, Yang Q, Liu J, Huang Z-P, Hu X, Chen D, Wang D-Z. 2017. Poly (C)-binding protein 1 (Pcbp1) regulates skeletal muscle differentiation by modulating microRNA processing in myoblasts. Journal of Biological Chemistry 292:9540-9550.
357. Benetti L, Roizman B. 2004. Herpes simplex virus protein kinase US3 activates and functionally overlaps protein kinase A to block apoptosis. Proceedings of the National Academy of Sciences 101:9411-9416.
358. Strumillo ST, Kartavykh D, de Carvalho Jr FF, Cruz NC, de Souza Teodoro AC, Sobhie Diaz R, Curcio MF. 2021. Host–virus interaction and viral evasion. Cell Biology International 45:1124-1147.
359. Kaufmann SH, Dorhoi A, Hotchkiss RS, Bartenschlager R. 2018. Host-directed therapies for bacterial and viral infections. Nature reviews Drug discovery 17:35-56.
360. Yang K, Baines JD. 2011. Selection of HSV capsids for envelopment involves interaction between capsid surface components pUL31, pUL17, and pUL25. Proceedings of the National Academy of Sciences 108:14276-14281.

361. Villanueva-Valencia JR, Tsimtsirakis E, Evilevitch A. 2021. Role of hsv-1 capsid vertex-specific component (Cvsc) and viral terminal dna in capsid docking at the nuclear pore. Viruses 13:2515.
362. Ryan CS, Schröder M. 2022. The human DEAD-box helicase DDX3X as a regulator of mRNA translation. Frontiers in Cell and Developmental Biology 10:1033684.
363. Riva V, Maga G. 2019. From the magic bullet to the magic target: exploiting the diverse roles of DDX3X in viral infections and tumorigenesis. Future medicinal chemistry 11:1357-1381.
364. Brai A, Trivisani CI, Poggialini F, Pasqualini C, Vagaggini C, Dreassi E. 2022. DEAD-box helicase DDX3X as a host target against emerging viruses: New insights for medicinal chemical approaches. Journal of Medicinal Chemistry 65:10195-10216.
365. Wang H, Kim S, Ryu W-S. 2009. DDX3 DEAD-Box RNA helicase inhibits hepatitis B virus reverse transcription by incorporation into nucleocapsids. Journal of virology 83:5815-5824.
366. Kramer T, Greco T, Enquist L, Cristea I. 2011. Proteomic characterization of pseudorabies virus extracellular virions. Journal of virology 85:6427-6441.
367. Khadivjam B. 2017. Impact of ATP-dependent RNA Helicase DDX3X on Herpes Simplex Type 1 (HSV-1) Replication.
368. Kato A, Kawaguchi Y. 2018. Us3 protein kinase encoded by HSV: the precise function and mechanism on viral life cycle. Human Herpesviruses 1045:45-62.
369. Schmidt T, Striebinger H, Haas J, Bailer SM. 2010. The heterogeneous nuclear ribonucleoprotein K is important for Herpes simplex virus-1 propagation. FEBS letters 584:4361-4365.
370. Shimada K, Kondo K, Yamanishi K. 2004. Human herpesvirus 6 immediate-early 2 protein interacts with heterogeneous ribonucleoprotein K and casein kinase 2. Microbiology and immunology 48:205-210.
371. Lamarche N, Matton G, Massie B, Fontecave M, Atta M, Dumas F, Gaudreau P, Langelier Y. 1996. Production of the R2 subunit of ribonucleotide reductase from herpes simplex virus with prokaryotic and eukaryotic expression systems: higher activity of R2 produced by eukaryotic cells related to higher iron-binding capacity. Biochemical Journal 320:129-135.

372. Frey AG, Nandal A, Park JH, Smith PM, Yabe T, Ryu M-S, Ghosh MC, Lee J, Rouault TA, Park MH. 2014. Iron chaperones PCBP1 and PCBP2 mediate the metallation of the dinuclear iron enzyme deoxyhypusine hydroxylase. Proceedings of the National Academy of Sciences 111:8031-8036.
373. Romeo AM, Christen L, Niles EG, Kosman DJ. 2001. Intracellular chelation of iron by bipyridyl inhibits DNA virus replication: ribonucleotide reductase maturation as a probe of intracellular iron pools. Journal of Biological Chemistry 276:24301-24308.
374. Berggård T, Linse S, James P. 2007. Methods for the detection and analysis of protein–protein interactions. Proteomics 7:2833-2842.
375. Manders E, Stap J, Brakenhoff G, Driel Rv, Aten J. 1992. Dynamics of three-dimensional replication patterns during the S-phase, analysed by double labelling of DNA and confocal microscopy. Journal of cell science 103:857-862.
376. Wiseman PW, Squier JA, Ellisman M, Wilson K. 2000. Two-photon image correlation spectroscopy and image cross-correlation spectroscopy. Journal of microscopy 200:14-25.
377. Li Q, Lau A, Morris TJ, Guo L, Fordyce CB, Stanley EF. 2004. A syntaxin 1, Gαo, and N-type calcium channel complex at a presynaptic nerve terminal: analysis by quantitative immunocolocalization. Journal of Neuroscience 24:4070-4081.
378. Manders EM, Verbeek F, Aten J. 1993. Measurement of co-localization of objects in dual-colour confocal images. Journal of microscopy 169:375-382.
379. Cordelieres FP, Bolte S. JACoP v2. 0: improving the user experience with co-localization studies 174: p 181.
380. Adler J, Parmryd I. 2021. Quantifying colocalization: The case for discarding the Manders overlap coefficient. Cytometry Part A 99:910-920.
381. Adler J, Parmryd I. 2010. Quantifying colocalization by correlation: the Pearson correlation coefficient is superior to the Mander's overlap coefficient. Cytometry Part A 77:733-742.
382. Costes SV, Daelemans D, Cho EH, Dobbin Z, Pavlakis G, Lockett S. 2004. Automatic and quantitative measurement of protein-protein colocalization in live cells. Biophysical journal 86:3993-4003.
383. Aaron JS, Taylor AB, Chew T-L. 2019. The Pearson's correlation coefficient is not a universally superior colocalization metric. Response to ‘Quantifying colocalization: the

MOC is a hybrid coefficient–an uninformative mix of co-occurrence and correlation'. Journal of Cell Science 132:jcs227074.

384. Cordelieres FP, Bolte S. 2014. Experimenters' guide to colocalization studies: finding a way through indicators and quantifiers, in practice. Methods in cell biology 123:395-408.

385. Aaron J, Chew T-L. 2018. Analysis of Image Similarity and Relationship. Basic Confocal Microscopy 11:309-333.

Chapter 8: Annex

Table 5.1. List of HSV-1 genes (inspired by *Dogrammatzis et al., 2020* (66))

Gene	Protein	Location/Function
UL1	gL	Envelope/Virus entry and egress
UL2	UNG	Accessary/Nucleic acid metabolism
UL3	pUL3	Accessary/Nuclear phosphoprotein
UL4	pUL4	Accessary/Latency, reactivation, and virus growth
UL5	HPI (DNA helicase)	NS/DNA Primase helicase complex
UL6	PORT	Capsid/Cleavage of replicated concatemeric DNA
UL7	EEP	Tegument/Virulence, virion assembly, and egress
UL8	HPIII	NS/DNA Primase helicase complex
UL9	ORI-B	NS/DBP, Replication
UL10	gM	Envelope/Virus entry, fusion, and cell-cell spread
UL11	CETP	Tegument/Nucleocapsid envelopment and egress
UL12	NUC	NS/DNA recombination
UL13	VPK	Tegument/viral kinase, regulate NEC positioning
UL14	ECP	Tegument/Viral replication and Secondary envelopment
UL15	TERI	NS/DNA terminase complex
UL16	CETPbp	Tegument/Mitochondrial metabolism, Replication, Egress
UL17	CTTP	Capsid/C-capsids egress, DNA Packaging, and retention
UL18	VP23	Capsid/antiviral immunity
UL19	VP5	Capsid/Antigenic component
UL20	pUL20	Tegument/Capsid egress
UL21	CEF2	Tegument/Virus propagation and Genome retention
UL22	gH	Envelope/Virus entry, egress, and cell-cell spread

UL23	TK	Tegument/Nucleolus dispersal and glycoprotein trafficking
UL24	pUL24	Accessary/Inhibits NF-κB activation
UL25	PCP	Capsid/DNA packaging, Genome retention
UL26	VP21 and VP24	Capsid/Serine protease
UL26.5	VP22a	Capsid/Scaffolding protein
UL27	gB	Envelope/Virus entry
UL28	TER2/ICP18.5	NS/DNA Packaging and viral proteins expression
UL29	ICP8	NS/Direct replication compartments to ND10
UL30	POL	NS/DNA Polymerase
UL31	pUL31	Accessary/NECI, Primary envelopment
UL32	CTNP	NS/DNA Packaging and Capsid localization
UL33	TTS2	NS/Helicase-Terminase complex
UL34	pUL34	Accessary/NECII, Promotes primary envelopment
UL35	VP26	Capsid/Capsids assembly and trafficking
UL36	ICP1/2	NS/Inhibit IFN-β production and NF-κB activation
UL37	LTPbp	Tegument/Nuclear egress
UL38	VP19C	Capsid/viral gene expression
UL39	RR1	NS/Replication
UL40	RR2	NS/Replication
UL41	VHS	Tegument/Viral RNAse, inhibit antiviral immunity
UL42	PPS	NS/DNA Polymerase
UL43	NEMP	NS/Virus entry and fusion
UL44	gC	Envelope/Virus binding to host receptors and virus entry
UL45	pUL45	Envelope/Low pH-dependent virus entry and gB-induced fusion
UL46	VP11/12	Tegument/Inhibits TBK1and STING signaling
UL47	VP13/14	Tegument/Regulate transcription and IE gene expression

UL48	VP16	Tegument/IE gene expression
UL49	VP22	Tegument/DNA replication and viral protein expression
UL49.5	gN	Envelope/gM partner
UL50	dUTPase	Tegument/transcriptional activator
UL51	CEF1	Tegument/Viral replication and pathogenicity
UL52	HP2	NS/Primase-Helicase
UL53	gK	Envelope/virus entry and capsids egress
UL54	ICP27	NS/Gene expression regulation
UL55	pUL55	Tegument/Cytoplasmic envelopment
UL56	pUL56	Tegument/Cytoplasmic envelopment
US1	ICP22	Accessary/Primary envelopment and Late gene expression
US2	pUS2	Tegument/Protein trafficking
US3	PK	Tegument/antiapoptotic, NEC positioning and nuclear egress
US4	gG	Envelope/Chemokines regulation
US5	gJ	Envelope/antiapoptotic
US6	gD	Envelope/Virus entry and spread
US7	gI	Envelope/anterograde transport and cell-cell spread
US8	gE	Envelope/neurovirulence and cell-cell spread
US8.5	pUS8.5	Accessary/localized to nucleolus
US9	pUS9	Tegument/anterograde transport and neurovirulence
US10	pUS10	Tegument/capsids associated protein
US11	pUS11	Tegument/RNA binding, Inhibit PKR and IFN induction
US12	1CP47	Accessary/downregulate MHC-I
RL1	ICP34.5	Tegument/Neurovirulence factor, Prevent autophagy

RL2	ICP0	Tegument/E3 ubiquitin ligase modulates endocytosis
RS1	ICP4	Tegument/Regulator of gene expression